Delft University of Technology

Delft University of Technology
Faculty of Electrical Engineering, Mathematics and Computer Science
Delft Institute of Applied Mathematics

Multivariable feedback control of a Dividing Wall Column

A thesis submitted to the
Delft Institute of Applied Mathematics
in partial fulfilment of the requirements

for the degree

MASTER OF SCIENCE
in
APPLIED MATHEMATICS

by

RUBEN C. VAN DIGGELEN

Delft, the Netherlands
March 2007

Delft University of Technology

MSc THESIS APPLIED MATHEMATICS

"Multivariable feedback control of a Dividing Wall Column"

RUBEN C. VAN DIGGELEN

Delft University of Technology

Daily supervisor	**Responsible professor**
Dr.ir. A. A. Kiss	Prof.dr.ir. A.W. Heemink

Other thesis committee members

dr.ir. K.J. Keesman, Wageningen University

dr. J.W. van der Woude

August, 2009 Delft, The Netherlands

Table of Contents

1 Introduction

Following the literature review, it is clear that while a variety of controllers are used for binary distillation columns, only a few control structures were studied for dividing-wall columns (DWC). In most of the cases multi-loop PID controllers were used to steer the system to the desired steady state. However, control of a DWC using model predictive control has also been successfully studied (Adrian, et al 2004).

Nevertheless, there is still a gap between multi-loop PID control structures and a MPC strategy. Hence, the applicability and possible advantage of more advanced control strategies should be investigated. Moreover, a major problem of the previously reported case studies is the difficulty if not impossibility to make a fair comparison of the control structures, as different ternary systems were used for separation in a DWC. To solve this problem we apply all the investigated control structures to the same DWC, thus allowing a non-biased comparison of the control performance.

The general design goal is to maintain the product qualities at their given set points even in the presence of the disturbances. In this work, the set points are chosen equally for the three product compositions. Moreover, since we try to achieve a sharp separation there are no changes made to the set point. As a consequence, reference tracking – the performance of the overall system in case the reference changes – is not investigated. We exert two types of disturbances: 10% increase of feed flow rate and 10% increase of the molar fraction of component A in the feed. Note also that the disturbances are not exerted simultaneously.

The time needed by the controller for steering the product purities in a small neighborhood of the set points after the exertion of disturbance is measured and used for comparison of the controller performance. Since in an industrial environment the measurements can be distorted by noise and measurement delays we carry out additional simulations using the controllers that satisfy the general design goal. Hence, the controller performance is investigated in case of a measurement delay of one minute and added measurement noise. The noise is filtered which results in a more peak shaped noise signal instead of a block signal. The gain of the filter is such that the average noise strength is 1% of the nominal measured value.

Literature Review

The literature study reveals that a variety of controllers are used for distillation columns. Although there is an abundance of literature available about distillation control, most of the studies are on the control of binary separations. Some of them are interesting from a theoretic point of view, while others present a more practical approach.

Viel et al. (1997) proposed a stable control structure for binary distillation column based on a nonlinear Lyapunov controller. The controller satisfied the design goals to maintain the product qualities at their given set-points, despite the presence of typical disturbances in the feed flow rates and in the feed

composition. The model used to design the controller is a relative simple constant molar overflow model. In such model pressure is taken constant, and thermal balances are neglected. The performance of the controller

controllers performed better than the linear model predictive controller (QDMC). In presence of unmeasured disturbance to the process and parametric uncertainty the IOL-QDMC is much better than simple IOL-PI.

The Generic Model Control (GMC) described by Lee and Sullivan (1988) is a process model based control algorithm that incorporates the nonlinear state-space model of the process directly within the control algorithm. In addition to this, a variant of GMC also known as Distillation Adaptive Generic Model Control (DAGMC) was applied to two typical nontrivial distillation units (Rani and Gangiah, 1991). Note that when the relative order of a nonlinear system is equal to one, the control law of GMC is the same as the control law obtained by IOL (To et al., 1996).

A different robust controller was designed by (Da-Wei Gu, 2005). The control structure consisted of a two level control: inventory control was compared with another nonlinear controller based on the input-output linearization (IOL) technique (Isidori, 1989). Therefore, this Lyapunov based controller can achieve set-point tracking and asymptotic disturbance rejection with better robustness than in the case of using a decoupling matrix obtained by input/output linearization.

In addition to nonlinear control structures, Biswas et al. (2007) noticed that input-output linearizing controllers suffer due to constraints on input and output variables. Hence, they augmented IOL controllers with quadratic matrix controller (IOL-QDMC). The performance of this controller was compared to a quadratic dynamic matrix controller and input-output linearization with PI controller (IOL-PI). Consequently, the two nonlinear and composition control. The inventory of the non-linear model was simply done by two P controllers. The composition control is done by a two-degree-of freedom (2DOF) H_∞ loop shaping controller and a μ-controller. Both controllers ensure robust stability of the closed loop system and fulfilment of a mixture of time domain and frequency domain specifications. Although the design of the controller is based on a reduced linearized model, the simulation of the closed loop system with the nonlinear distillation column model shows very good performance for different reference and disturbance signals as well as for different values of the uncertain parameters.

Several authors studied the design phase of the dividing-wall column (DWC) in order to improve the energy efficiency. The design stage of a DWC is very important as in this phase there are two DOF that can be used for optimization purposes. In this perspective we mention the study reported by Halvorsen and Skogestad (1997) about understanding of the steady-state behaviour. The optimal solution surface of the minimal boil up is given as a function of the control variable *liquid split* and the design variable *vapour split*. Furthermore candidate feedback variables are suggested that can be used to control the system such that the boil up is minimized. One of the feedback variables is the measure of symmetry (DTs) in the temperature profile along the column. In case of optimal operation the temperature profile in the column is symmetric. Hence a 4x4 system is obtained where the inputs are reflux flow rate, vapour flow rate, side product flow rate and liquid split (L_0, V0, S, R_L), and the measured outputs are the three product purities and DTs (x_A, x_B, x_C, DTs), respectively. A suitable set

point for the variable DTs makes sure that the operating point is on the bottom of the optimal solution surface – hence the boil up is minimized.

A plant is considered to be controllable if there is a controller that yields acceptable performance for all expected plant variations (Serra et al., 2000). Hence, two for two cases optimal and non-optimal operating two different designs were compared using linear analysis tools – Morari resiliency index (MRI), condition number (CN), relative gain array (RGA), and closed loop disturbance gain (CLDG) – although non-linear analysis could also be applied (Kiss et al., 2007). For DB inventory control adding more trays can improve the CN – this is not the case for LV inventory control. A non-optimal design improves the controllability when DB inventory control is used – again this is not the case for LV inventory control.

The energy efficiency of the DWC may be improved by allowing heat transfer through the wall (Suphanit, 2007). Although the energy savings that are obtained are small, their suggestion can be taken into account when one is designing a DWC unit.

A more practical approach is suggested by Serra et al. (1999). A linearized model is used to obtain a feedback control by PI control. The inventory level consists of two PI loops in order to keep the liquid in the tank and the liquid in the reboiler at a nominal level. From the candidate manipulated variables: L_0, V_0, D B, S, R_L and R_V, typically the DB, LB, DV or LV is used for inventory control. The remaining variables can be used for composition control. The control structures are compared by SVD and RGA frequency dependent analysis for two cases: optimal en non-optimal operation. The boil up flow rate of the optimal operation is 25% lower than the boil up flow rate of the non-optimal operation. As a result LV inventory control where the control variables D, S and B are used, respectively for composition control is the preferred control structure for optimal operation.

A more advanced approach for a DWC is the MPC strategy reported by Adrian et al. (2004). The MPC controller outperforms a single PI loop. Three temperatures are controlled by the reflux ratios, the liquid split and side-draw flow rate, respectively. The disturbed variable in this case was the feed flow rate.

The null space method is a self-optimizing control method that selects the control variables as combinations of measurements (Alstad and Skogestad, 2007). For the case of a Petlyuk distillation setup this resulted into the following candidate measurements: temperature at all stages and all flow rates. Using the null space method a subset of six measurements was obtained, resulting in a practically implementation.

A very recent control structure is proposed by Ling and Luyben (2009). Their case study resulted in an energy minimizing control structure consisting of PID controllers. They concluded that the composition of the heavy component at the top of the prefractionator is an implicit and practical way to minimize energy consumption in the presence of feed disturbances. This specific composition was controlled by the liquid split variable (R_L).

Controller performance can be benchmarked in a systematic way based on operating records (i.e. data from plant) or using a plant model (Ordys et al., 2007). For example if a PID controller is required to control a plant, the LQG cost functions can be used to provide the lowest practically achievable performance bound. The optimal LQG based controller can be used then to compute the optimal PID

controller. This optimal controller can be compared to the actual controller and hence the performance can be determined. This approach has been applied on a simulation of DWC proprietary BASF (Ordys et al., 2007).

DWC distillation

As a thermal separation method, distillation is one of the most important separation technologies in the chemical industry. Basically, all of the chemicals produced worldwide go through at least one distillation column on their way from crude oil to final product. Considering its many well-known benefits, distillation is and it will remain the separation method of choice in the chemical industry – with over 40 000 columns in operation around the world. Despite the flexibility and the widespread use, one important drawback is the considerable energy requirements, as distillation can generate more than 50% of plant operating cost. (Taylor et al., 2003) An innovative solution to diminish this energy consumption drawback is using advanced process integration techniques (Olujic et al., 2003).
Conventionally, a ternary mixture can be separated via a direct sequence (most volatile component is separated first), indirect sequence (heaviest component is separated first) or distributed sequence (mid-split) consisting of 2-3 distillation columns. This separation sequence evolved to the Petlyuk column configuration (Petlyuk et al., 1965) consisting of two fully thermally coupled distillation columns. Eventually, this led to the concept known today as dividing-wall column (DWC) that integrates in fact the two columns of a Petlyuk system into one column shell (Kaibel, 1987; Christiansen et al., 1997; Schultz et al., 2002; Kolbe and Wenzel, 2004). Figure 1 illustrates the most important ternary separation alternatives.

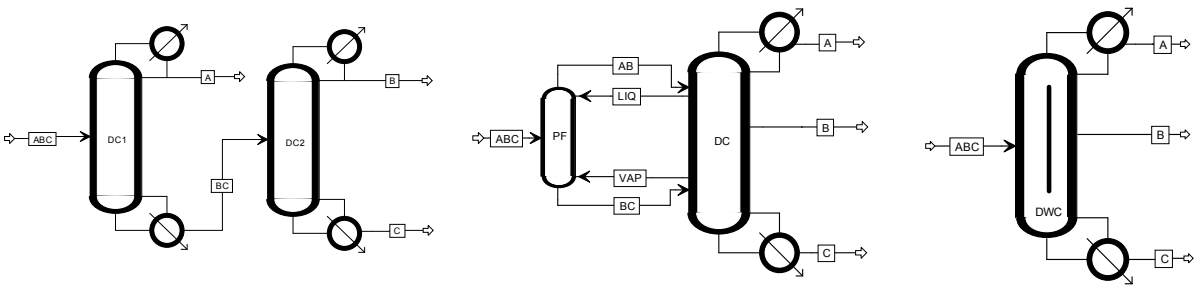

Figure 1: Separation of a ternary mixture via direct distillation sequence (left), Petlyuk configuration (centre) and dividing-wall column (right).

The name of DWC (dividing-wall column or divided wall-column) is given because the middle part of the column is split into two sections by a wall, as illustrated in Figure 1. Feed, typically containing three or more components, is introduced into one side of the column facing the wall. Deflected by the wall, the lightest component A flows upward and exits the column as top distillate while the heaviest component C drops down and is withdrawn from the bottom of the column. The intermediate boiling component B is initially entrained up and down with both streams, but the fluid that goes upward

subsequently separates in the upper part and falls down on the opposite side of the wall. Similarly, the amount of B that goes toward the bottom separates in the lower part then flows up to the back side of the wall, where the entire B product is recovered by a side draw stream. Note however that using a DWC requires a proper match between the operating conditions of the two stand-alone columns in a conventional direct or indirect sequence (Becker et al., 2001).

DWC is very appealing to the chemical industry – with Montz and BASF as the leading companies (Kaibel et al., 2006) – because it can separate three or more components in a single distillation tower, thereby eliminating the need for a second unit, hence saving the cost of building two columns and cutting operating costs by using a single condenser and reboiler. In fact, using dividing-wall columns can save up to 30% in the capital invested and up to 40% in the energy costs (Schultz et al., 2002; Isopescu et al., 2008), particularly for close boiling-species (Perry's Handbook, 2008). In addition, the maintenance costs are also lower.

Compared to classic distillation design arrangements, DWC offers the following benefits:

- High purity for all three or more product streams reached in only one column.
- High thermodynamic efficiency due to reduced remixing effects.
- Lower capital investment due to the integrated design.
- Lower energy consumption compared to conventional direct, indirect and distributed separation sequences.
- Small footprint due to the reduced number of equipment units compared to conventional separation configurations.

Moreover, the list of advantages can be extended when DWC is further combined with reactive distillation leading to the more integrated concept of reactive DWC (Kiss et al., 2009). Note however that the integration of two columns into one shell leads also to changes in the operating mode and ultimately in the controllability of the system (Wang and Wong, 2007). Therefore, all these advantages are possible only under the condition that a good control strategy is available and able to achieve the ternary separation objectives.

Although much of the literature focuses on the control of binary distillation columns, there are only a limited number of studies on the control of DWC. The brief literature review that follows makes a critical overview of the most important DWC control studies up to date.

In this work we explore the main DWC control issues and make a comparison of various multi-loop PID control strategies (DB/LSV, DV/LSB, LB/DSV, LV/DSB) and more advanced controllers such as LQG/LQR, GMC, and high order controllers based on the H_∞ norm μ-synthesis. The performances of these control strategies and the dynamic response of the DWC is investigated in terms of products composition and flow rates, for various persistent disturbances in the feed flow rate and composition. These control strategies are applied to an industrial case study – a dividing-wall column (DWC) used for the ternary separation of benzene-toluene-xylene.

2 Model

Because the model will be used to develop a controller it is recommend using linearized liquid dynamics instead of neglecting the liquid dynamics (Skogestad, 1988; 1992; 2005). For the long run there will be no difference between neglecting liquid dynamics and linearizing liquid dynamics. When the liquid dynamics are not neglected but simplified by a linearization the initial response will be more realistic. Hence, linearized liquid dynamics will be incorporated. The vapour split is impractical to control hence it considered as a design variable. Unfortunately, because it is noticed that with a variable vapour split the energy loss in the presence of feed disturbances is approximately 10 times lower than with a fixed vapour split. (Alstad and Skogestad, 2007).For the dynamic model a number of simplifying assumptions were made:

1. constant pressure,
2. no vapour flow dynamics,
3. linearized liquid dynamics and
4. Neglecting the energy balances and changes in enthalpy.

Note that the DWC is thermodynamically equivalent to the Petlyuk distillation system that is modelled using the following equations:

$$\begin{aligned} \dot{x} &= f(x,u,d,t) \\ y &= g(x) \end{aligned} \tag{2.1}$$

Where u = [L_0 S V_0 D B R_L R_V] is the input vector, d = [F z_1 z_2 q] the disturbance vector and y = [x_A x_B x_C H_T H_R] the output vector.

The dynamic model is implemented in Matlab® (Mathworks, 2007) and it is based on a Petlyuk model previously reported in literature (Halvorsen and Skogestad, 1997). For the detailed mathematical description of the model the reader is referred to the appendix.

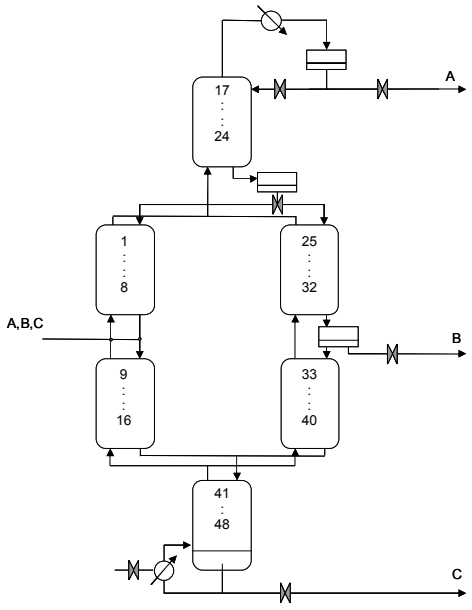

Figure 2: Schematics of the simulated dividing-wall column

Figure 2 illustrates the simulated dividing-wall column. The column is divided into 6 sections each containing 8 trays. Hence, we have 32 trays in the main column and 16 in the prefractionator. When disturbances are not present we assume the flow rate to be F=1, the enthalpy factor to be q=1 en the compositions are equally large. The liquid hold-ups are set as follow: for the reflux tank and the reboiler the hold-up is 20. For the prefractionator the liquid hold-up is 0.5 for the main column, section 3, 4, 5, 6 we have as liquid hold up 1, 0.5, 0.5 and 1 respectively. Furthermore, according to the assumption we have:

$$V_i = V_{i-1} \tag{2.2}$$

This means that inside a section the vapour flow is constant. In addition, the linearized approximation for the liquid flow (Halvorsen & Skogestad, 1997) is:

$$L_i \approx k_0 + k_1 M_i + k_2 V_{i-1} \tag{2.3}$$

The constants k_0, k_1 and k_2 have to be chosen properly. Especially the constant k_2 have an impact on the control properties of the column while the variable V is assumed to be a control variable.

Note that in the literature quite a range of set points for the product purities has been used for ternary separation. Most recent industrial examples mentioned are the separation of ternary mixtures: benzene, toluene and o-xylene (Ling and Luyben, 2009) and benzene-toulene p-xylene (Suphanit et al., 2007). The authors used for the set points of the product purities the values [0.99 0.99 0.99] and [0.95 0.95 0.95], respectively. In this work, we use the same ternary mixture (benzene-toluene-xylene) and the reasonable set points [0.97 0.97 0.97] for the product specifications. Figure 3 provides the composition profiles inside the DWC.

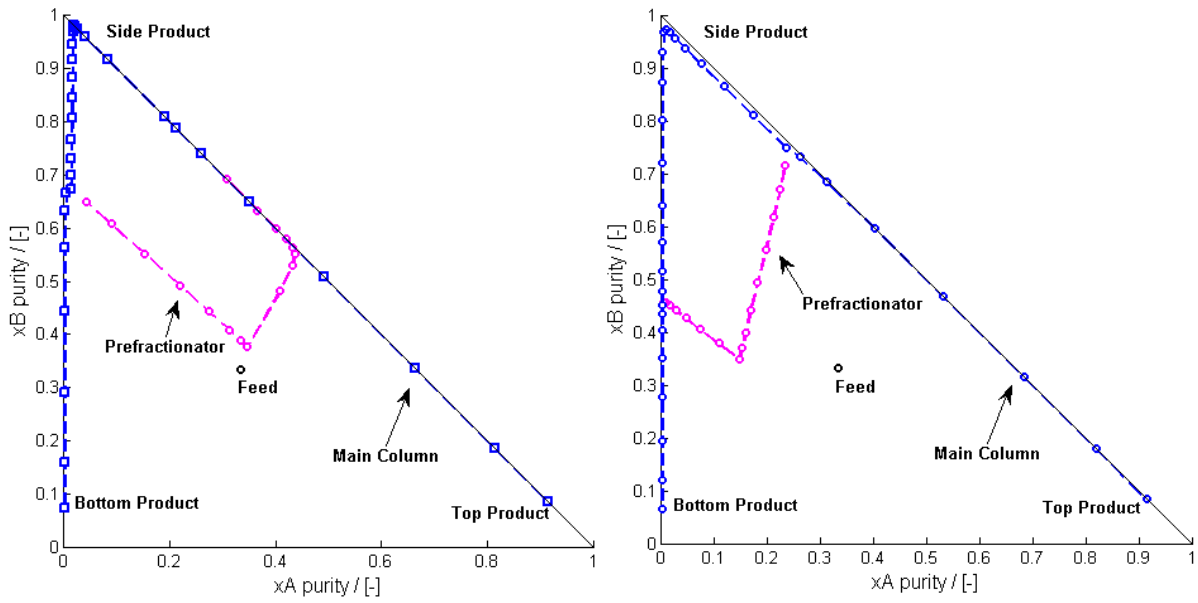

Figure 3: Composition profile inside the dividing-wall column, as ternary diagram for two cases: saturated liquid feed (q=1, left) and liquid-vapour feed (q=0.5, right).

Linear model.

A linear model around the equilibrium (x*, u*) is obtained by numerical differentiation. Hence, the linear model is only valid in a neighborhood of this equilibrium (x*, u*). The linear model will be represented in input-state-output form consisting of the matrices:

$$A(i,j) = \frac{f(x+h,u,d,t) - f(x-h,u,d,t)}{2h}$$

$$B_{input}(i,j) = \frac{f(x,u+h,d,t) - f(x,u-h,d,t)}{2h} \qquad B_{disturbance}(i,j) = \frac{f(x,u,d+h,t) - f(x,u,d-h,t)}{2h} \tag{2.4}$$

$$C(i,j) = \frac{g(x+h,u,d,t) - g(x-h,u,d,t)}{2h}$$

$$D(i,j) = \frac{g(x,u+h,d,t) - g(x,u-h,d,t)}{2h}$$

Note that the matrices B_{input} and $B_{disturbance}$ are two input matrices. The input signal vector u can be chosen by the user while the disturbance vector d is determined the circumstances.

$$\dot{x} = Ax + B_{input}u + B_{disturbance}d$$
$$y = Cx + Du \tag{2.5}$$

The model has 156 states (96 compositions of the components xA and xB, 8 xA and xB composition for the two splitters, reflux tank and reboiler respectively, 48 tray hold-ups and the hold-ups for the two splitters, reflux tank and reboiler), 5 control signals u and 4 disturbances d like the nonlinear model.
The quality of the linear model with respect to the non-linear model is visible in the following two graphs where the nonlinear and the linear response are given on a temporary disturbance in the feed flow rate (Figure 4). The inputs where set at nominal level and only the tank level and reboiler level where controlled while they appear to be unstable.

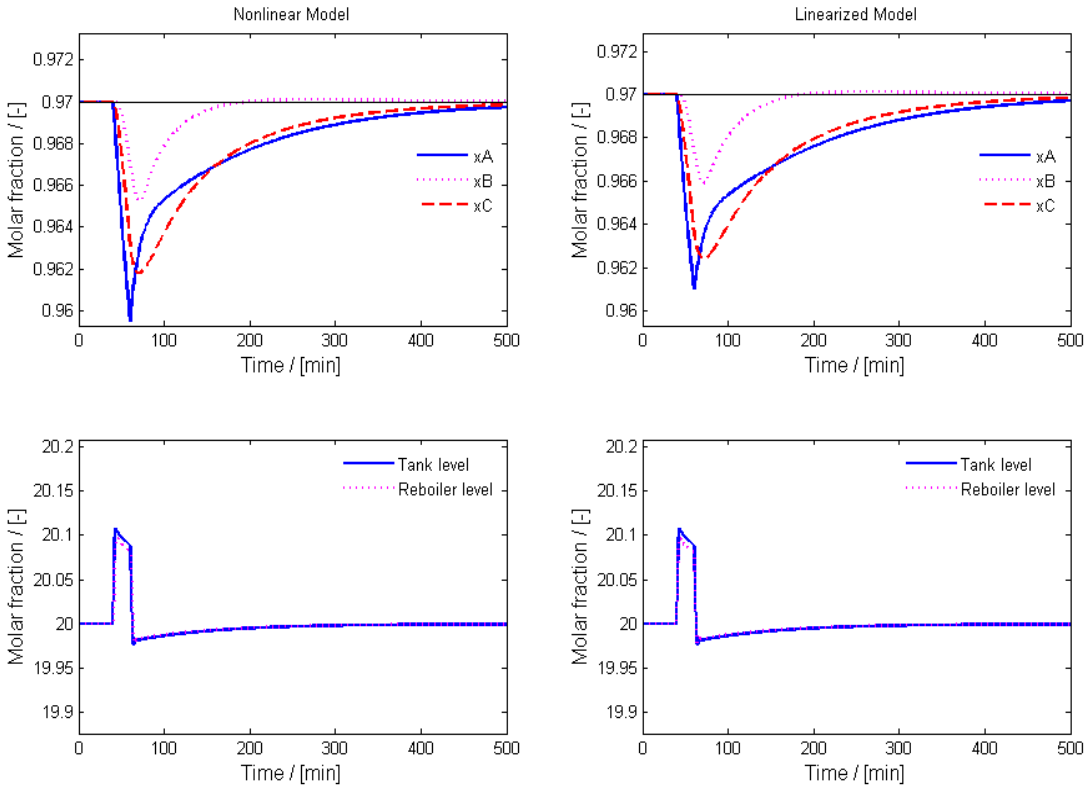

Figure 4: Comparison between the non-linear and linearized system: response after a non-persistent disturbance of +10% in the feed flow rate for 20 minutes (t=40...60)

3 System and Control

Controllability and Observability

From System and Control there are methods available for analysis of the model with respect to the controllability of the plant and other properties which give insight to the performance of the plant. Among the mathematical models we can distinguish roughly two types: linear and non-linear models. After linearization we have obtained a linearized model in state space form:

$$\begin{aligned} \dot{x} &= Ax + Bu \\ y &= Cx \end{aligned} \tag{3.1}$$

The term state controllability is system theoretical concept and originates from Kalman. A system is controllable in practical sense if there exist a controller that yields acceptable performance for all expected plant variations. In addition, there are also examples of systems which are state controllable but which are not controllable in practical sense. On the other hand, state controllability can be used to proof properties in an analytical way. For example if a system has eigenvalues with a positive real part we know that the system is unstable. However, if the system is state controllable we able to choose a feedback gain matrix that achieves an arbitrary pole location. And hence we can stabilize the system.

State Controllability

Definition 1: The dynamical system (3.1) is said to be state controllable if, for any initial state x(0)=x0, any time t1 > 0 and any final state x1, there exists an input u(t) such that x(t1) = x1. Otherwise the system is said to be state uncontrollable.

Remark that if a system is state controllable it is not a priori true that: one can hold the system at a given value if t $\rightarrow\infty$,the required inputs may be very large with sudden changes, some of the state may be of no practical importance.
There exists several tests to verify whether a system (A,B) is state controllable. For example the controllability matrix:

$$\begin{bmatrix} B & AB & A^2B & \dots & A^{n-1}B \end{bmatrix} \tag{3.2}$$

has full row rank if and only if the system (A,B) with n states is state controllable.

An other test, given in the next theorem, gives insight about state controllability by considering the individual poles of the system.
Theorem 1Let pi be an eigenvalue of A.
The eigenvalue pi is state controllable if and only if

$$u_{p,i} = B^H q_i \neq 0 \tag{3.3}$$

for all left eigenvectors q_i or linear combinations associated with p_i. Otherwise the pole is uncontrollable. A system is state controllable if and only if every pole pi is controllable.
In practice many system are not state controllable but are controllable in practical sense. Furthermore, the other way around is also possible; it is shown in the example that a system can be state controllable but is not controllable in practice (Skogestad and Postletwaite, 2005)

Example Water tanks in Series.
Consider the following system in state-space representation

$$A = \begin{pmatrix} -1/\tau & 0 & 0 & 0 \\ 1/\tau & -1/\tau & 0 & 0 \\ 0 & 1/\tau & -1/\tau & 0 \\ 0 & 0 & 1/\tau & -1/\tau \end{pmatrix} \quad B = \begin{pmatrix} 1/\tau \\ 0 \\ 0 \\ 0 \end{pmatrix} \quad C = \begin{pmatrix} 0 & 0 & 0 & 1 \end{pmatrix} \tag{3.4}$$

Matrix A has the eigenvalue -1/τ with multiplicity 4; the corresponding left eigenvectors of A are the columns of the following matrix

$$Q = \begin{pmatrix} 1 & -1 & 1 & -1 \\ 0 & 0 & 0 & 0 \\ 0 & 0 & 0 & 0 \\ 0 & 0 & 0 & 0 \end{pmatrix} \tag{3.5}$$

In order to check the controllability of the poles we calculate $B^T q_i = \pm 1/\tau$. As a result, all the poles are state controllable. Hence the system is controllable.
The system is a series of four first order systems. Moreover a physical interpretation could be the temperature of four water tanks in series. Assuming that there is no heat loss we have the following energy balances as transfer functions:

$$T_4 = \frac{1}{\tau s + 1} T_3 \quad T_3 = \frac{1}{\tau s + 1} T_2 \quad T_2 = \frac{1}{\tau s + 1} T_1 \quad T_1 = \frac{1}{ts + 1} T_0 \tag{3.6}$$

Hence the states are the four tank temperatures: $x=[T_1,T_2,T_3,T_4]^T$, the input $u=T_0$ is the inlet temperature and $\tau=100s$ is the residence time in each tank.
For example, if we want to reach from steady state ($T_i=0$, i=1…4) the state $x_1=[1,-1,1,-1]^T$. Due to the state controllability property this is possible and the input signal and the system response is given in the following picture:

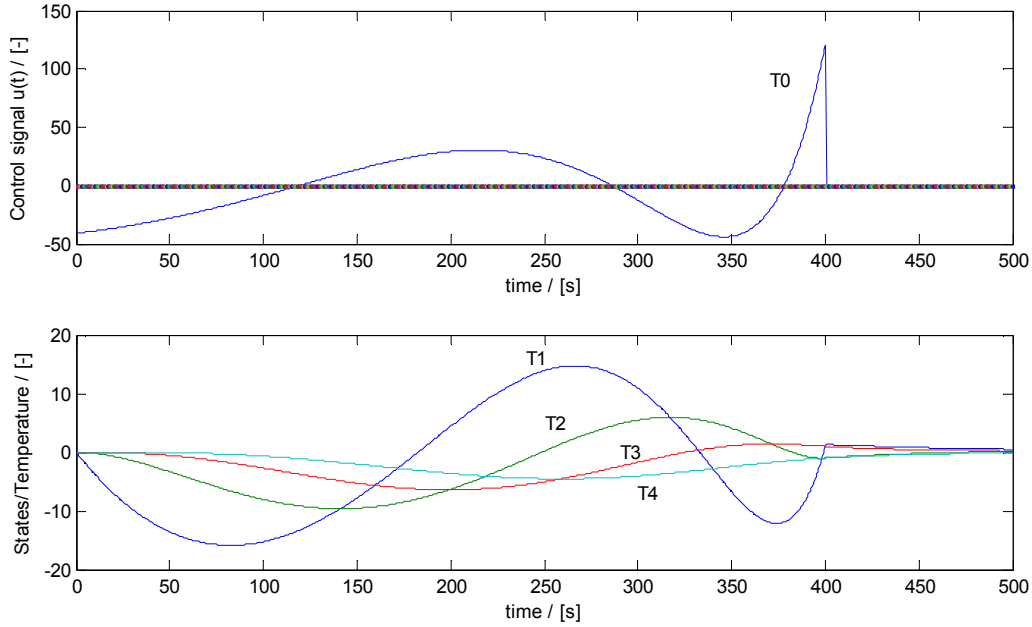

Figure 5: The control signal to the 4 water tanks (top); the corresponding temperature trajectory in each tank (bottom) From Skogestad and Postlethwaite, 2005.

It is demonstrated that the system could reach the state x_1 at finite time 400s. However, when the state is reached the system is not at steady state and the desired state is only attended for a very short time. In addition, the control signal is at some time very high; 100 times higher than the desired state. While the system in theory is controllable in practice it would be very doubtful if the same results can be obtained.

As a result, Skogestad and Postlethwaite suggest that a better name for state-controllability is point-wise state controllability.

State Observability

Definition 2 The pair (A,C) of a dynamic system is said to be state observable if, for any time t1>0, the initial state x(0)=x0 can be determined from the time history of the input u(t) and the output y(t) in the interval [0,t1]. Otherwise the pair (A,C) is said to be state unobservable.

There exists several test for state observability. For example the observability matrix

$$\begin{bmatrix} C \\ CA \\ \vdots \\ CA^{n-1} \end{bmatrix} \tag{3.7}$$

has full column rank if and only if the system (A,C) is state observable.

Like in the case of controllability we can investigate individual poles on observability

Theorem 2 Let p_i be an eigenvalue of A.

The eigenvalue pi is observable if and only if

$$u_{p,i} = B^H q_i \neq 0 \tag{3.8}$$

for all right eigenvectors ti or linear combinations associated with pi. Otherwise the eigenvalue is unobservable.

A system is observable if and only if every eigenvalue pi is observable.

Singular values

The singular value decomposition can be useful for analysis of the MIMO system G(s) with m inputs and l outputs. The problem is that eigenvalues measure the gain only for the special case when the inputs and outputs are in the same direction: the direction of the eigenvector.

For a fixed frequency, a matrix G(jω) may be decomposed into its singular value decomposition:

$$G = U\Sigma V^H \tag{3.9}$$

Where Σ is a diagonal matrix with dimensions (lxm); the k=min(l,m) non-negative singular values σ_i are arranged in descending order along the diagonal. The singular values are the positive square roots of the eigenvalues of G^HG, where G^H is the complex conjugate transpose of G,

$$\sigma_i(G) = \sqrt{\lambda_i(G^HG)} \tag{3.10}$$

Moreover, U is an l x l unitary matrix of output singular vectors u_i, V is an m x m unitary matrix of input singular vectors v_i. A unitary matrix is an n x n complex matrix M such that $MM^H=M^HM=I$.

Any matrix can be decomposed into an input rotation, scaling and output rotation. To illustrate this as example is given for any 2 x 2 matrix:

$$G = \underbrace{\begin{pmatrix} \cos\theta_1 & -\sin\theta_1 \\ \sin\theta_1 & \cos\theta_1 \end{pmatrix}}_{U} \underbrace{\begin{pmatrix} \sigma_1 & 0 \\ 0 & \sigma_2 \end{pmatrix}}_{\Sigma} \underbrace{\begin{pmatrix} \cos\theta_2 & \pm\sin\theta_2 \\ -\sin\theta_2 & \pm\cos\theta_2 \end{pmatrix}^T}_{V^T} \tag{3.11}$$

where U is the output rotation, Σ the scaling matrix and V the input rotation. As a result, the input and output directions are related through the singular values. Since V is a unitary matrix we deduce from (3.11) that

$$Gv_i = \sigma_i u_i \tag{3.12}$$

Thus for an input in direction v_i (column vector of V) the output will be in direction u_i (column vector of U) and scaled by σ. Note that the column vector of the matrices U and V are orthogonal and have unit length. Hence the i'th singular value gives the gain of the transfer matrix G in the direction v_i:

$$\sigma_i(G) = \|Gv_i\|_2 = \frac{\|Gv_i\|_2}{\|v_i\|_2} \tag{3.13}$$

In addition, the above equation can be used to calculate a lower and upper bound for any input direction. The maximum singular value is an upper bound:

$$\bar{\sigma}(G) \equiv \sigma_1(G) = \max_{d\neq 0} \frac{\|Gd\|_2}{\|d\|_2} = \frac{\|Gv_1\|_2}{\|v_1\|_2} \tag{3.14}$$

and the minimum singular value

$$\underline{\sigma}(G) \equiv \sigma_k(G) = \min_{d \neq 0} \frac{\|Gd\|_2}{\|d\|_2} = \frac{\|Gv_k\|_2}{\|v_k\|_2} \tag{3.15}$$

And of course

$$\underline{\sigma}(G) \leq \frac{\|Gd\|_2}{\|d\|_2} \leq \bar{\sigma}(G) \tag{3.16}$$

Performance

In the following figure a negative feedback system is shown:

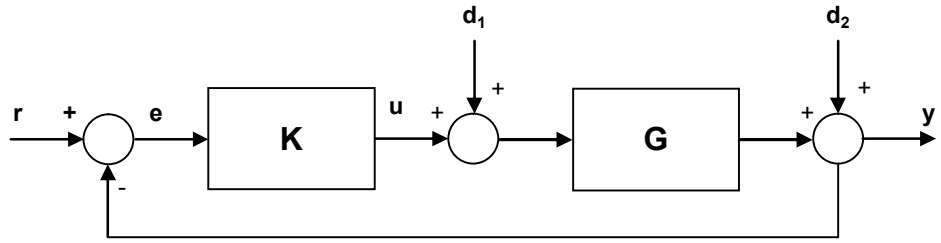

Figure 6: Negative feedback control system with disturbances.

The transfer function for the open loop system is given by

$$L = GK \tag{3.17}$$

The sensitivity and complementary sensitivity are then defined as

$$S = (I + L)^{-1} \qquad T = I - S = L(I + L)^{-1} \tag{3.18}$$

For the sensitivity function we can also calculate the minimum and maximal singular value resulting in

$$\underline{\sigma}(S(j\omega)) \leq \frac{\|e(\omega)\|_2}{\|r(\omega)\|_2} \leq \bar{\sigma}(S(j\omega)) \tag{3.19}$$

Good performance is expected when the maximal singular value of the sensitivity function remains small for all frequencies.

When synthesizing (i.e. formal way of designing) advanced controllers or analysis of control structures often the H_∞ norm is used. Using a performance weighting we can estimate the maximal singular value of the sensitivity function and hence, we can determine a performance weighting in a reasonable manner. Starting that the inverse performance weight is always larger than the maximal singular value of the sensitivity function:

$$\begin{aligned} \bar{\sigma}(S(j\omega)) < \frac{1}{|\omega_P(j\omega)|}, \quad \forall\omega \quad &\Leftrightarrow \quad \bar{\sigma}(\omega_P(j\omega)) < 1, \quad \forall\omega \\ &\Leftrightarrow \quad \|\omega_P S\|_\infty < 1 \end{aligned} \tag{3.20}$$

The H_∞ norm can be defined as:

$$\|M\|_\infty = \max_\omega \bar{\sigma}(M(j\omega)) \tag{3.21}$$

Condition Number

If the gain of a system varies considerably with the input direction then the system has a strong directionality. A measure for quantification of the directionality is the condition number and the relative

gain array (RGA). The condition number of a matrix is defined as the ratio between the maximum and minimum singular value

$$\gamma(G) = \bar{\sigma}(G)/\underline{\sigma}(G) \tag{3.22}$$

A system G with a large condition number is said to be ill-conditioned. The condition number can be used as an input output controllability measure. Moreover, a large condition number indicates possibly sensitivity to uncertainty. Although, this is not true in general, the reverse holds. Thus, in case of a small condition number, multivariable effects of uncertainty are not expected to be serious.

In case of a large condition number (>10) we have a possible indication for control problem (Skogestad and Postlewaite, 2005): First of all, a large condition number may be caused by a small minimal singular value. Because of the large condition number and small minimal singular value the system has a small gain for some input direction while in other directions there is a huge gain; this is in general undesirable and can lead to control problems. On the other hand the minimal condition number can be large and possibly some RGA elements are also large (in the range 5-10 or larger). If this is the case at frequencies important for control then this is an indication for fundamentally difficult for control due to strong interactions and sensitivity to uncertainty. Finally, a large condition number implies that the system is sensitive to unstructured input uncertainty. While this uncertainty does not occur in practice we cannot generally conclude that a plant with a large condition number is sensitive to uncertainty.

Input-Output controllability

Before starting to design a control structure or even synthesize an advanced controller we carry out some preliminary analysis. The analysis give insight to the practical controllability and limitations induced by the nature of the plant like: poles, zeros, disturbances, input constraints and uncertainty.

Poles

Poles are the eigenvalues of the state-space matrix A. The solution of a general linear dynamical system $\dot{x} = Ax + Bu$ is the sum of exponential terms $e^{\lambda_i t}$ each containing an eigenvalue. Hence, the dynamical system will be stable if and only if are all in the close left hand plane (LHP). As a result, the dynamical system will be unstable if and only if there is at least one pole such that $Re(p_i) \geq 0$.

Zeros

If a system has a zero it can happen that despite the input is non-zero the output is zero.

Definition: z_i is a zero of G(s) if the rank of $G(z_i)$ is less than the maximal rank of G(s). The zero polynomial is defined as $z(s) = \prod_{i=1}^{n_z}(s - z_i)$ where n_z is the number of finite zeros of G(s).

The sensitivity function S and the complementary sensitivity function T will be used often. From (3.18) we conclude that S+T=I and moreover,

$$|\bar{\sigma}(S)-1|\le \bar{\sigma}(T)\le \bar{\sigma}(S)+1$$
$$|\bar{\sigma}(T)-1|\le \bar{\sigma}(S)\le \bar{\sigma}(T)+1 \tag{3.23}$$

From this we concluded that it is not possible that S and T are both close to zero simultaneously. Furthermore, the latter inequalities give rise to

$$|\bar{\sigma}(S)-\bar{\sigma}(T)|\le 1 \tag{3.24}$$

Hence, the magnitudes of the maximal singular values of S and T differ by most 1 at a given frequency.

Stability and minimum peaks on S and T

In order to have stability of the feedback system where G(s) has a RHP-zero z; the following interpolation constraints should be satisfied:

$$y_z^H T(z)=0 \qquad y_z^H S(z)=y_z^H \tag{3.25}$$

Where y_z is the corresponding output direction to the zero z.

We have a similar result for the case that G(s) has a RHP-pole. For internal stability the following interpolation constraint should be satisfied

$$S(p)y_p=0 \qquad T(p)y_p=y_p \tag{3.26}$$

These two results can be generalized for various closed-loop transfer functions and lead to lower bounds. First of all we demonstrate that the minimum peaks for S and T can be calculated for any stabilizing controller K. These two minima are defined as:

$$M_{S,min}=\min_K \|S\|_\infty \qquad M_{T,min}=\min_K \|T\|_\infty \tag{3.27}$$

Theorem *Sensitivity peaks* Consider a system G(s) with no time delay, where z_i are the RHP-zeros of G(s) with unit output direction vectors $y_{z,i}$; let p_i be the RHP-poles of (G) with unit output pole directions vectors $y_{p,i}$. In addition, assume that z_i and p_i are all distinct. Then:

$$M_{S,min}=M_{T,min}=\sqrt{1+\bar{\sigma}^2\left(Q^{-1/2}Q_{zp}Q_p^{-1/2}\right)} \tag{3.28}$$

Where the elements of the matrix Q_z, the matrix Q_p and the matrix Q_{zp} are given by

$$\left[Q_z\right]_{ij}=\frac{y_{z,i}^H y_{z,j}}{z_i+\bar{z}_j} \qquad \left[Q_p\right]_{ij}=\frac{y_{p,i}^H y_{p,j}}{\bar{p}_i+p_j} \qquad \left[Q_{zp}\right]_{ij}=\frac{y_{z,i}^H y_{p,j}}{z_i-p_j} \tag{3.29}$$

It can be useful to extend the previous result by including weightings. Assuming that the weights $W_1(s)$ and $W_2(s)$ contain no RHP-poles or RHP-zeros we consider the function W_1SW_2 and W_1TW_2 in the following theorem:

Theorem *Weighted (complementary) sensitivity peaks* Consider a system G(s) with no time delays and no poles or zeros on the imaginary axis; let p_i be the RHP-poles of (G) with unit output pole directions vectors $y_{p,i}$. In addition, assume that z_i and p_i are all distinct. Then:

$$\gamma_{S,min}=\inf_K \|W_1SW_2\|_\infty \qquad \gamma_{T,min}=\inf_K \|W_1TW_2\|_\infty \tag{3.30}$$

Then

$$\gamma_{S,min} = \inf_K \left\| W_1 S W_2 \right\|_\infty \quad \gamma_{T,min} = \inf_K \left\| W_1 T W_2 \right\|_\infty \tag{3.31}$$

$$\gamma_{S,min} = \inf_K \left\| W_1 S W_2 \right\|_\infty \quad \gamma_{T,min} = \inf_K \left\| W_1 T W_2 \right\|_\infty \tag{3.32}$$

where λ_{max} is the largest eigenvalue and the elements of the Q-matrices are given by:

$$\begin{aligned}
[Q_{z1}]_{ij} &= \frac{y_{z,i}^H W_1^{-1}(z_i) W_1^{-H}(z_j) y_{z,j}}{z_i + \bar{z}_j}, \quad [Q_{z2}]_{ij} = \frac{y_{z,i}^H W_2(z_i) W_2(z_j) y_{z,j}}{z_i + \bar{z}_j} \\
[Q_{p1}]_{ij} &= \frac{y_{p,i}^H W_1^H(p_i) W_1(p_j) y_{p,j}}{\bar{p}_i + p_j}, \quad [Q_{p2}]_{ij} = \frac{y_{p,i}^H W_2^{-H}(p_i) W_2^{-1}(p_j) p_{z,j}}{\bar{p}_i + p_j} \\
[Q_{zp1}]_{ij} &= \frac{y_{z,i}^H W_1^{-1}(z_i) W_1(p_j) y_{p,j}}{z_i - p_j}, \quad [Q_{zp2}]_{ij} = \frac{y_{z,i}^H W_2(z_i) W_2^{-1}(p_j) y_{p,j}}{z_i - p_j}
\end{aligned} \tag{3.33}$$

For a special class of weightings: the scalar case there are two other lower bounds.

Theorem Consider a system G(s) which as one RHP-zero at s=z. Choose $W_1=\omega_P(s)$ and $W_2=1$, where $\omega_P(s)$ is a scalar stable transfer function. Then for closed-loop stability the weighted sensitivity function must satisfy

$$\left\| \omega_P S \right\|_\infty \geq \left| \omega_P(z) \right| \tag{3.34}$$

A similar result is available in case the plant G(s) has an RHP-pole at s=p.

Theorem Consider a system G(s) which as one RHP-pole at s=p. Choose $W_1=\omega_T(s)$ and $W_2=1$, where $\omega_P(s)$ is a scalar stable transfer function. Then for closed-loop stability the weighted complementary sensitivity function must satisfy.

$$\left\| \omega_T S \right\|_\infty \geq \left| \omega_T(z) \right| \tag{3.35}$$

In addition, we will give some other useful results; minimum peaks for other closed-loop transfer functions:

SG. Using the theorem on Weighted (complementary) sensitivity peaks we can also obtain a bound for SG: W1=1 and W2 = $G_{ms}(s)$ where $G_{ms}(s)$ denotes the “minimum-phases, stable version” of G(s). In case of more inputs than outputs (G(s) is non-square) the pseudo inverse of G(s) should be obtained in order to find bounds on SG.

SG_d. In general we want that $\left\| SG_d \right\|_\infty$ to be small. Similar to the latter case we replace G_d by the “minimum-phases, stable version” of $G_d(s)$.

KS. A bound on the transfer function KS:

$$\left\| KS \right\|_\infty \geq 1/\underline{\sigma}(U(G)^*) \tag{3.36}$$

For a plant with a single real RHP-pole the equality can be simplified to

$$\left\| KS \right\|_\infty \geq \left\| u_p^H G_s(p)^{-1} \right\|_2 \tag{3.37}$$

KSG_d. In case when a disturbance model, G_d, is known, the bound KS can be generalized as

$$\|KSG_d\|_\infty \geq 1/\underline{\sigma}(U(G_{d,ms}^{-1}G)^*) \tag{3.38}$$

where $U(G_{d,ms}^{-1}G)^*$ is the mirror image of the anti-stable part of $G_{d,ms}^{-1}G$. Similar to bound on KS we can obtain a tight bound for a sing RHP-pole p:

$$\|KSG_d\|_\infty \geq \left\|u_p^H G_s(p)^{-1} G_{d,ms}(p)\right\|_2 \tag{3.39}$$

S_I and T_I. S_I is the input sensitivity function and T_I the input complementary sensitivity function and are defined as:

$$S_I = (I+L)^{-1} \qquad T_I = I - S_I = L(I+L)^{-1} \tag{3.40}$$

The theorem on sensitivity peaks can be used to obtain bounds on the input sensitivity and complementary sensitivity functions. The output pole and zero direction should then be replaced by input pole and zero direction.

		Want small for		Bound on peak
		Signals	Stability robustness	General Case
1	S	Performance Tracking e=-Sr	Multiplicative inverse output uncertainty	(3.25)
2	T	Performance Noise e=-Tn	Multiplicative additive output uncertainty	(3.25)
3	KS	Input usage u=KS(r-n)	Additive uncertainty	(3.41)
4*	SG_d	Performance disturbance $e=SGd_u$	G_d=G: Inverse uncertainty	(3.42) where W_1=I and $W_2=G_{d,ms}$
5*	KSG_d	Input usage disturbance u=KSGd	G_d=G: Multiplicative additive input uncertainty	(3.43)
6	S_I	Actual plant input $u+d_u=S_I d_u$	Inverse multiplicative input uncertainty	(3.25) with output directions replaced by input directions (u_p,u_z)

*Special case: Input disturbance G_d=G

Table 1: Bounds on peaks of important closed-loop transfer functions (Skogestad and Postlethwaite, 2005)

Functional controllability

The term controllability gives rise to confusion while it has different meanings. Due to the state space framework controllability is often changed with state controllability. State controllability is a more or less a academic concept while we can give example of systems which are perfectly state controllable but not controllable in practice. On the other hand there are also many examples of systems which are not state controllable but are perfectly controllable in practice.
An other definition is the following:

Definition 3: The dynamical system G(s) is said to be functional controllable if the rank r of G(s), for s is not a member of the set of zeros, is equal to the number of outputs l. Hence the plant G(s) is functional controllable if G(s) has full row rank. A plant is functionally uncontrollable if r<l.

As a result of the definition a minimal requirement for functional controllability is that we have at least as many inputs as outputs. In addition, a strictly proper plant (D=0) is functional controllable if rank(B)<l, or if rank(C)<l, or if rank(sI-A)<l. This follows from the definition $G(s)=C(sI-A)^{-1}B$ and that the rank of product matrices is less or equal to minimum rank of the individual matrices.
In case that a plant is functional uncontrollable then there are l-r output directions which cannot be affected. Hence, there are output directions y_0^H varying with frequency such that

$$y_0^H(j\omega)G(j\omega) = 0 \tag{3.44}$$

The uncontrollable output directions $y_0(j\omega)$ are the last l-r columns of $U(j\omega)$ where the matrix U results from a singular value decomposition $G(s)=U\Sigma V^H$.
Analysis of these directions can result in an increase of actuators in order to increase the rank of G(s).

RHP-zeros
The existence of RHP-zeros for a plant limits the control performance directly. This is true for tracking performance as well as for disturbance rejection. In case of an ideal integrated square error optimal control problem there is a direct relation between the RHP-zeros and control performance. The resulting integrated error is given by

$$J_0 = \eta^T H \eta \tag{3.45}$$

where η is some disturbance and H is some positive definite matrix with the property that: $\text{trace}(H)=2\sum_i 1/z_i$. Hence, RHP-zeros close to the origin imply poor control performance.

4 PID Control

Because of it simplicity and its effectiveness to control industrial processes PID controller are the most used controllers in industry and particularly controlling distillation columns. PID controllers can be applied in many ways. For design of a control structure PID controllers can be used to form the following specific control configurations (Skogestad):

- Decentralized Control structure consists of independent control loops: Each system output is coupled to one system input Multivariate PID The manipulated inputs of the system can by linked with one or more outputs of the system.
- Cascade control: The output from one controller is the input to another controller. Feed forward elements: The measured disturbance is linked via a controller the a system input.
- Decoupling elements: Links one set of manipulated inputs with another set of manipulated inputs. This is done in order to improve the performance of the decentralized controller.

In addition:

- Selectors: Depending on the condition of the system a selector selects inputs or outputs for control.

Decentralized feedback control

Assuming that the system to be controlled is a square mxm plant the decentralized controller has the following form:

$$K(s) = \begin{pmatrix} k_1(s) & & \\ & \ddots & \\ & & k_m(s) \end{pmatrix} \tag{4.1}$$

There are many possibilities in the way the loops can be chosen: m!. By arranging the in and outputs we can obtain a diagonal controller for every pairing. By restricting ourselves to diagonal controllers we might have performance loss. However, there are some strong theoretical results. Perfect control with decentralized control is possible for plants with no RHP-zeros (Zames and Benoussan, 1983). Moreover, for a stable plant it is possible to use integral control in all channels to achieve perfect steady-state control if and only if G(0) is non-singular (Campo and Morari, 1994). With full multivariable control these conditions are also required. Although, there is performance loss with decentralized control applied to interactive plants and finite bandwidth controllers. Moreover, the interaction caused by off-diagonal non-zero elements of the plant G(s), may cause instability. Interaction problems may be solved by choosing good pairings between inputs and outputs. Hence the design of a decentralized controller consists of two steps:

1. Choosing of the loop paring between plant input and plant output.
2. The design and tuning of each controller ki(s).
3. Verify stability and performance.

RGA

An important tool needed to choose the optimal loop paring is an analyis using Relative Gain Array (Bristol, 1966). Complementary to the selection rules using RGA is the use of physical insight of the plant.

The RGA of a non-singular complex matrix G is a square complex matrix defined as:

$$RGA(G) = \Lambda(G) \triangleq G \times (G^{-1})^{T} \tag{4.2}$$

where x is the Hadamard element by element multiplication. The RGA matrix gives insight of the interaction between an input and output. This can be understood by the following argumentation. For a particular input-output pair u_j and y_j of the MIMO plant G(s) we have two extreme cases:

all other loops open: $u_k=0$, for all $k \neq j$ or

all other loops closed with perfect control: $y_k = 0$, for all $k \neq i$.

For these two cases we can evaluate the gain $\partial y_i / \partial u_j$:

$$\left(\frac{\partial y_i}{\partial u_j}\right)_{u_k=0,k\neq j} = g_{ij} \tag{4.3}$$

$$\left(\frac{\partial y_i}{\partial u_j}\right)_{y_k=0,k\neq i} = \hat{g}_{ij} \tag{4.4}$$

where $g_{ij} = [G]_{ij}$ is the ij'th element of G, whereas $\hat{g}_{ij}$ is the inverse of the ji'th element of G^{-1}

$$\hat{g}_{ij} = \frac{1}{\left[G^{-1}\right]_{ji}}. \tag{4.5}$$

This can be derived after noting that

$$y=Gu \Rightarrow \left(\frac{\partial y_i}{\partial u_j}\right)_{u_k=0,k\neq j} = \left[G\right]_{ij} \tag{4.6}$$

we obtain after interchanging the roles of G and G^{-1}, u and y, and of i and j:

$$u=G^{-1}y \Rightarrow \left(\frac{\partial u_j}{\partial y_i}\right)_{y_k=0,k\neq i} = \left[G^{-1}\right]_{ji}. \tag{4.7}$$

Finally, Bristol defined the ij'th relative gain as:

$$\lambda_{ij} = \frac{g_{ij}}{\hat{g}_{ij}} = \left[G\right]_{ij}\left[G^{-1}\right]_{ji} \tag{4.8}$$

After calculation of the RGA for a MIMO plant the following rules help to choose the optimal paring:

Paring rule 1: Prefer pairings such that the rearranged system, with the selected pairings along the diagonal, has an RGA matrix close to identity at frequencies around the closed-loop bandwidth.

Paring rule 2: If possible avoid paring on negative steady-state RGA elements.

Furthermore, we mention some useful properties of the RGA:

- Scaling of the model has no influence of the RGA.
- The row and columns of the RGA sum up to one.
- For a lower/upper triangular system the RGA is the identity matrix. Plants with large RGA elements are always ill-conditioned.

While the RGA is frequency dependent is should be considered not only for the steady state s=0 but for a range of frequency. In addition, the elements of the RGA might be complex hence the magnitude can be used to plot the phase of the RGA elements. As an result, an undesirable paring elements -1 can be mistaken with a desirable paring element. A solution for this is the so called RGA number, defined as:

$$\text{RGA number} = \left\| \Lambda(G) - M_{\text{control structure}} \right\|_{\text{sum}} \tag{4.9}$$

where the sum norm is chosen arbitrarily and is defined as: $||A||_{sum} = \sum_{i,j} |a_{ij}|$. The matrix $M_{control\ structure}$ represents the control structure which is subject of analysis. For example, in case of an off-diagonal paring control structure for a 2x2 system the $M_{control\ structure}$ is:

$$M_{\text{control structure}} = \begin{pmatrix} 0 & 1 \\ 1 & 0 \end{pmatrix} \tag{4.10}$$

Note that for any other configuration the RGA number have to be recomputed.

DWC

In the literature the RGA analysis is already carried out for different divided wall columns. As a result, 4 different control structures are derived, see Figure 7. Naturally, the physical insight of the plant is import to exclude some senseless control structures among the 5!=120 possibilities. Although, the plant has seven inputs only five of them are used in the development of the control strategy. One of the excluded inputs is the vapour split R_V, because this variable cannot be controlled in practice and is only a design variable. Justification of the decision that R_L is a design variable is a result of previous work on the control of DWC (M. Serra et al, 1999). In this work the RGA and other controllability analysis were carried out. Two cases were subject of controllability analysis: optimal and non-optimal operation. An important different between these two cases is the boilup flowrate. In case of optimal operation the boilup flowrate is 25% lower than in case of non-optimal operation. Furthermore, an other good reason for exclusion of R_L is only recently known (Ling & Luyben, 2009). Consequently, the variable R_L can be used for optimization purposes. The idea is to control the heavy component compositions at the top of the prefractionator side of the wall by manipulation of R_L. This approach is independent of the inventory and regulatory control, respectively.

While M. Serra et, al concluded that the control structure LV/DSB has a well behaved RGA only a temporary change in feed flow rate F was exerted. A persistent disturbance caused instability. Hence, we choose to incorporate all four PI based control strategies in our comparison. Furthermore, we did not put much effort in comparing RGA analyses. The literature provided sufficient information on choosing the pairings. Moreover, preliminary simulations revealed which pairings were good and not applicable. In the following figure the used PI control structures are shown:

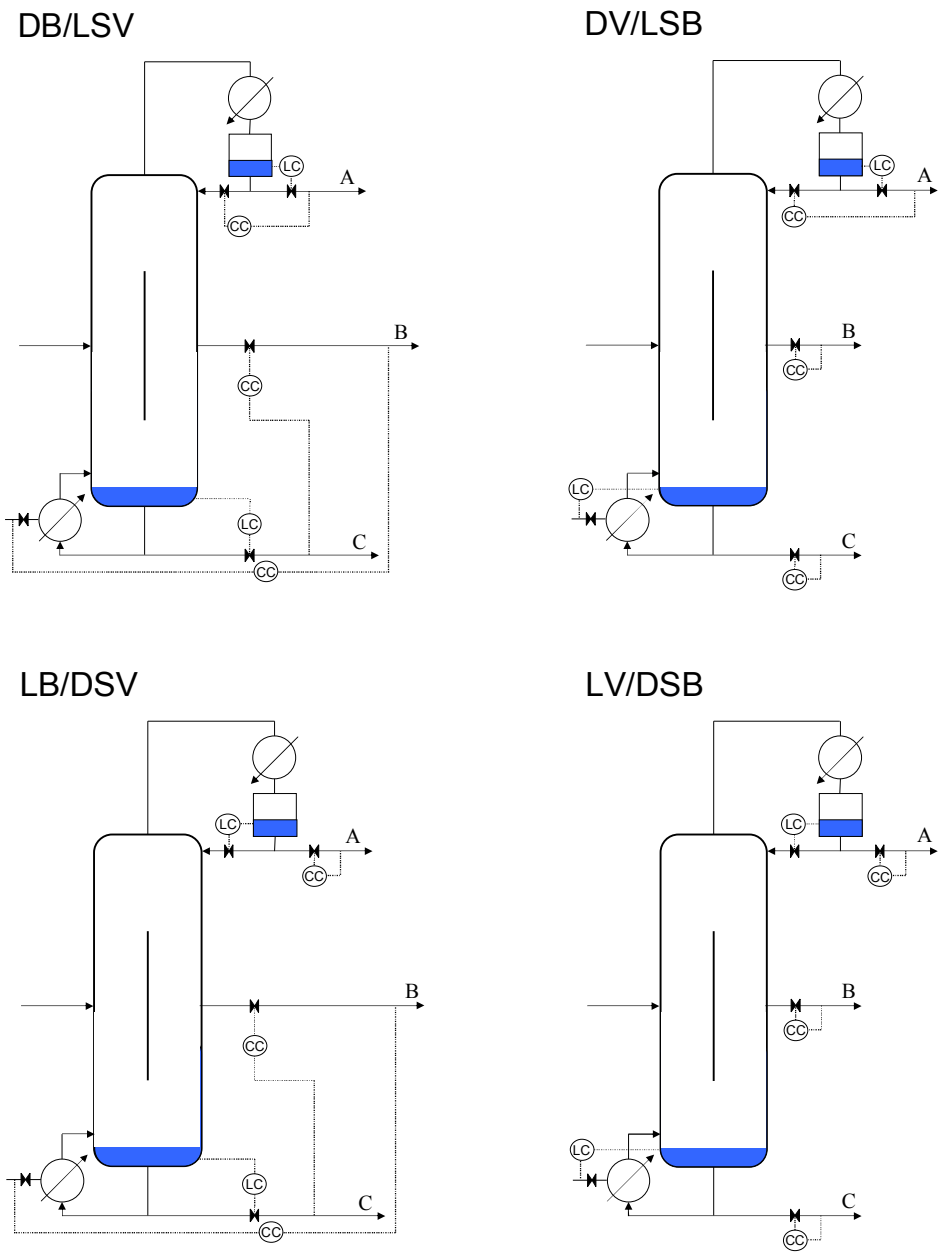

Figure 7: Multi-loop PID control structures: DB/LSV, DV/LSB, LB/DSV, LV/DSB.

Restricted Structure Optimal Control

The optimal Linear Quadratic Gaussian (LQG) framework can be used to design and tune PID controllers. This two fold goal can be achieved by solving a different LQG time domain cost function then the one which has the Algebraic Ricatti Equation as solution. Therefore, we assume that the optimal solution of the LQG problem is a desirable controller solution. After computing the full order controller of the LQG problem it be reduced to:

- Reduced-Structure controller (RS-LQG)
- PID controller
- Lead-lag controller

The reduction will be a trade off between an optimal controller and practical feasible controller.

SISO

In the SISO case the LQG cost function is defined as:

$$J = \lim_{T\to\infty} E\left\{\frac{1}{2T}\int_{-T}^{T}\left\{\left[(H_q * e)(t)\right]^2 + \left[(H_r * u)(t)\right]^2\right\}dt\right\} \tag{4.11}$$

where * is the convolution operator.

In the frequency domain the cost function becomes:

$$J = \frac{1}{2\pi j}\oint_D \left[Q_c(s)\Phi_{ee}(s)R_c(s)\Phi_{uu}(s)\right]ds \tag{4.12}$$

where Q_c and R_c are dynamic weighting elements acting on the spectrum of the error $\Phi_{ee}(s)$ and the spectrum of the feedback control signal $\Phi_{uu}(s)$. The weighting term R_c is assumed to be positive. On the D contour of the s-plane Q_c is assumed to be positive semi-definite. The integrand will be manipulated in order to minimize the integral. Before we start deriving the solution to the optimization problem we define the control system and its equations.

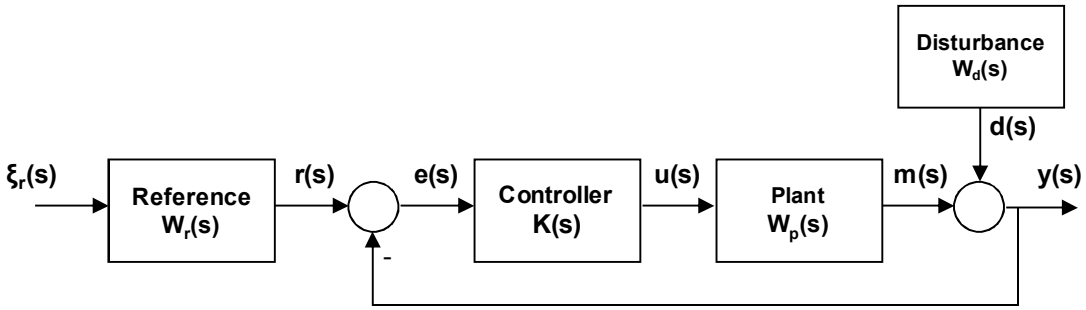

Figure 8: SISO/MIMO single degree of freedom feedback control system.

The above system may be represented in polynomial form:

$$\begin{aligned} &\text{Plant Model} && W = A^{-1}B \\ &\text{Reference generator} && W_r = A^{-1}E \\ &\text{Input disturbance} && W_d = A^{-1}C_d \end{aligned} \tag{4.13}$$

In addition, the cost function equation weightings can also be rewritten from transfer function to polynomial form:

$$\begin{aligned} &\text{Error signal weigth} && Q_c = Q_n/(A_q^* A_q) \\ &\text{Control signal weigth} && R_c = R_n/(A_r^* A_r) \end{aligned} \tag{4.14}$$

Where Aq is a Hurwitz polynomial and Ar is a strictly Hurwitz polynomial.

The system equations are:

$$\begin{aligned} &\text{Output} && y(s)=W(s)u(s)+d(s)\\ &\text{Input disturbance} && d(s)=Wd(s)d(s)\\ &\text{Reference} && r(s)=Wr(s)r(s)\\ &\text{Tracking error} && e(s)=r(s)-y(s)\\ &\text{Control signal} && u(s)=C_0e(s) \end{aligned} \tag{4.15}$$

The disturbance and reference are driven by the white noise sources and the system functions are represented as transfer function of the Laplace transform variable. We assume that the white noise sources are zero mean and independent.

Furthermore, for the SISO case we assume the plant W has no unstable hidden modes and the reference model W_r and subsystem W_d are asymptotically stable.

The transfer sensitivity function and control sensitivity function are defined, respectively as:

$$\begin{aligned} &\text{Sensitivity} && S(s)=(I+WC_0)^{-1}\\ &\text{Control Sensitivity} && M(s)=C_0(s)S(s)=C_0(I+WC_0)^{-1} \end{aligned} \tag{4.16}$$

where C_0 is the full order controller. Enabling us to write the output, error and control signal in terms of the reference and disturbance signal:

$$y(s)=WMr(s)+Sd(s) \tag{4.17}$$

$$e(s)=(1-WM)r(s)-Sd(s) \tag{4.18}$$

$$u(s)=SC_0(r(s)-d(s)) \tag{4.19}$$

First of all, we expand the spectra $\Phi_{ee}(s)$ and $\Phi_{uu}(s)$ using the control sensitivity function (4.14):

$$\Phi_{ee}(s) =(1-WM)\Phi_{rr}(1-WM)^{*}+(1-WM)\Phi_{dd}(1-WM)^{*} \tag{4.20}$$

The above expression will we simplified using the spectrum of the composite signal f(s)=r(s)-d(s), denoted by $\Phi_{ff}(s)$. En passant a generalised spectral factor Y_f is defined from this spectrum. In mathematics this leads to:

$$\Phi_{rr}(s)+\Phi_{dd}(s)=\Phi_{ff}(s) =Y_f\,Y_f^{*} \tag{4.21}$$

Then the spectrum $\Phi_{ee}(s)$ and similarly $\Phi_{uu}(s)$ are simplified to:

$$\begin{aligned} &\Phi_{ee}(s) =(1-WM)\Phi_{ff}(1-WM)^{*}\\ &\Phi_{uu}(s) =M\Phi_{ff}M^{*} \end{aligned} \tag{4.22}$$

Since the preparation is ready we can work towards the derivation of the full order solution. Proceeding by substitution of the error power spectrum and control input spectrum into the cost criterion:

$$J=\frac{1}{2\pi j}\oint_D (W^{*}Q_cW+R_c)M\Phi_{ff}M^{*}-Q_cWM\Phi_{ff}-Q_cW^{*}M^{*}\Phi_{ff}+Q_c\Phi_{ff}ds \tag{4.23}$$

The control spectral factor Yc(s) is defined as:

$$Y_cY_c^{*}=W^{*}Q_cW+R_c=\left[D_cA^{-1}\right]^{*}\left[D_cA^{-1}\right] \tag{4.24}$$

And hence

$$Y_c = \left[D_c A^{-1} \right] \tag{4.25}$$

Moreover, the generalized spectral factor Y_f can shown to be $Y_f=A^{-1}D_f$. The disturbance model is assumed to be such that D_f is strictly Hurwitz and satisfies

$$D_f D_f^* = EE^* + C_d C_d^* \tag{4.26}$$

Further substitutions are leading to the cost

$$J = \frac{1}{2\pi j} \oint_D (Y_c M Y_f)(Y_C M Y_f)^* - Y_c M Y_f \frac{Q_c W \Phi_{ff}}{Y_c Y_f} - Y_c^* M^* Y_f^* \frac{Q_c W^* \Phi_{ff}}{Y_c^* Y_c^*} Q_c \Phi_{ff} ds \tag{4.27}$$

Using the mathematical trick of: completing the squares the cost function is changed into

$$J = \frac{1}{2\pi j} \oint_D \left((Y_c M Y_f) - \frac{Q_c W^* \Phi_{ff}}{Y_c^* Y_f^*} \right) \left((Y_c M Y_f) - \frac{Q_c W^* \Phi_{ff}}{Y_c^* Y_f^*} \right)^* - \frac{W^* W Q_c^* Q_c \Phi_{ff}^* \Phi_{ff}}{Y_c^* Y_c^*} + Q_c \Phi_{ff} ds \tag{4.28}$$

The product term in the integrand is expanded by substituting the various polynomial definitions resulting in

$$\left((Y_c M Y_f) - \frac{Q_c W^* \Phi_{ff}}{Y_c^* Y_f^*} \right) = \frac{\left(B^* A_r^* Q_n D_F \right) B A_r C_{0n}}{D \; Ac \left(A C_{0d} + B C_{0n} \right)} - \frac{B^* A_r^* Q_n D_f}{D_c^* A A_q} \tag{4.29}$$

The right hand side can be splitted in a strictly stable and a strictly unstable term using the Diophantine equation pair:

$$\begin{aligned} D_c^* G_0 + F_0 A A_q &= B^* A_r^* Q_n D_f \\ D_c^* H_0 - F_0 B A_r &= A^* A_q^* R_n D_f \end{aligned} \tag{4.30}$$

Hence, equation (4.29) becomes

$$\left((Y_c M Y_f) - \frac{Q_c W^* \Phi_{ff}}{Y_c^* Y_f^*} \right) = \frac{C_{0n} H_0 A_q - C_{0d} G_0 A_r}{A_w \left(A C_{0d} + B C_{0n} \right)} - \frac{F_0}{D_c^*} \tag{4.31}$$

The first term of the RHS is strictly stable and the second term strictly unstable. By writing the first stable term as $T_1^+(s)$ and the unstable term $T_1^-(s)$.

Using this decomposition the cost function can be written as

$$J = \frac{1}{2\pi j} \oint_D \left(T_1^+ + T_1^- \right) \left(T_1^+ + T_1^- \right)^* + \Phi_0 ds \tag{4.32}$$

While the unstable term $T_1^-(s)$ and Φ_0 are independent of the controller C0 the final minimization problem is reduced to finding the controller C0 in order minimize

$$J = \frac{1}{2\pi j} \oint_D T_1^+ (T_1^+)^* ds \tag{4.33}$$

Finally, the full order controller which minimize the cost function (4.11)) is given by

$$C_0(s) = \frac{G_0 A_r}{H_0 A_q} \tag{4.34}$$

MIMO

Like the SISO case the system is represented in polynomial matrix form:

$$\begin{bmatrix} W & W_d & W_r \end{bmatrix} = A^{-1}\begin{bmatrix} B & D & E \end{bmatrix} \tag{4.35}$$

It is assumed that the system can be written in the above form and that the system matrices W, W_d and W_r are coprime. The corresponding MIMO LQG cost function is:

$$J_{LQG} = \frac{1}{2\pi j}\oint_D \mathrm{tr}\left(Q_c(s)\Phi_{ee}(s)\right) + \mathrm{tr}\left(R_c(s)\Phi_{uu}(s)\right)ds \tag{4.36}$$

where D denotes the usual D contour taken over the right half of the s-plane and $\Phi_{ee,}$ Φ_{uu} denote the real rational matrix spectral density transfer functions for the error e(s) the control u(s) respectively.

The algorithm

Here we will give the derivation of the algorithm for the computation of the full order controller. Like the SISO we will work towards two Diophantic equations which solutions are elements of the full order controller.

Furthermore, the multivariable dynamic weights have to be chosen such that the required response of the closed-loop system is achieved. The dynamic weights are defined as:

$$\begin{aligned} Q_c(s) &= A_q^{-*}B_q^*B_qA_q^{-1} = Q_c^*(s) \\ R_c(s) &= A_r^{-*}B_r^*B_rA_r^{-1} = R_c^*(s) \end{aligned} \tag{4.37}$$

where the adjoint operator is defined as: $[X(s)]^* = [X^T(-s)]$ and Q_c, R_c should be positive semidefinite on the D-contour, hence A_q, A_r, B_q and B_r should be chosen appropriately.

Starting by introducing the weighted system transfer function:

$$W_{WT} = A_q^{-1}A^{-1}BA_r = B_1A_1^{-1} \tag{4.38}$$

In addition, the control spectral factors is defined as

$$Y_c^*Y = W^*Q_cW + R_c = \left[D_c(A_rA_l)^{-1}\right]^*\left[D_c(A_rA_l)^{-1}\right] \tag{4.39}$$

where the polynomial matrix $D_c(s)$ is the fraction of:

$$B_l^*B_q^*B_qB_l + A_l^*B_r^*B_rA_l = D_c^*D_c \tag{4.40}$$

The polynomial matrix filter spectral factor $D_f(s)$ is:

$$D_fD_f^* = EE^* + DD^* \tag{4.41}$$

and will be used to compute the generalized spectral factor $Y_f \in \Re^{m\times m}$

$$Y_fY_f^* = \left[A^{-1}D_f\right]\left[A^{-1}D_f\right]^* \tag{4.42}$$

The generalized spectral factor is related to the total spectrum of the signals $e(s) \in \Re^m$ and is denoted by $\Theta_{TT}(s) \in \Re^{m\times m}$:

$$\Theta_{TT} = \Theta_{rr} + \Theta_{dd} = Y_f Y_f^* \tag{4.43}$$

Now we are ready to pose the two Diophantic equations. Solve the following equations in order to obtain H_0, G_0 and F_0 with F_0 of smallest row degree:

$$\begin{aligned} D_c^* G_0 + F_0 A_2 &= B_1^* B_q^* B_q D_2 \\ D_c^* H_0 + F_0 B_2 &= A_1^* B_r^* B_r D_3 \end{aligned} \tag{4.44}$$

with right coprime decompositions

$$\begin{aligned} A_2 D_2^{-1} &= D_f^{-1} A A_q \\ B_2 D_3^{-1} &= D_f^{-1} B A_r \end{aligned} \tag{4.45}$$

We will pose two theorems, the first theorem states that the cost criterion can be split up in two parts. Subsequently the second theorem states that minimizing only one particular term is necessary to solve the minimization problem.

Theorem (Multivariable LQG cost function decomposition)

$$J_{LQG} = \quad J_A + J_{BC}$$

where

$$\begin{aligned} J_A &= \frac{1}{2\pi j} \oint_D \mathrm{tr}\left(X_A^* X_A \right) ds \\ J_{BC} &= \frac{1}{2\pi j} \oint_D \mathrm{tr}\left(X_B^* X_B + X_C \right) ds \end{aligned} \tag{4.46}$$

and

$$\begin{aligned} X_A(s) &= \left(H_0 D_3^{-1} A_r^{-1} K_n - G_0 D_2^{-1} A_q^{-1} K_d \right) \left(A K_d + B K_n \right)^{-1} \\ X_B(s) &= -D_C^{-*}(s) F_0(s) \\ X_c(s) &= \left(Q_c - Q_c W^* \left(Y_c^* Y_c \right)^{-1} W Q_c \right) \Theta_{TT} \end{aligned} \tag{4.47}$$

Corollary (Optimal multivariable LQG control and cost values)

$$J_{LQG}^{min} = J_{BC}$$

and this minimum is obtained using the optimal controller $K_{opt}(s)$ given by

$$K_{opt}(s) = A_r(s) D_3(s) H_0^{-1}(s) G_0(s) D_2^{-1}(s) A_q^{-1}(s) \tag{4.48}$$

Proof: The cost function has only the term J_A available for optimization with respect to controller parameters. J_A is positive semidefinite thus minimization is achieved when X_A=0:

$$X_A(s) = \left(H_0 D_3^{-1} A_r^{-1} K_n K_d^{-1} - G_0 D_2^{-1} A_q^{-1} \right) \left(A + B K_n K_d^{-1} \right)^{-1} D_f = 0 \tag{4.49}$$

As a result the optimal controller is

$$K_{opt}(s) = Ar(s) D3(s) H_0^{-1}(s) G_0(s) D_2^{-1}(s) A_q^{-1}(s) \tag{4.50}$$

Using this controller we have $J_{LQG} = 0 + J_{BC} = J_{LQG}^{min}$.

MIMO RS-controller

The full order controller which achieves the minimization of J_{LQG} has in general complex structure consisting of higher order terms. In industrial application a diagonal PI controller is always preferred. However, it is also possible to perform the minimization step with the demand that all controller elements have the following restricted structure:

$$C_0(s) = K_0 + K_1 \frac{1}{1 - z^{-1}} + K_2 \frac{\left(1 - z^{-1}\right)}{\left(1 - \tau_d z^{-1}\right)} \tag{4.51}$$

where

$$K_i = \begin{pmatrix} k_{11}^i & k_{12}^i & \cdots & k_{1r}^i \\ k_{21}^i & k_{22}^i & \cdots & \vdots \\ \vdots & \ddots & \ddots & \vdots \\ \vdots & \ddots & \ddots & \vdots \\ k_{m1}^i & \cdots & \cdots & k_{mr}^i \end{pmatrix} \quad i = 0,1,2 \tag{4.52}$$

In this case the restricted structure consists of an P,I and D control action. A parametric optimization algorithm should be used to compute the matrices K with respect to the LQG cost function J_A. The full order solution can be used as a benchmark to asses the performance loss. In addition, the restricted structure can be simplified by demanding that some terms have an decreased order or are even zero. The algorithm has an iteration loop and is not included.

Example –The hot strip Mill Looper system-

The following figure represents a stand used in the steel industry and this plant will serve as an example (Johnson & Moradi, 2005). The stand is used to achieve a certain thickness of the strip.

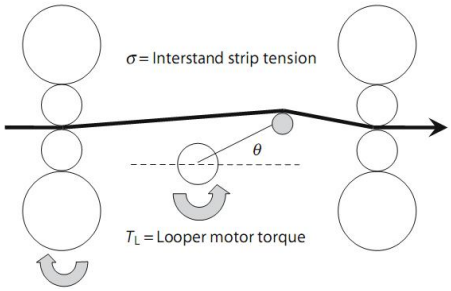

Figure 9: View on the Looper model. From Johnson & Moradi, 2005.

The model can be represented in the following transfer function:

$$\begin{pmatrix} \Delta\sigma \\ \Delta\theta \end{pmatrix} = \begin{pmatrix} \frac{-120}{s+1.2} & \frac{100s+9}{s^2+9s+s} \\ \frac{24}{s+1.2} & \frac{0.9s+9}{s^2+9s+s} \end{pmatrix} \begin{pmatrix} \Delta V_R \\ \Delta T_L \end{pmatrix} \tag{4.53}$$

where the two inputs are roll velocity V_R, loop motor torque T_L and the two outputs are the strip tension and Looper angle. In the following table some of the possible control structures and corresponding cost function values are given.

	Multivariate Control structure	Number of controller parameters	Cost function value
1	$\begin{pmatrix} K_{LQG} & K_{LQG} \\ K_{LQG} & K_{LQG} \end{pmatrix}$	47	937.346
2	$\begin{pmatrix} K_{PI} & K_{PI} \\ K_{PI} & K_{PI} \end{pmatrix}$	8	1110.798
3	$\begin{pmatrix} K_{PI} & K_{PI} \\ 0 & K_{PI} \end{pmatrix}$	6	1291.538
4	$\begin{pmatrix} 0 & K_{PI} \\ K_{PI} & 0 \end{pmatrix}$	4	1175.139
5	$\begin{pmatrix} K_{PI} & 0 \\ 0 & K_{PI} \end{pmatrix}$	4	50018.35

Table 2: Multivariate control structures and the corresponding cost function value. From Johnson & Moradi, 2005.

From the table some conclusion can be drawn. First of all, a relative simple control structure, consisting of only four PI control loops achieves a relative low cost function value. Which, is a very useful result for a practical application. Secondly, if the controller elements K_{11} and K_{22} fall out we obtain a diagonal controller, number 4 in the table, which again performs relative good. However, there is a loss comparing the cost function value with the full order solution. Furthermore, the asymmetric control structure, number 3, performs relative bad. Finally, a wrong chosen diagonal controller performs very bad because the cost function is very high.

DWC

Unfortunately, the above method has not been applied for the DWC due to numerical computational problems. This problem occurred in the computation of the full order controller. While the full order controller is needed in the algorithm for the restricted structure solution no restricted structures are computed. In the computation of the above example a similar problem occurred. The cause of the computational error is the range of the zero frequency gains or static gain of the full-order transfer function. For the Looper model this range was 3.1×10^{-3} to 10^{8}. Hence, in case of the Looper model example, a clean demonstration model was used.

In order to avoid computational problems we performed several model reductions. The system can be reduced into a stable and unstable part. Incorporating the unstable part results in a static gain range exceeding 10^{8} which is causing computational problems. On the other hand, only using the stable solved this problem and made that the static gain range was approximately only 37. However, the assumption of the system matrices being coprime is being violated when only the stable part of the model is used while there is no solution for the equation:

$$W(s)X + W_r(s)Y = I \tag{4.54}$$

5 LQR

Considerate the following state space model:

$$\begin{aligned} \dot{x} &= Ax + Bu, \\ y &= Cx + Du. \end{aligned} \tag{5.1}$$

For simplicity we assume that D=0. We assume that the desired measured output is the zero vector. Hence, the system has to be driven to the origin, x=0, starting from a non-zero initial state x(0). The optimal linear quadratic regulation (LQR) problem is defined as follows:

$$J_{LQR} := \int_0^\infty x(t)^T Q x(t) + \rho u(t)^T R u(t) dt, \tag{5.2}$$

where ρ>0. Hence, when time goes to infinity we want to minimize the energy of the controlled output (first term of integral) and the control signal (second term). The design constant ρ establish a trade off between the two objectives.

The optimal solution, for any initial state is: u(t) = -K x(t), where $K=R^{-1}B^TX$ and X is symmetric, positive semi-definite solution of the algebraic Riccati equation (ARE)

$$A^T X + XA - XBR^{-1}B^T + Q = 0. \tag{5.3}$$

Due to the fact that the solution needs the full state is called optimal state feedback. The optimal gain matrix K exist when the pair $(A,B,Q^{½})$ is stabilizable and $(A,W^{½}, C)$ are stabilizable and detectable.

The feedback system is asymptotically stable if the resulting system:

$$\dot{x} = (A - BK)x \tag{5.4}$$

is asymptotically stable.

Full-order observer

In order to implement the LQR controller the whole state should be available and hence be measured by a sensor. Often this is not the case while in case of the DWC the composition along the column can not be measured in practice. Nevertheless, while the process dynamics are known it is possible to construct a deterministic observer which reconstructs the states based on only inputs and measurements. A common name for the algorithm that reconstruct not physically measured quantities is soft sensor. Using the dynamics we start the estimation of x; the estimation is denoted by $\hat{x}$. Moreover we have using the dynamics:

$$\dot{\hat{x}} = A\hat{x} + Bu \tag{5.5}$$

The error of the state estimation is $e := x - \hat{x}$ and hence the dynamics of the error is given by

$$\dot{e} = Ax - A\hat{x} = Ae \tag{5.6}$$

Independent of the input u, the error will converge to zero when A is asymptotically stable. Hence, the state will be estimated without an error. In case of an unstable A we can include a correction term using the measurements:l

$$\dot{e} = Ax - A\hat{x} - L(y - \hat{y}) = (A - LC)e \tag{5.7}$$

The error will converge if A-LC is asymptotically stable. Note that even in case of an unstable A there is a possibility that L can be chosen such that A-LC is stable. Finally, the full-order observer is given by

$$\dot{\hat{x}} = (A - LC)\hat{x} + Bu + Ly \tag{5.8}$$

The inputs are u and y and the output is the estimated state $\hat{x}$ obtained after solving the differential equation by integration.

LQG

In case of measurement noise and disturbance the dynamics are influenced. For this reason, the state space model is extended in order to incorporate the measurement noise and disturbance.

For the development of the controller, measurement noise and disturbance noise is assumed to be Gaussian white noise. Because for this type of noise there strong theoretical results have been developed. Gaussian white noise is defined as the generalized derivative of the Wiener process W_t. Although, the Wiener process is not differentiable there exists a generalized derivative defined symbolically:

$$g(t)W_t = \int_0^t g(s)\dot{W}_s ds + \int_0^t \dot{g}(s)W_s ds \tag{5.9}$$

where g(t) is any smooth function with compact support. This generalized derivative is called Gaussian white noise ω(t). As a result, it can be proven that the Gaussian process has zero mean and covariances:

$$E\left[\omega(t)\omega(s)^T\right] = \delta(t-s) \tag{5.10}$$

where δ is the Dirac's Delta.

The disturbance d and measurement noise n can be modelled in the state space frame work as follows:

$$\begin{aligned} \dot{x} &= Ax + Bu + B_d d \\ y &= Cx + n \end{aligned} \tag{5.11}$$

As a result a more advanced observer is needed which filters out the noise. Similar to the full order observer the error dynamics are

$$\begin{aligned} \dot{e} &= Ax - A\hat{x} - L(y - \hat{y}) \\ &= (A - LC)e + B_d - Ln \end{aligned} \tag{5.12}$$

The linear quadratic Gaussian (LQG) problem is to find a matrix L such that the expected estimation will be minimized. Mathematically we write

$$\lim_{t\to\infty} E\left[\left\|e(t)\right\|^2\right] \tag{5.13}$$

Assuming that d(t) and n(t) are zero-mean, uncorrelated Gaussian noise stochastic processes having constant power density matrices W and V there is a solution. In other words, the stochastic processes d(t) and n(t) are gaussian white noise processes with covariances

$$E\left[d(t)d(t)^T\right] = W\delta(t-\tau)$$
$$E\left[n(t)n(t)^T\right] = V\delta(t-\tau) \tag{5.14}$$

and

$$E\{d(t)n(t)^T\} = 0$$
$$E\{n(t)d(t)^T\} = 0 \tag{5.15}$$

The optimal LQG estimator gain is the matrix:

$$L = PC^T V^{-1} \tag{5.16}$$

The matrix P is the unique positive-definite solution to the ARE

$$AP + PA^T - B_d W B_d^T - PC^T V^{-1} C = 0 \tag{5.17}$$

Using the matrix L obtained by the LQG problem in the equation (5.8) one obtain the so called *Kalman-Bucy* filter. This system is asymptotically stable if two conditions are satisfied: observability of the system (5.11) and state controllability of system (5.11) when the control input u is ignored and d is regarded as the input.

Output Feedback

The two previous techniques of linear quadratic regulation (LQR) and linear quadratic Gaussian estimation (LQG) can of course be combined together. As a result, the following control structure is obtained:

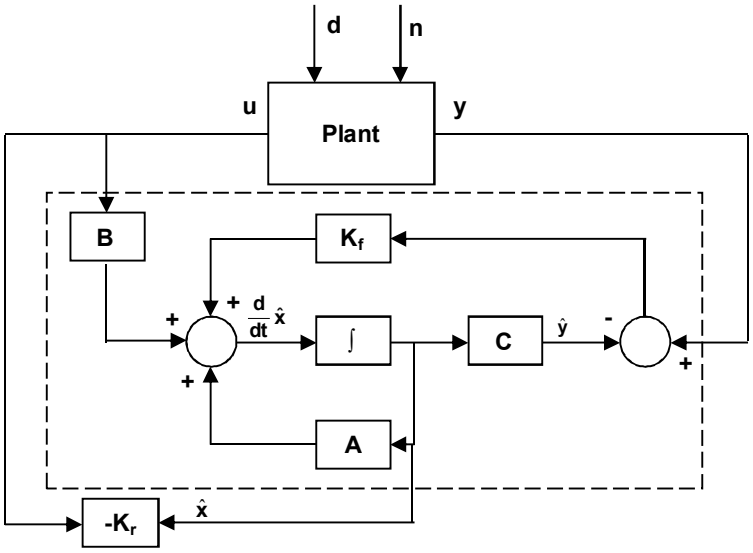

Figure 10: The plant is controlled via an optimal linear quadratic regulation; while the state is being estimated via the Kalman-Bucy filter (dashed box).

6 Advanced Controller Synthesis

Introduction

The ∞-norm can be used to calculate a controller for a plant. By choosing a suitable closed-loop system the control error can be minimized. As a result a controller can be obtained which is robust against plant uncertainties and exogenous error signals. Apart from H_∞ optimal control design by μ-Synthesis aims at reducing the peak value of the structured singular value. Therefore, optimization with respect to robustness and performance optimization can be achieved.

A multivariate PID control structure is obtained by a two step procedure. First the pairings are selected and then a diagonal controller is designed. In general, such two-step design procedure results in a sub-optimal design. Therefore better results can obtained by synthesize directly a multivariable controller based on minimizing some objective function like a norm. Often the word synthesize is be used rather than design; while these approaches are more a formalized approach.

General control configuration

Firstly, we define a system consisting of the plant P and the controller K(s). The general control configuration is shown in the following figure. Note that model uncertainty is not yet incorporated.

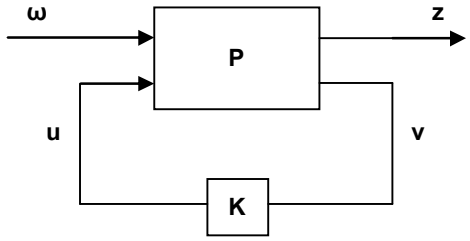

Figure 11: The general control configuration for H_∞ control and μ-Synthesis.

In the figure u is a vector of control signals, v is a vector measured outputs, ω is a vector of weighted exogenous inputs and z is a vector of weighted exogenous outputs. As weightings functions transfer functions are often used. Hence, the weightings are differentiated between specific frequency ranges. For example a low-pass filter can be used to filter the error signal z; high zero-mean frequency noise can be neglected while low frequency steady state errors are controlled away.

Secondly, we extended the model with uncertainty. The matrix Δ is a block-diagonal matrix that includes all possible perturbations and is useful for controller synthesis:

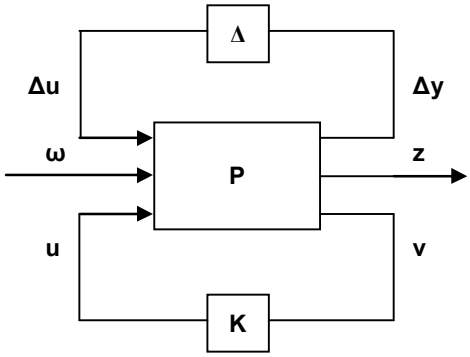

Figure 12: Extension of the general configuration with model uncertainty.

For controller synthesis in the H_∞ control frame work as well as for the μ-Synthesis a closed loop transfer function N is needed. If a controller is available :

$$z = N\omega \tag{6.1}$$

The transfer function N can be used to analyze the robust performance of the closed loop system. The plant P in the general control configuration is often portioned as:

$$P = \begin{pmatrix} P_{11} & P_{12} \\ P_{21} & P_{22} \end{pmatrix} \tag{6.2}$$

The dimension should be such that the following hold:

$$\begin{aligned} z &= P_{11}\omega + P_{12}u \\ v &= P_{21}\omega + P_{22}u \end{aligned} \tag{6.3}$$

As a result the transfer N is given by:

$$N = P_{11} + P_{12}K(I - P_{22})^{-1}P_{21} = F_l(P,K) \tag{6.4}$$

The $F_l(P,K)$ denotes a linear fractional transformation (LFT) of P with parameter K. The subscript l stands for lower LFT while the lower loop has been closed (see Figure 12). Furthermore, the upper loop can be closed; the general block with included uncertainty is shown in the next figure:

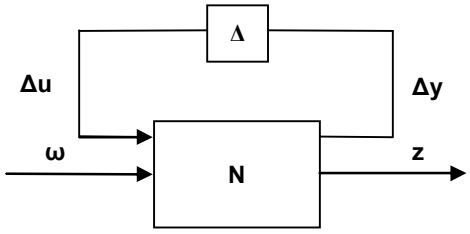

Figure 13: The general closed loop system; uncertainty is included.

The transfer function of the system shown in Figure 13 is given by the upper LFT:

$$z = F_u(N,\Delta)\omega \quad F_u(N,\Delta) = N_{22} + P_{21}\Delta(I - PN_{11})^{-1}N_{12} \tag{6.5}$$

The state-space realization of the generalized plant P is given by:

$$P = \left(\begin{array}{c|cc} A & B_1 & B_2 \\ \hline C_1 & D_{11} & D_{12} \\ C_2 & D_{21} & D_{22} \end{array}\right) \tag{6.6}$$

In order to solve the H_∞ and H_2 control problem the following assumptions are typically made:

1. (A,B_2) is stabilizable and (C2,A) is detectable.
2. D12 and D21 have full rank.
3. $\begin{pmatrix} A - j\omega I & B_2 \\ C_1 & D_{12} \end{pmatrix}$ has full column rank for all ω.
4. $\begin{pmatrix} A - j\omega I & B_1 \\ C_2 & D_{21} \end{pmatrix}$ has full column rank for all ω.
5. $D_{11}=0$ and $D_{22}=0$.

Assumptions (1) makes sure that there exists an existing stabilizing controller. The second assumptions is sufficient to ensure the controllers are proper and realizable. Assumption (3) ensure that P12 and P21 have full column and full row rank on the imaginary axis which avoids that that the optimal controller cancel poles or zeros on the imaginary axis which would result in closed-loop instability.

Assumption (5) simplifies the algorithm in case of H_∞ optimal control problem, significantly and can be made without loss of generality. Moreover, in H_2 this assumption is conventional and makes P_{11} strictly proper. We note that the H_2 consists of all strictly proper stable transfer functions. The assumption $D_{22}=0$ simplifies the algorithm and is made without loss of generality.

6. $D_{12} = \begin{pmatrix} 0 \\ I \end{pmatrix}$ and $D_{21} = \begin{pmatrix} 0 & I \end{pmatrix}$.
7. $D_{12}^T C_1 = 0$ and $B_1 D_{21}^T = 0$.

(A,B_1) is stabilizable and (A,C_1) is detectable.

Assumption (6) can be achieved, by a scaling of u and v and a unitary transformation of w and z. Assumption (7) is common in H_2 control and comes to down to the absence of cross-terms in the cost function ($D_{12}^T C_1 = 0$), and process noise and measurement noise are uncorrelated ($B_1 D_{21}^T = 0$).

If (7) holds then (3) and (4) may be replaced by (8).

Example: LQG in a H_2 control setting

In addition to the H_∞ framework we can also compute an optimal controller K with respect to the the H_2 norm. The standard H_2 optimal control problem is to find a controller K which minimizes general closed loop system with respect to the norm:

$$\|F(s)\|_2 = \sqrt{\frac{1}{2\pi}\int_{\infty}^{\infty} \mathrm{tr}\left[F(j\omega)F(j\omega)^H\right] d\omega} \tag{6.7}$$

If the exogenous input ω is white noise of unit intensity then the expected error signal z is then given by:

$$\begin{aligned} E\left[\lim_{T\to\infty}\frac{1}{2T}\int_{-T}^{T} z(t)^T z(t)\,dt\right] &= \mathrm{tr}\,E\left[z(t)^T z(t)\right] \\ &= \sqrt{\frac{1}{2\pi}\int_{\infty}^{\infty} \mathrm{tr}\left[F(j\omega)F(j\omega)^H\right] d\omega} \\ &= \|F\|_2^2 = \|F_l(P,K)\|_2^2 \end{aligned} \tag{6.8}$$

Hence, by minimizing the H_2 norm of the overall system the root-mean-square value of z is minimized. Similar assumptions like the H_∞ control problem are typically made for the H_2 control problem.

Recall the standard LQG problem: Find a feedback controller K such that LQG cost criterion J is minimized:

$$J = E\left[\lim_{T\to\infty}\frac{1}{T}\int_0^T x(t)^T Q x(t) + u(t)^T R u(t)\,dt\right] \tag{6.9}$$

where $Q=Q^T \geq 0$ and $R=R^T \geq 0$. The control signal $u=Kx$ and x is the state vector of the stochastic system:

$$\begin{aligned} \dot{x} &= Ax + Bu + \omega_d \\ y &= Cx + \omega_n \end{aligned} \tag{6.10}$$

The stochastic signals ω_d and ω_n are Gaussian white noise with the property

$$E\left[\begin{pmatrix}\omega_d(t)\\ \omega_n(t)\end{pmatrix}\begin{pmatrix}\omega_d(t) & \omega_n(t)\end{pmatrix}^T\right] = \begin{pmatrix}W & 0\\ 0 & V\end{pmatrix}\delta(t-\tau) \tag{6.11}$$

Casting the above problem in the standard H_2 problem we have to define the error signals z, the exogenous signals w and the generalized plant P. Firstly we define the error signal z as

$$z = \begin{pmatrix} Q^{\frac{1}{2}} & 0 \\ 0 & R^{\frac{1}{2}} \end{pmatrix}\begin{pmatrix} x \\ u \end{pmatrix} \tag{6.12}$$

And secondly represent the stochastic inputs ω_d and ω_n as

$$\begin{pmatrix}\omega_d\\ \omega_n\end{pmatrix} = \begin{pmatrix} W^{\frac{1}{2}} & 0 \\ 0 & V^{\frac{1}{2}} \end{pmatrix}\omega \tag{6.13}$$

Hence, the exogenous input of unit intensity is scaled in order to have similar inputs for the given LQG system. Then the generalized plant is defined in (6.108) and computation lead to:

$$P = \begin{pmatrix} P_{11} & P_{12} \\ P_{21} & P_{22} \end{pmatrix} = \left(\begin{array}{c|ccc} A & W^{\frac{1}{2}} & 0 & B \\ \hline Q^{\frac{1}{2}} & 0 & 0 & 0 \\ 0 & 0 & 0 & R^{\frac{1}{2}} \\ \hline C & 0 & V^{\frac{1}{2}} & 0 \end{array}\right) \tag{6.14}$$

With this expression for P we have a closed-loop transfer function from ω to z: $z=F_l(P,K)\omega$. Using the expression (6.110) we convert the LQG cost function J (6.111) into the H_2 norm of the closed loop of the system which is the H_2 optimal control problem.

H_∞ control

The standard H_∞ optimal control problem is to find all stabilizing controllers K which minimize

$$\left\|F_l(P,K)\right\|_\infty \tag{6.15}$$

This objective can be interpreted in two ways. Firstly, there is a clearly intuitive interpretation in the time domain:

$$\left\|F_l(P,K)\right\|_\infty = \max_{\omega(t)\neq 0} \frac{\left\|z(t)\right\|_2}{\left\|\omega(t)\right\|_2} \tag{6.16}$$

Secondly, the H_∞ norm is equal to:

$$\|F_l(P,K)\|_\infty = \max_{\omega(t)\neq 0} \bar{\sigma}(F_l(P,K)(j\omega)) \tag{6.17}$$

Hence, in the control problem the peak of the maximum singular value corresponding to the general control configuration.

Theorem (Existence of controller for the standard H_∞ problem)
For the plant in Figure 8 with the corresponding assumptions 1-8 there exists a stabilizing controller for which $\|H\|_\infty < \gamma$ if and only if the following three conditions hold:

$AQ + QA^T + Q(\frac{1}{\gamma^2}C_1^TC_1 - C_2^TC_2)Q + B_1B_1^T = 0$ has a stabilizing solution $Q \geq 0$,

$PA + A^TP + P(\frac{1}{\gamma^2}B_1^TB_1 - B_2^TB_2)P + C_1C_1^T = 0$ has a stabilizing solution $P \geq 0$,

All eigenvalues of QP have magnitude less than γ^2.

If these conditions are satisfied then the controller that stabilizes and achieves $\|H\|_\infty < \gamma$ is the controller with realization

$$\begin{cases} \dot{\hat{x}} = (A + (\frac{1}{\gamma^2}B_1^TB_1 - B_2^TB_2)P)\hat{x} + (I - \frac{1}{\gamma^2}QP)^{-1}QC_2^T(y - C_2\hat{x}) \\ u = -B_2^TP\hat{x} \end{cases} \tag{6.18}$$

H_∞ control loop-shaping design

Basically, loop shaping is designing a controller such that some objective transfer function is shaped to the desired frequency response. However, for complicated systems the classic approach is not suitable. For example, unstable systems are hard to stabilize using this technique. In the H_∞ framework we can computed a robust stabilizing controller for a plant which has been pre- and post-compensated. Via the compensation the shape of the open-loop singular values can be changed to a shape with better control properties. Thus, the H_∞ loop-shape design procedure consist of two steps: first shape the plant and then synthesize a controller.
This systematic procedure is used practice and has the benefits that no specific performance requirements have to given. The procedure is proposed by McFarlane and Glover in 1990.

Robust Stabilization
In order to make a mathematical model similar to reality a model can be extended with uncertainty. In order to be able to define the uncertainty model we recall the left and right normal coprime factors of the plant G:

$$\begin{aligned} G &= M_l^{-1}(s)N_l(s) \\ G &= N_r(s)M_r^{-1}(s) \end{aligned} \tag{6.19}$$

such that there exists stable systems $U_l(s)$, $V_l(s)$, $U_r(s)$ and $V_r(s)$ satisfying the two equations:

$$U_r(s)N_r(s)+V_r(s)M_r(s)=I$$
$$N_l(s)U_l(s)+M_l(s)V_l(s)=I \tag{6.20}$$

Inclusion of coprime uncertainty results in a perturbed plant G_p:

$$G_p = (M_l + \Delta_M)^{-1}(N_l + \Delta_N) \tag{6.21}$$

where Δ_M, Δ_N are stable and unknown transfer functions. The resulting model is shown in the following figure:

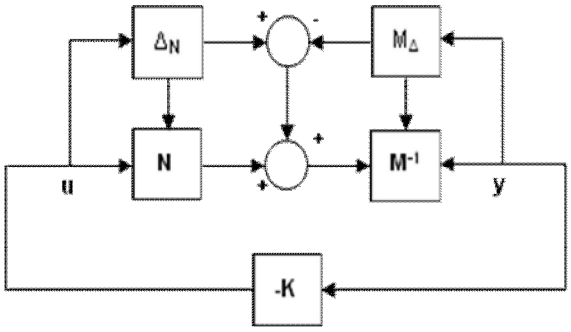

Figure 14: Coprime uncertainty: The plant is represented by the coprime factors N and M^{-1} and coprime factor uncertainty is added.

Whereas, for example multiplicative input uncertainty used later in the μ-Synthesis for DWC has a clear intuitive interpretation this is unclear for the coprime uncertainty model. However, the coprime uncertainty is very general while it allows both zeros and poles to cross into the RHP. Hence, the obtained controller will robustly stabilize the perturbed plant for a very general uncertainty. More mathematically, the objective of robust stabilization is to find a controller such that every element of the following set is stabilized

$$G_P\left\{(M_l + \Delta_M)^{-1}(N_l + \Delta_N) : \left\|\begin{bmatrix}\Delta_N & \Delta_M\end{bmatrix}\right\|_\infty < \varepsilon\right\} \tag{6.22}$$

Robust stability is obtained if and only if the nominal feedback system is stable and

$$\gamma_K = \left\|\begin{bmatrix}K\\ I\end{bmatrix}(I - GK)^{-1}M^{-1}\right\|_\infty \le \frac{1}{\varepsilon} \tag{6.23}$$

The lowest achievable value of γ_K is given by

$$\gamma_{min} = \left\{1 - \left\|\begin{pmatrix}N & M\end{pmatrix}\right\|_H^2\right\}^{-1/2} = (1+\rho(XZ))^{1/2} \tag{6.24}$$

where $\|\cdot\|_H$ denotes the Hankel norm and ρ denotes the spectral radius what is the maximum eigenvalue. X and Z are the unique positive definite solution of two algebraic Riccati equations. Consider the minimal realization (A,B,C,D) of G then Z is the solution of:

$$(A - BS^{-1}D^TC)Z + Z(A - BS^{-1}D^TC)^T - ZC^TR^{-1}CZ + BS^{-1}B^T = 0 \tag{6.25}$$

where

$$R = I + DD^T, \quad S = I + D^T D \tag{6.26}$$

X is the solution of the equation

$$(A - BS^{-1}D^T C)X + X(A - BS^{-1}D^T C) - XBS^{-1}B^T X + C^T R^{-1} C = 0 \tag{6.27}$$

Loop-shaping

In order to improve performance the plant is shaped prior to robust stabilization. The shaped plant is given by

$$G_s = W_2 G W_1 \tag{6.28}$$

Hence, a controller K is synthesized in order to achieve robust stability for the following control system:

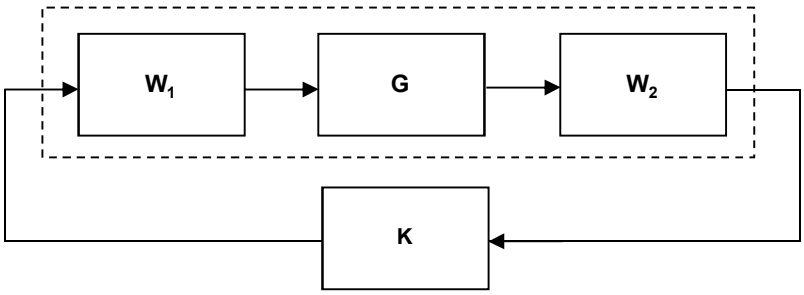

Figure 15: Loop-shaping: Synthesis of robust controller K for shaped G_s.

For the shaped plant G_s there should exists a normalized left coprime factorization. The feedback controller for the plant is given by $K=W_1 K_s W_2$. Where W_2 is the identity matrix and W_1 is a diagonal matrix with the following transfer function on the diagonal:

$$W_1(i,i) = 2 \cdot \frac{s+1}{10s} \tag{1}$$

The value 2 is chosen for the gain of the filter, in order to ensure a small steady-state error. Larger gains lead to smaller steady-state errors but worse transient response (Gu, 2005). In addition, for larger values the closed loop system is unstable in the presence of the measurements noise and time delay. The result on the singular values is given in the following figure:

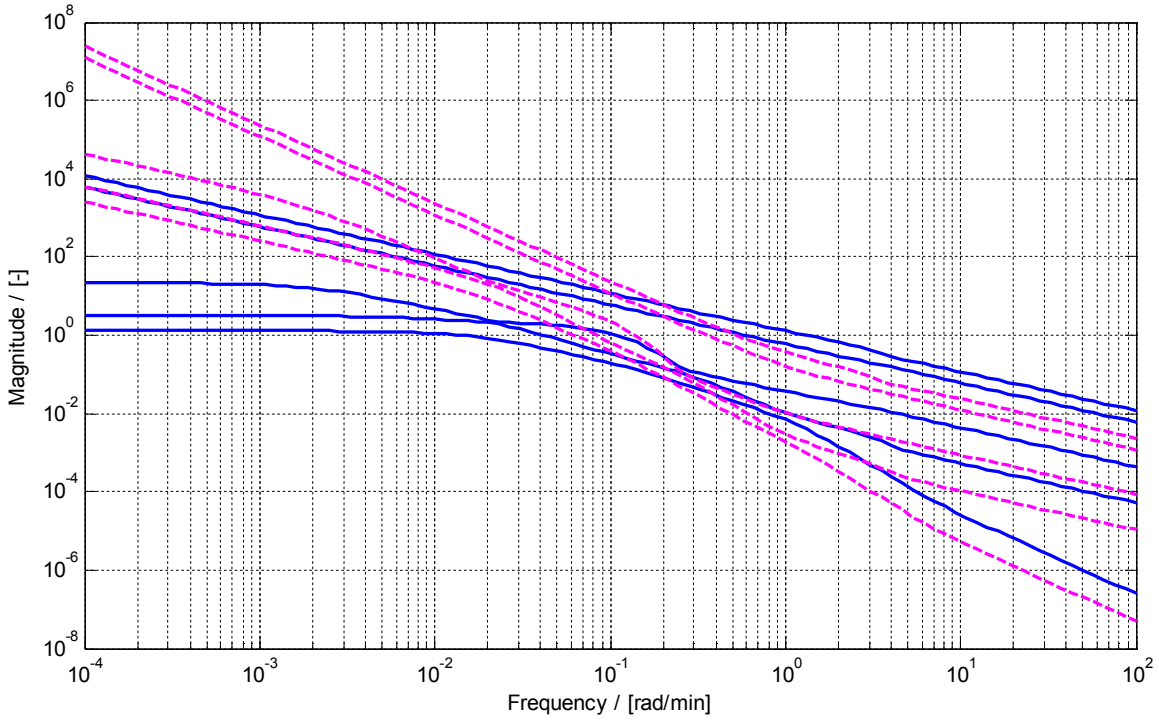

Figure 16: The frequency response of the plant G (-) and of the shaped plant(--).

μ-Synthesis via DK-iteration

The question how to synthesize a μ-optimal controller for the system shown in Figure 12 is still an open question. Although, in general the DK-iteration algorithm can finds a μ-suboptimal controller. With this controller we can achieve robust stability and robust performance.

Here we give a short introduction on the DK-iteration which is a very common procedure to synthesize a μ- suboptimal controller.

From the general plant P we can obtain a interconnection matrix N. The interconnection matrix N is a function of the system G, controller K and the uncertainty weights Δ_U. This structure is used for robust performance analysis. The weightings, which are incorporated in the plant P, are chosen such that $||\Delta_U||_\infty \leq 1$. As a result, a family of plants is obtained. Only complex pertubations are considered. The performance is specified by weights in P, chosen such that when the H_∞-norm of N is less than 1 means that the control objectives are achieved.

The following scheme is used for robustness analysis:

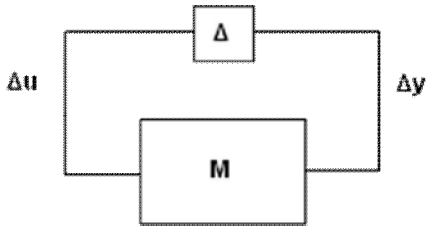

Figure 17: The M interconnection structure for robust stability analysis.

where $\Delta=\{ \Delta_U, \Delta_P\}$, consisting of block-diagonal perturbation matrix $\Delta_U=\text{diag}\{\Delta_1,....,\Delta_n\}$ and a full complex perturbation matrix Δ_P with $||\Delta_P||_\infty \leq 1$. The M function is derived from N by connecting ω to z via Δ_P. It can be shown that robust performance (RP) is equivalent with:

$$\text{RP} \quad \Leftrightarrow \quad \mu_{RP} = \sup_{\omega} \mu_{\Delta}\left(M(j\omega)\right) < 1 \tag{6.29}$$

The value μ is computed through upper and lower bounds and frequency-by-frequency. The upper bound is given by:

$$\mu_{\Delta}\left(M(j\omega)\right) \leq \inf_{D \in \mathbf{D}} \bar{\sigma}\left(DMD^{-1}\right) \tag{6.30}$$

where $\mathbf{D}=\{D \mid D\Delta=\Delta D\}$

De DK-iteration solves the following minimization problem:

$$\min_{K} \inf_{D \in \mathbf{D}} \sup_{\omega} \bar{\sigma}\left(DMD^{-1}\right) \tag{6.31}$$

M is a function of K, by alternating minimization of $\bar{\sigma}\left(\mathrm{DMD}^{-1}\right)$ for either K or D. The minimization steps are convex in K and D. However, joint convexity is not guaranteed.

Step 1: Scale M with a stable and minimum phase rational transfer matrix D(s) with the appropriate structure.

Step 2: Synthesize and H_∞ controller for the scaled problem: $\min_K \sup_\omega \bar{\sigma}\left(\mathrm{DMD}^{-1}\right)$, (K-step).

Step 3: Continue to iterate until performance is satisfactory or H_∞ does not increase any more.

Step 4: Compute the upper bound on μ to obtain new D-scales as a function of frequency. The new D(jω) minimizes at each frequency $\bar{\sigma}\left(\mathrm{DMD}^{-1}\right)$ with fixed M, (D-step_.

Step 5: Fit the magnitude of each element of D(jω) to a stable and minimum phase rational transfer function. Go to step 1.

DWC

The two degree of freedom setup which is used is given in the following figure:

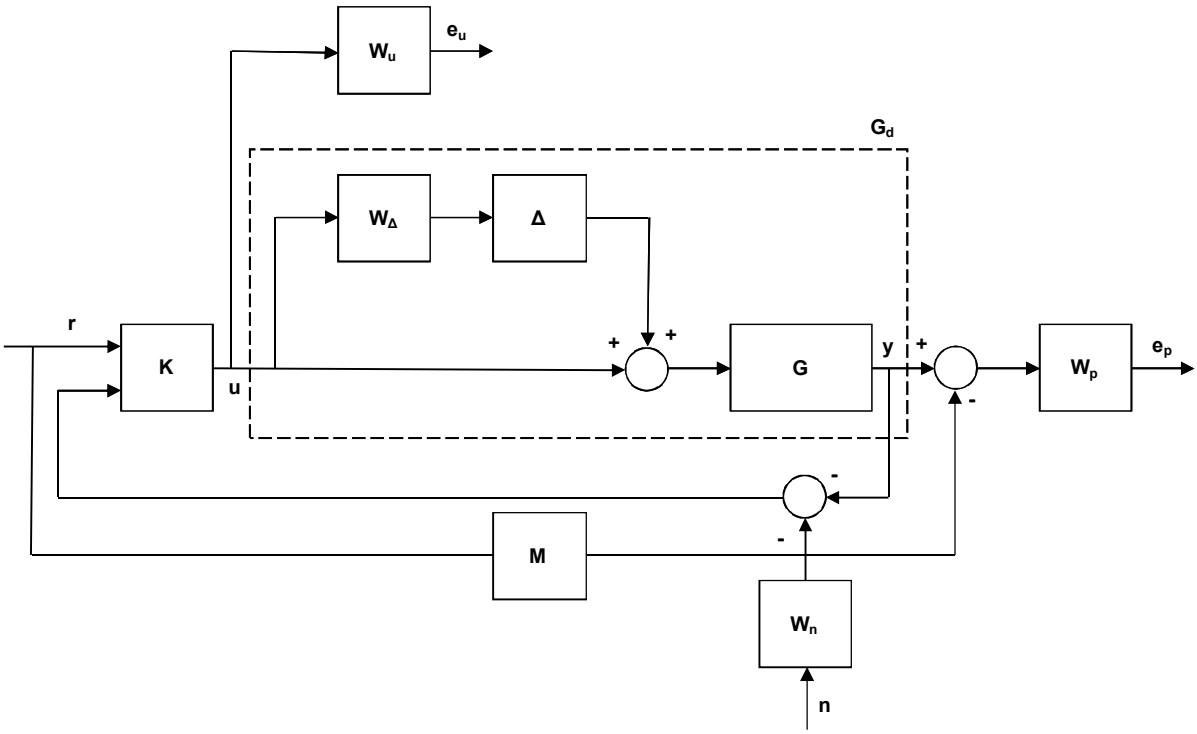

Figure 18: Block diagram for two degree of freedom controller. From Gu, 2005.

The plant G is extended with multiplicative input uncertainty. This is the sub loop consisting of W_Δ and Δ within Gd. Consequently, Consequently, the inputs are perturbed by an gain uncertainty and a input delay. Hence, G_d is a set of plants; controller synthesis is performed with respect to all possible perturbations in W_Δ and Δ. Two weightings W_U and W_P are incorporated to increase the performance. The matrix W_n is a noise shaping filter, used for adding noise to the measurements. True block pulses have more impact compared to pointed noise pulses shaped by the filter W_n. The matrix M is used to increase the tracking performance and represents the desired dynamics.

The weightings are:

$$W_u = \begin{pmatrix} k_1 e^{-\Theta_1 s} & & \\ & \ddots & \\ & & k_1 e^{-\Theta_1 s} \end{pmatrix} \tag{6.32}$$

where $k_i \in [0.8,1.2]$ and $\Theta_i \in [0,1]$ for i = 1,…,5.

The matrix W_u can be split up into two matrices:

$$\Delta = \begin{pmatrix} \Delta_1 & & \\ & \ddots & \\ & & \Delta_5 \end{pmatrix} \qquad W_\Delta = \begin{pmatrix} W_{\Delta_1} & & \\ & \ddots & \\ & & W_{\Delta_5} \end{pmatrix} \tag{6.33}$$

where $|\Delta_i| \leq 1$ for i=1,…,5. The functions in the matrix W_Δ are obtained via a fitting procedure in the frequency domain (Gu, 2007):

$$W_{\Delta_i} = \frac{2.2138s^3 + 15.9537s^2 + 27.6702s + 4.9050}{1s^3 + 8.3412s^2 + 21.2393s + 22.6705}, i = 1,...,5 \tag{6.34}$$

This function is the upper bound of 200 realizations of the relative uncertainty. Hence, an uncertainty set consisting of plants G_d is obtained, while the parameters of the uncertainty are within certain ranges.

The off-diagonal elements are 0.03, such that the products and liquid levels will go to their prescribed set points. The function wp has the effect that for a low frequency range the set points are achieved. The functions W_u limit the control action over the frequency range ω≥150 and the gains are chosen independently, such that in case of strong measurement noise over-steering is avoided. This results in:

$$W_u = \begin{pmatrix} wu_1 & & & & \\ & wu_2 & & & \\ & & wu_3 & & \\ & & & wu_4 & \\ & & & & wu_5 \end{pmatrix} \qquad \begin{aligned} wu_i &= g_i \frac{s+1}{s+1}\, i = 1...3 \\ wu_i &= g_i \frac{s+1}{0.01s+1}\, i = 4..5 \end{aligned} \tag{6.35}$$

The weights g_i are chosen to ensure good performance and robust control: $g_1=g_2=g_3=10.44$ and $g_4=g_5=0.2175$. The measurement noise on the five measurements is filtered by:

$$W_n = \begin{pmatrix} wn & & & & \\ & wn & & & \\ & & wn & & \\ & & & wn_4 & \\ & & & & wn_5 \end{pmatrix}, \quad wn = 0.01\frac{s}{s+1}, \quad wn_4 = wn_5 = 0.2\frac{s}{s+1} \tag{6.36}$$

The reference is linked to the output of the plant G_d via a model M. The model is represented by a diagonal matrix with zero off-diagonal elements and the following transfer functions (wm), on the diagonal:

$$M = \frac{1}{1080s^2+288s+1} \tag{6.37}$$

The off-diagonal elements are zero to avoid interaction and the constants are chosen such that the settle time after an impulse is ~150s. Inclusion of such a model makes it easier to achieve desired dynamics.

In order to obtain a function M needed for the DK-iteration we have to specify Δ:

$$\Delta = \left\{ \begin{pmatrix} \Delta_U & 0 \\ 0 & \Delta_P \end{pmatrix} : \Delta_U \in \mathbb{C}^{5\times 5}, \Delta_P \in \mathbb{C}^{10\times 10} \right\} \tag{6.38}$$

The first block Δ_U is used to model the uncertainty of the column and its dimension is 5. This block represents the multiplicative input uncertainty withing G_d. Furthermore, the fictitious uncertainty Δ_P is used to include performance objectives: the inputs are e_u and e_p, the outputs being the exogenous inputs to r and n.

The μ-synthesis procedure – performed in Matlab® using the command *dksyn* – results in the iteration steps listed in the following table**:**

Iteration	Controller order	Maximum value of μ	Achieved γ
1	147	3.754	4.717
2	163	1.049	1.148
3	169	0.702	0.703

Table 3: Results of the μ-synthesis.

Robust stability analysis reveals that the maximum value of μ is 0.3629. Hence the system is stable under perturbations that satisfy: ||Δ|| < 1/0.3629. Likewise the maximum value of μ in case of the robust performance analysis is 0.9847. Hence the system achieves robust performance for all the specified uncertainties. The obtained controller has an order of 218 – note that the controller is reduced to an order of 25 as there are negligible difference between the reduced controller and the full order controller.

7 Results and discussion

In the dynamic simulations performed in this study, disturbances of +10% in the feed flow rate (F) and +10% in the feed composition (x_A) were used, as these are among the most significant ones at industrial scale. Note that persistent disturbances give a better insight of the quality of the controller than zero mean disturbances, as typically after a temporary disturbance the product compositions return to their given set points. However, the reflux and reboiler levels are unstable and need to be stabilized. For the PI controllers of the four investigated structures the tuning parameters (proportional gain and integral term) listed in Table 1 were used, along with the control loop direction.

DB/LSV	P ($^{\%}/_{\%}$)	I (min)	D (min)	Control direction
xA → L	3	80	0	+
xB → S	3	80	0	–
xC → V	3	80	0	+
Tank Level → D	0.5	100	0	–
Reboiler Level → B	0.5	100	0	–

DV/LSB	P ($^{\%}/_{\%}$)	I (min)	D (min)	Control direction
xA → L	1	100	0	+
xB → S	1	100	0	–
xC → B	1	100	0	–
Tank Level → D	0.1	400	0	–
Reboiler Level → V	0.1	400	0	–

LB/DSV	P ($^{\%}/_{\%}$)	I (min)	D (min)	Control direction
xA → D	3	75	0	–
xB → V	3	75	0	+
xC → S	3	75	0	+
Tank Level → L	0.5	400	0	–
Reboiler Level → B	0.5	400	0	–

LV/DSB	P ($^{\%}/_{\%}$)	I (min)	D (min)	Control direction
xA → D	1	100	0	–
xB → S	1	100	0	–
xC → B	1	100	0	–
Tank Level → L	0.5	400	0	–
Reboiler Level → V	0.5	400	0	–

Table 4: Tuning parameters of PI controllers.

The dynamic simulations were carried out in Mathworks Matlab® combined with Simulink®. As shown next by the dynamic simulations, all PI control structures cope well with persistent disturbances. However, the control structure DV/LSB and LV/DSB make the DWC return to steady state only after a long time (>1000 min).

The LQG controller with feed forward control has only good results for (persistent) disturbances in the feed flow rate. For other disturbances the tuning of the feed forward terms is less straightforward. The controller has no feedback on the error term that is the difference of the set points and the measured values. As a result offset in the product purities appears. To solve this problem, the LQG controller is combined with an integral term.

A stop criterion is used for all test cases in order to have a fair comparison of the controllers – the simulation is stopped if the condition $||(x_A,x_B,x_C)-(0.97,0.97,0.97)||^2 < 1e^{-10}$ holds at time t_1 and also holds at time $t_2=t_1 + 40$ min, where $t_1<t_2$. The resulting times (smaller values means better control) are shown in the following table:

Control structure	+10% Feed flow rate	+10% x_A in feed
DB/LSV	714	525
DV/LSB	>> 1000	>> 1000
LB/DSV	790	561
LV/DSB	>> 1000	>> 1000
LQR/LGQ (Feed forward)	432.5	N/A
LQR/LGQ (Integral action)	510	839
LSDP	645	569
μ-controller	152.8	148

Table 5: Settle time to reach steady state for different persistent disturbances.

The effect of measurement noise on the control performance was also investigated. At the five measurements, filtered white noise was added using the following filter:

$$f_{gain} \cdot \frac{s}{s+1} \tag{8.2}$$

Hence for frequencies ω>1 the damping is 0 dB and for ω≤1 there is a damping of 20 dB per decade. The gain f_{gain} =0.01 for the composition channels and 0.2 for the tank and reboiler level sensor, respectively, and the noise source is a block signal with mean 1 and sample time 0.1 minute. Consequently, the gain is 1% of the nominal value.

After a constant load disturbance in the feed at first instance all product purities decrease (Figure 19, left) but then, the top and bottom purities decrease significantly while the middle product purity increases. The product flow rates D and B are steered by the controller above the new nominal values in order to stabilize the product purities. The compositions load disturbance is handled faster and there is no serious overshoot (Figure 19, right). Since, the maximum difference between the set points and

the measured product purity in case of feed flow rate disturbance is between 0.015-0.020, and approximately 0.008 in case of feed composition disturbance.

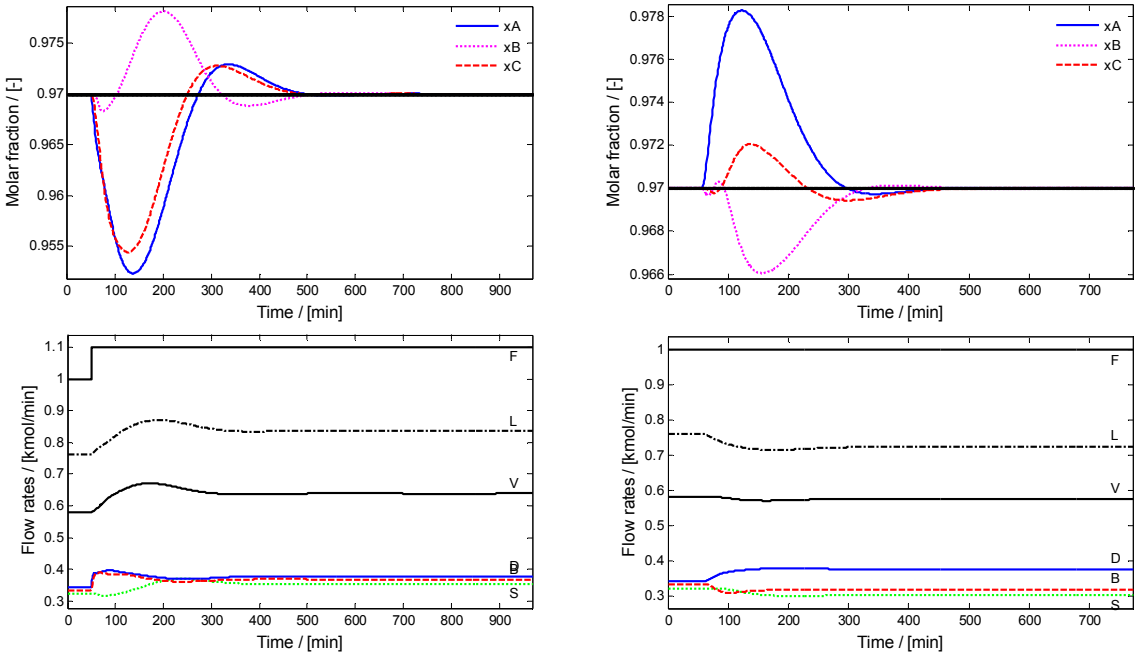

Figure 19: Dynamic response of the DB/LSV control structure, at a persistent disturbance of +10% in the feed flow rate (left) and +10% x_A in the feed composition (right)

Unlike the previous PI control structure, DV/LSB needs a long period to stabilize the plant around the new steady state (Figure 20, left). The overshoot in the purity of xA in case of feed composition disturbance is large: approximately 0.08 (Figure 20, right).

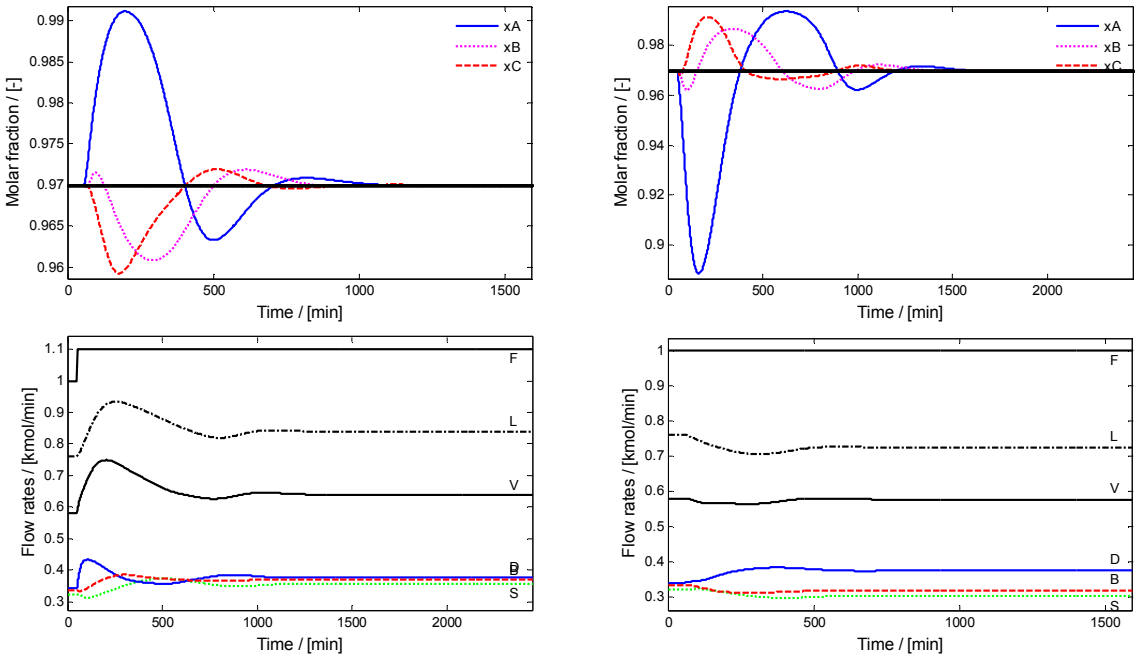

Figure 20: Dynamic response of the DV/LSB control structure, at a persistent disturbance of +10% in the feed flow rate (left) and +10% x_A in the feed composition (right)

The PI control structure LB/DSV controls the DWC in a similar timescale to DB/LSV (Table). The disturbances resulting from the changes in the nominal feed are controlled away; showing only a small overshoot in the product purities; less than 0.02 for both cases (Figure 21).

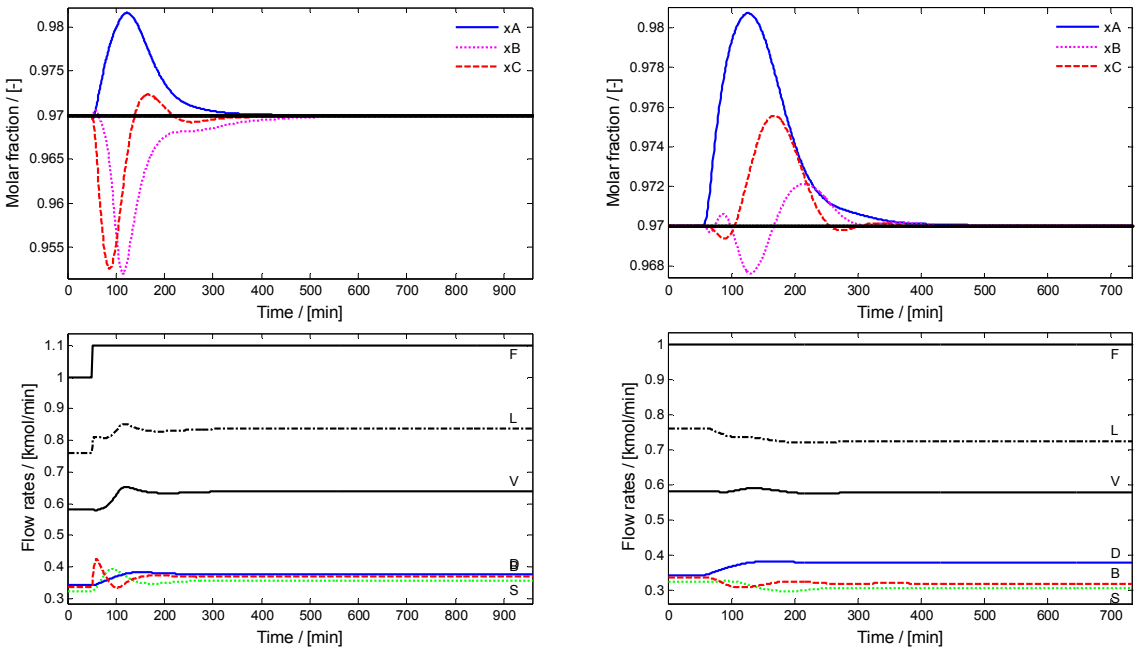

Figure 21: Dynamic response of the LB/DSV control structure, at a persistent disturbance of +10% in the feed flow rate (left) and +10% xA in the feed composition (right)

The control structure of the LV/DSB configuration is such that there are amplifying effects due to the outcome of the control action of both inventory and regulatory control. As a result, the feed flowrate disturbance leads to an increase of L_0 and V_0 to maintain the demanded tank and reboiler level. Consequently, the product purities increase and the levels of the tank and reboiler drop very fast due to the synergy effect of the inventory and regulatory control (Figure 22, left). This phenomenon is also present for the compositions load but less strong (Figure 22, right). Nevertheless the steady state can only be reached after a long time and the feed flow rate disturbance leads to an error of 0.05 in the purity of product B. In addition, compared to the three previous control structures, relative high flow rates are used to control the DWC: $L_0 > 1.1$ and $V_0 > 1.3$.

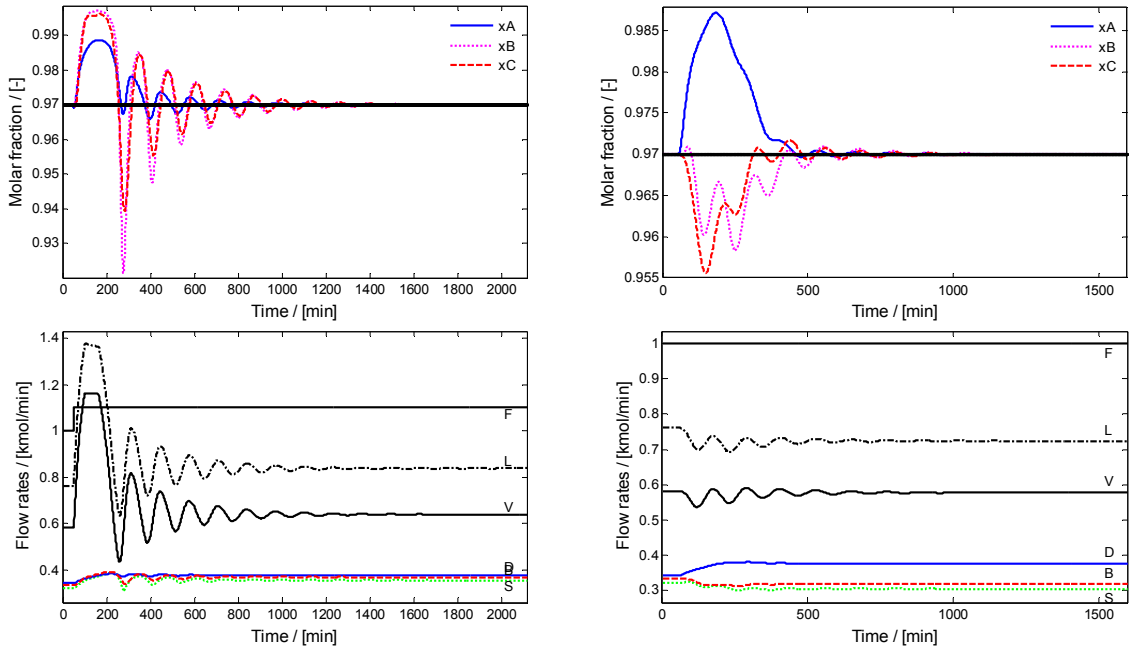

Figure 22: Dynamic response of the LV/DSB control structure, at a persistent disturbance of +10% in the feed flow rate (left) and +10% x_A in the feed composition (right)

While the LQG controller results in optimal state feedback in case of zero-mean noise, problems occur in case of persistent disturbance. Hence, the LQG controller needs to be expanded in order to handle the load disturbances. Combined with the feed forward controller the feed flow rate disturbance can easily be controlled and results in a small settle time (Figure 23, left). In case of compositions disturbance there is no clear relationship between the amount of input and output – as it was for flow rate – and hence the feed forward leads to bad control resulting in a different steady state error (Figure 23, right).

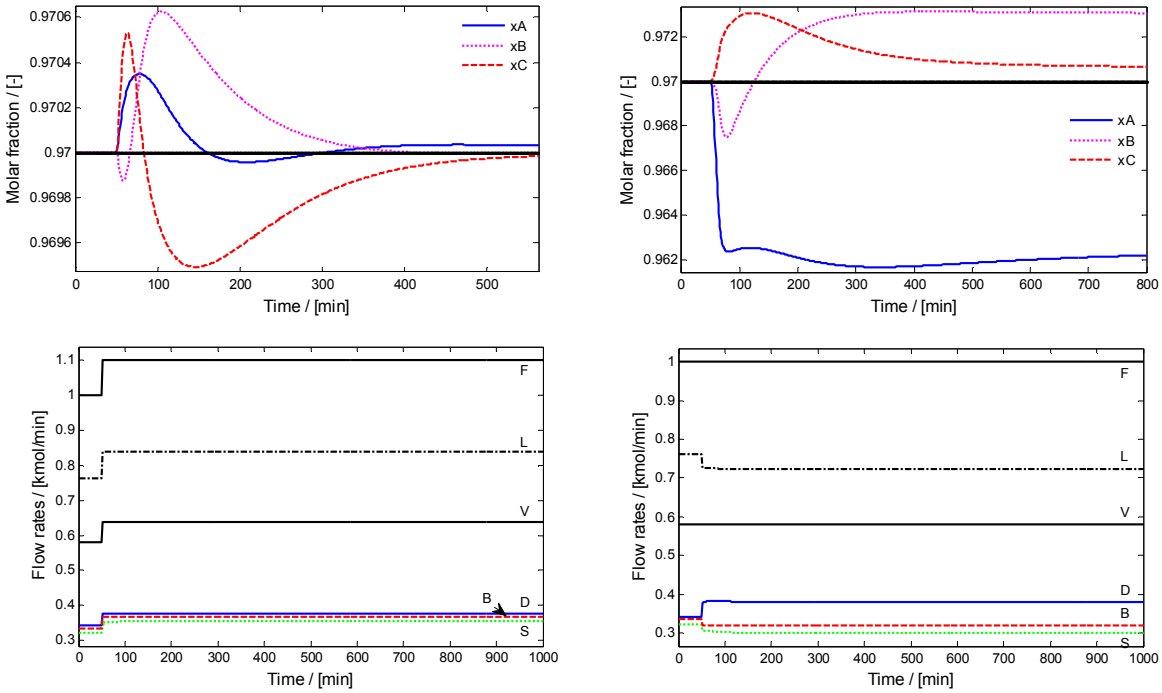

Figure 23: Dynamic response of LQG controller with feed forward, at a persistent disturbance of +10% in the feed flow rate (left) and +10% x_A in the feed composition (right).

The LQG combined with an integral action stabilizes the column around the demanded set points for all the disturbances (Figure 24). In both cases the maximum error in the product compositions is less then 0.005. Furthermore, there is a striking contrast between settle time after a feed flow rate disturbance and a feed composition disturbance: in the latter case the settle time is much longer.

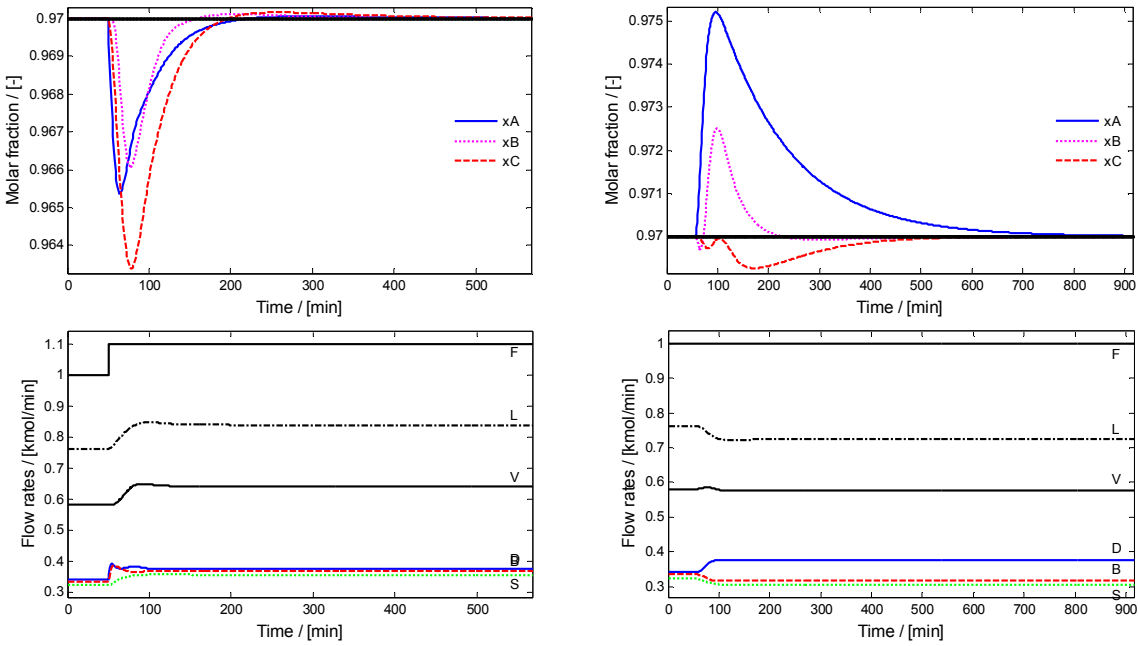

Figure 24: Dynamic response of the LQG combined with Integral action control structure, at a persistent disturbance of +10% in the feed flow rate (left) and +10% x_A in the feed composition (right).

The controller obtained by the LSDP is implemented and the results are shown in Figure 25. The application of this advanced controller leads to significantly shorter settle times: about 6 times lower than the two best PI control structures. Remarkably, the maximal offset error in the product compositions are less then 0.002.

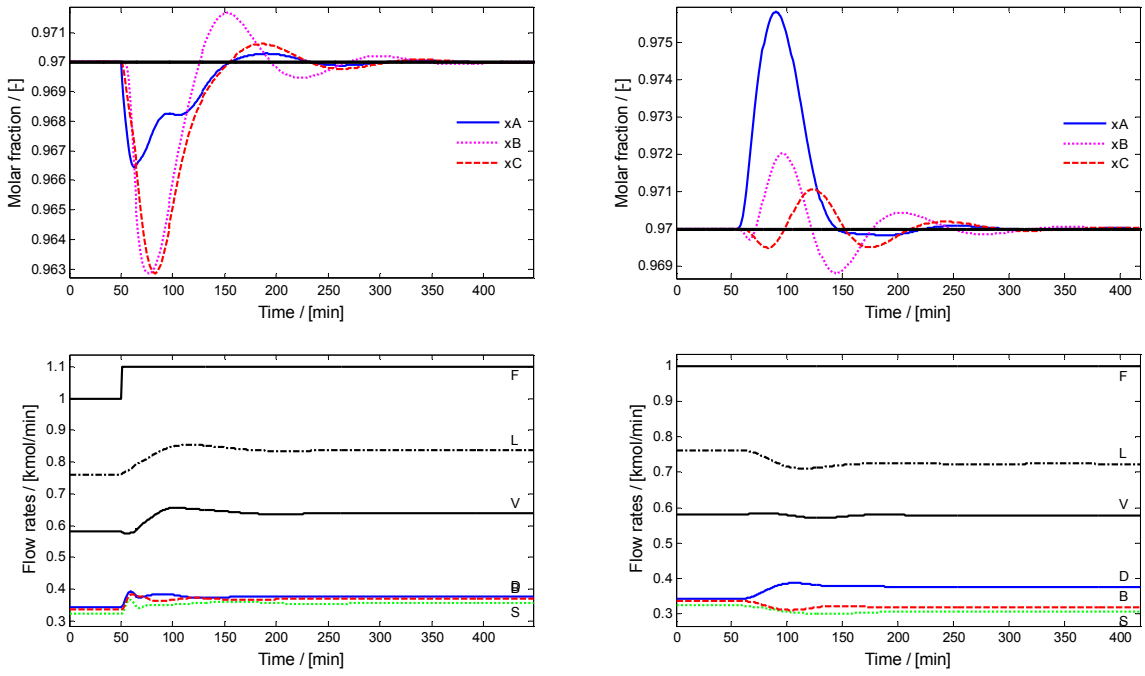

Figure 25: Dynamic response of the LSDP-controller, at a persistent disturbance of +10% in the feed flow rate (left) and +10% x_A in the feed composition (right).

Figure 26 shows that the □-controller is able to steer the system to the desired steady state after persistent disturbance. Similar to the LSDP-controller the settle time is significantly shorter compared to the PI control structures. And the maximal error in the product compositions is less then 0.002. Moreover, the settle time of the system controlled by the □-controller is the smallest of all compared control structures.

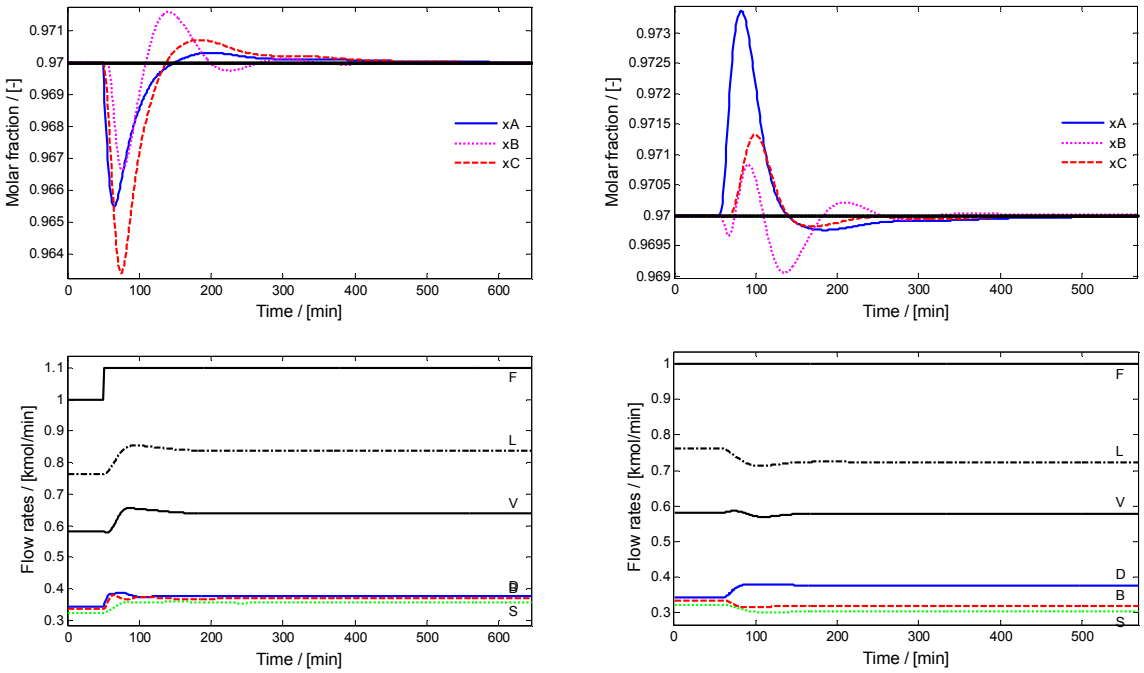

Figure 26: Dynamic response of the μ-controller, at a persistent disturbance of +10% in the feed flow rate (left) and +10% x_A in the feed composition (right).

In addition to the previous scenarios, noise and a time delay of 1 minute was added to each measurement channel. The added measurement noise is filtered using the filter described by the previous equation (8.2). This simulation was carried out only for the PI control structure DB/LSV, LQG with Integral action, LSDP-controller and the μ-controller as these controllers lead to the shortest settle times. The impact of noise and delay on the LB/DSV PI structure is expected to comparable with DB/LSV. The dynamic simulation of the PI control structure DB/LSV with measurement noise is shown in Figure 27.

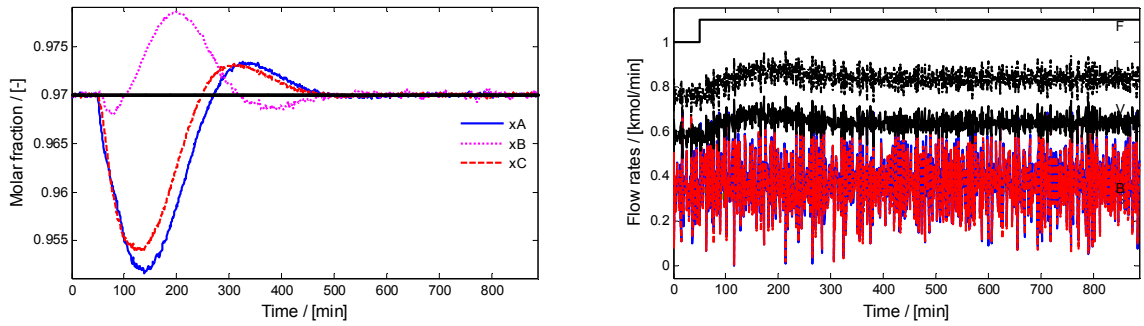

Figure 27: Dynamic response of the DWC with the DB/LSV control structure, at a persistent disturbance of +10% at t=50min in the feed flow rate while there is white measurement noise and a time delay.

The regulatory part of the control structure (DB) is controlling the tank level and the reboiler level. The measurements noise has more impact on the flow rates D and B than the other three flow rates (Figure 27, right). In addition, the persistent disturbance results in a serious offset for t < 500 minutes. However, the control structure is robust to the measurement noise and time delays.

In order to have a fair comparison with the PI control structure, the scales on the Y-axis are the same. The results for the LQG with Integral action control structure (Figure 28) shows similar chaotic behavior in the product composition compared with the PI control structure. Nevertheless, the maximal deviation in the product composition is less than 0.008 and the persistent disturbance in no longer visible after approximately t > 200 minutes. While the weighting of the integral error for the product compositions is much larger compared to the liquid levels, the noise has more impact on the control signals L_0, V_0 and S. In addition, the input weightings are also different: the weightings on L0 and V0 are larger than the weighting on S, and the weightings on S is larger than the weightings on B and D. Hence, there is a trade off in a fast control action and measurement noise reduction.

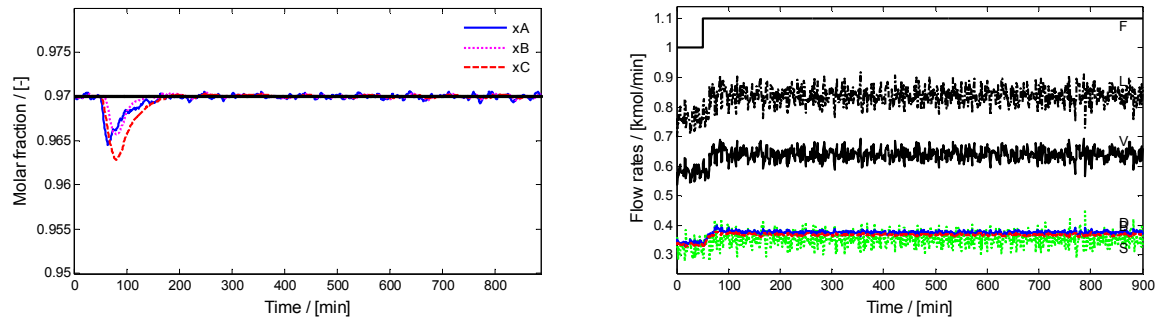

Figure 28: Dynamic response of the DWC with the LQG with Integral action control structure, at a persistent disturbance of +10% at t=50min in the feed flow rate while there is white measurement noise and a time delay.

The high order LSDP-controller is more sensitive to noise as shown by the chaotic behavior of the product purities plotted in Figure 29. The closed loop stable remains stable but when synthesizing the

controller the noise source is not taken into account. In the absence of measurement noise the control action is such that the settle time is short.

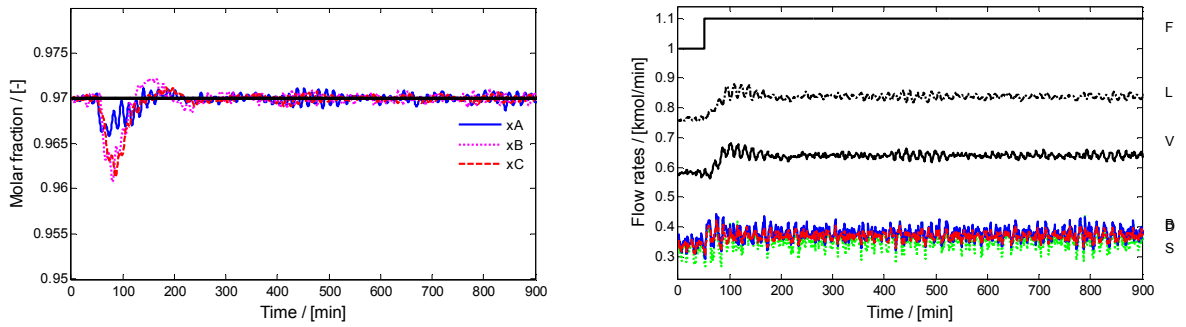

Figure 29: Dynamic response of the DWC with the LSDP-controller, at a persistent disturbance of +10% at t=50min in the feed flow rate while there is white measurement noise and a time delay.

The effect of measurement noise and delay on the system controlled by the μ-controller is shown in Figure 30. While there is chaotic behavior in the product compositions the control actions are very calm despite the present noise. Also, the maximum deviation in the product composition is small – less than 0.008.

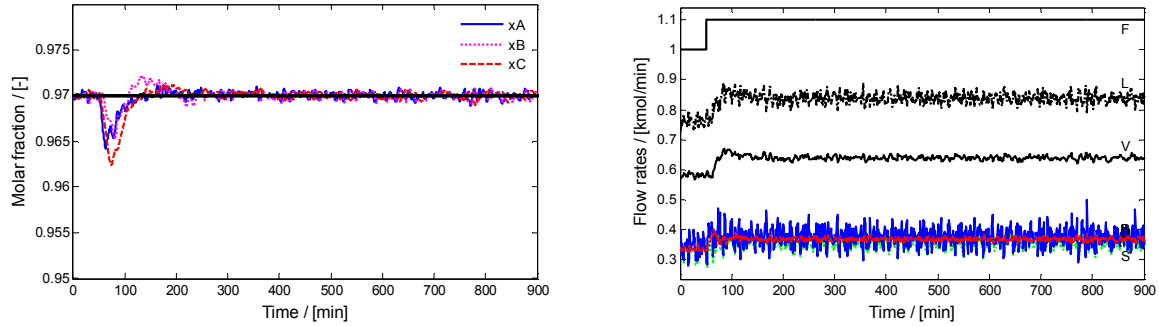

Figure 30: Dynamic response of the DWC with the μ-controller, at a persistent disturbance of +10% at t=50min in the feed flow rate while there is white measurement noise and a time delay.

Note that all the control structures investigated were tested for a large number of disturbances, but here we limit only to the ones that are relevant at industrial scale. Although the reported disturbances are not exerted at the same time, no serious problems – such as instability or lack of capability to reach the set points – were observed in case of simultaneous disturbances. The same holds for a decrease of 10% in the feed flow rate or feed composition. The exerted noise is filtered and the gain is approximately 1% of the nominal value on the channel. In an industrial case the filter should corresponds to the measurement sensor.

Remarkably, PI control structures are already for a long time the celebrated controllers in the chemical industry (Johnson and Moradi, 2005). Several reasons are given for their success:

1. Simplicity of the control structure,

2. Robustness with respect to model uncertainties and disturbances,
3. Relatively easy manual stabilization of the process with a multi-loop controller, when an actuator or sensor fails.

The LQG control structure offers optimal state estimation and an optimal control with respect to the cost function (5.2), providing that the matrices Q and R are chosen in an appropriate way. Unlike LQG, many control variables have to be chosen for the multi-loop PI structures. In addition, the LQG control structure guarantees stability of the closed loop system consisting of a linearized DWC, whereas the stability problem of the multi-loop PI structure is still open (Johnson and Moradi, 2005). The full model is nonlinear and the optimal state estimation and optimal control holds only for the linearized model. However, as shown by Figure 4 this should not lead to problems. Moreover, the dynamic simulations showed no control or stability problems of the closed loop system. Furthermore, there is a trade off between a short settle time in the case of no measurement delay and noise, and a very smooth control action in case of measurement noise. A short settle time results in a more chaotic control if noise is present.

The LSDP-controller has difficulties to cope with the measurement noise. The μ-controller has the shortest settle times and a relatively good behavior when measurement noise and delay is present. Unlike the μ-controller, controller reduction of the LSDP-controller leads to serious problems in the presence of the measurement noise and delay. As a result, the computer needs much more time to carry out a simulation of the DWC controlled by a LSDP-controller compared the other control structures.

In addition to the controllers compared in this work, Model Predictive Control is a serious candidate for controlling non-linear processes (Kiss et al., 1999; Nagy et al., 2007, Roman et al., 2009) and in particular DWC (Adrian et al, 2003). However, more advanced controllers such as MPC are out of the scope of the current study.

8. Conclusions

The comparison of control strategies performed in this work provides significant insight into the controllability of dividing-wall columns, and gives important guidelines for selecting the appropriate control structure. The dynamic model of DWC used in this study is not a reduced one, but a full-size non-linear model that is representative for industrial separations. Although the application of non-linear based controllers is very appealing – since linearization is not necessary – the general model controller (GMC) is not applicable in practice for the DWC as the open-loop model is not minimum phase.

Due to practical considerations based on the physical flows, there are basically four PI multi-loops control strategies possible for a DWC: DB/LSV, DV/LBS, LB/DSV, LV/DSB. The results of the dynamic simulations show that DB/LSV and LB/DSV are the best control structures among the decentralized multivariable PI structured controllers, being able to handle persistent disturbances in reasonable short times. However, the other two structures DV/LBS and LV/DSB needed an extremely long settle times, in case of persistent disturbances.

The DWC model is not only non-linear but also a true multi-input multi-output (MIMO) system, hence the applicability of a MIMO control structure starting with a LQG controller was also investigated. With the LQG controller there is an optimal tuning with respect to the corresponding cost function. In order to cope with persistent disturbances two options were explored: feed forward control and addition of an integral action. The LQG combined with a feed forward has good results for a persistent disturbance in the feed flow rate. However, for changes in the feed composition and condition it is difficult to find a good tuning. Moreover, other persistent disturbances than the ones used for tuning cannot be controlled with LQG. Nevertheless, combining LQG with an integral action and reference input solves the problem. Depending on the expected measurement noise the cost function can be determined. Moreover, robustness against measurement noise results in a more conservative tuning.

The loop-shaping design procedure (LSDP) used in this work leads to a feasible μ-controller that has some additional benefits, while specific model uncertainties can be incorporated in the control structure. In the DWC case described here, the obtained μ-controller is able to minimize the settle time when handling persistent disturbances. While PI control structures are also able to control the DWC, significantly shorter settle times can be achieved using MIMO controllers. Moreover, persistent disturbance are also controlled faster using a MIMO controller.

9 References

1. Adrian R., Schoenmakers H., Boll M., MPC of integrated unit operations: Control of a DWC, Chemical Engineering & Processing, 43 (2004), 347-355.
2. Alstad V., Skogestad S., Null Space Method for Selecting Optimal Measurement Combinations as Controlled Variables, Industrial & Engineering Chemistry Research, 46 (2007), 846-853.
3. Becker H., Godorr S., Kreis H., Partitioned distilliation columns - why, when & how, Journal of Chemical Engineering, January (2001), 68-74.
4. Biswas P. P., Ray S., Samanta A. N., Multi-objective constraint optimizing IOL control of distillation column with nonlinear observer, Journal of Process Control, 17 (2007), 73-81.
5. Campo, P.K. And Morari, M., Achievable closed-loop properties of systems under decentralized control: Conditions involving the steady-state gain, IEEE Transactions on Automatic Control AC-39(5): 932-942 (1994).
6. Diggelen, R.C., Kiss, A.A., Heemink, A.W., Comparison of Control Strategies for Dividing-Wall Columns, Industrial & Engineering Chemistry Research, to appear in 2009. See Appendix.
7. Gu D.W., Robust Control Design with Matlab®, Chapter 11, Springer, 2005.
8. Halvorsen I. J., Skogestad S., Optimizing control of Petlyuk Distillation: Understanding the Steady-State behaviour, Computers & Chemical Engineering, 21 (1997), 249-254.
9. Isidori, A., Nonlinear Control Systems: An Introduction, Springer Verlag, 1989.
10. Johnson M. A., Moradi H., PID Control: New Identification and Design Methods, Springer Verlag, London, 2005.
11. Kaibel B., Jansen H., Zich E., Olujic Z., Unfixed Dividing Wall Technology for Packed and Tray Distillation Columns, Distillation and Absorption, 152 (2006), 252-266.
12. Kaibel G., Distillation columns with vertical partitions, Chemical Engineering Technology, 10 (1987), 92–98.
13. Kiss A. A., Agachi S. P., Model Predictive Control of temperature of a PVC emulsion process, Hungarian Journal of Industrial Chemistry, 27 (1999), 117-124.
14. Kiss A. A., Bildea C. S., Dimian A. C., Design and Control of Recycle Systems by Non-linear Analysis, Computers & Chemical Engineering, 31 (2007), 601-611.
15. Kiss A. A., Pragt H., van Strien C., Reactive Dividing-Wall Columns - How to get more with less resources?, Chemical Engineering Communications, (2009), Advance Article.
16. Kolbe B., Wenzel S., Novel distillation concepts using one-shell columns, Chemical Engineering & Processing, 43 (2004), 339-346.
17. Lee P.L., Sullivan G.R., Generic Model Control (GMC), Computers & Chemical Engineering, 12 (1988), 573-580.
18. Ling H., Luyben W. L., New Control Structure for Divided-Wall Columns, Industrial & Engineering Chemistry Research, 48 (2009), 6034-6049.

19. Lundström, P., Skogestad,S., Doyle, J., Two degree of freedom controller design fora n ill-conditioned plant using μ-synthesis, European Control Conference, Groningen (The Netherlands), 1993.
20. MathWorks Inc., MATLAB® – Robust Control Toolbox Manual, 2007.
21. Mueller I., Kenig E. Y., Reactive Distillation in a Dividing Wall Column – Rate-Based Modeling and Simulation, Industrial & Engineering Chemistry Research, 46 (2007), 3709-3719.
22. Nagy Z. K., Mahn B., Franke R., Allgower F., Efficient output feedback nonlinear model predictive control for temperature control of industrial batch reactors, Control Engineering Practice, 15 (2007), 839-859.
23. Olujic Z., Kaibel B., Jansen H., Rietfort T., Zich E., Frey G., Distillation column internals/configurations for process intensification, Chemical & Biochemical Engineering Quarterly, 17 (2003), 301-309.
24. Ordys A., Uduehi D., Johnson M., Process Control Performance Assessment – From Theory to Implementation, Springer, London, 2007.
25. Perry R. H., Green D. W., Perry's Chemical Engineers' Handbook, 8th Edition, McGraw-Hill, 2008.
26. Petlyuk F. B., Platonov V. M., Slavinskii D. M., Thermodynamically optimal method for separating multicomponent mixtures, International Chemical Engineering, 5 (1965), 555-561.
27. Roman R., Nagy Z. K., Cristea M. V., Agachi S. P., Dynamic modelling and nonlinear model predictive control of a Fluid Catalytic Cracking Unit, Computers & Chemical Engineering, 33 (2009), 605-617.
28. Rouchon P., Dynamic simulation and nonlinear control of distillation columns. Ph.D. thesis, Ecole des Mines de Paris, France, 1990.
29. Schultz M. A., Stewart D. G., Harris J. M., Rosenblum S. P., Shakur M. S., O'Brien D. E., Reduce costs with dividing-wall columns, Chemical Engineering Progress, May (2002), 64-71.
30. Serra M., Espuña A., Puigjaner, L., Control and optimization of the divided wall column, Chemical Engineering and Processing, 38 (1999), 549-562.
31. Serra M., Espuña A., Puigjaner L., Study of the divided wall column controllability: influence of design and operation, Computers & Chemical Engineering, 24 (2000), 901-907.
32. Skogestad S., Dynamics and control of distillation columns – a critical survey, IFAC-symposium DYCORD+'92, Maryland, April 27-29, 1992.
33. Skogestad S., Morari M., Robust Control of Ill-Conditioned Plants: High-Purity Distillation, IEEE Transactions on Automatic Control, 33 (1988), no. 12.
34. Skogestad S., Postlethwaite I., Multivariable Feedback Control, 2nd edition, Wiley, 2005.
35. Suphanit B., Bischert A., Narataruksa P., Exergy loss analysis of heat transfer across the wall of the dividing-wall distillation column, Energy, 32 (2007), 2121-2134.
36. Taylor R., Krishna R., Kooijman H., Real-world modeling of distillation, Chemical Engineering Progress, 99 (2003), 28-39.
37. To L.C., Nonlinear Control techniques in Alumina Refineries, Ph.D. thesis, Curtin University of Technology, 1996.

38. Viel F., Busvelle A., Gauthiers J.P., A stable control structure for binary distillation columns, International Journal of Control, 67 (1997), 475-505.
39. Wang S. J., Wong D. S. H., Controllability and energy efficiency of a high-purity divided wall column, Chemical Engineering Science, 62 (2007), 1010-1025.
40. Zames, G. and Bensoussan, D., Multivariable feedback, sensitivity and decentralized control, IEEE Transactions on Automatic Control AC-28(11): 1030-1035 (1983).

10 Appendix

Notation

Disturbances

F	feed flow rate
z_1	feed composition, component A
z_2	feed composition, component B
q	feed condition

State space

f, g	functions
x	state vector
u	control vector
d	disturbance vector
t	time

Subscripts

i	tray number $i \in \{1 \ldots N\}$
j	component $j \in \{1, 2, 3\}$

Control inputs

L_0	reflux flow rate
V_0	vapour flow rate
D	top product flow rate
S	side product flow rate
B	bottom product flow rate
D	distillate product flow rate
R_L	ratio liquid split
R_V	ratio vapour split

Measured Outputs

x_A	top composition, component A
x_B	side composition, component B
x_C	bottom composition, component C
H_T	liquid hold up in reflux tank
H_R	liquid hold up in Reboiler

Other variables

k_i	constant hydraulic factor $i \in \{0, 1, 2\}$
N	number of trays
T	temperature
$x_{i,j}$	liquid composition
$y_{i,j}$	vapour composition
H	liquid hold up
α_j	relative volatility

Model Equations

The nonlinear model of the DWC is described by the following mathematical equations:

$$\dot{x} = f(x,u,d,t)$$
$$y = g(x) \qquad \text{A.1}$$

Where u = [L_0 S V_0 D B R_L R_V] and d = [F z_1 z_2 q]. Furthermore, the state vector x consists of 104 compositions for the first two components and 52 liquid hold ups. The output vector is y=[x_A x_B x_C H_T H_R].

State equations.

Numbering is from top to bottom starting in the prefractionator and then continuing in the main column.

$$H_{i,j}\frac{d}{dt} = L_{i,j}\,(x_{liquid\_split,j}-x_{i,j}) + V_{i-1,j}(y_{i-1,j} - y_i) \qquad i = 1 \qquad \text{A.2}$$

$$H_{i,j}\frac{d}{dt} = L_{i,j}\,(x_{i+1,j}-x_{i,j}) + V_{i-1,j}(y_{i-1,j}-y_i) \qquad i = 2\ldots8 \qquad \text{A.3}$$

$$H_{i,j}\frac{d}{dt} = L_{i,j}\,(x_{in\_2,j}-x_{i,j}) + V_{i-1,j}(y_{i-1,j} - y_i) \qquad i = 9 \qquad \text{A.4}$$

$$H_{i,j}\frac{d}{dt} = L_{i,j}\,(x_{i+1,j}-x_{i,j}) + V_{i-1,j}(y_{i-1,j}-y_i) \qquad i = 10\ldots16 \qquad \text{A.5}$$

$$H_{i,j}\frac{d}{dt} = L_{i,j}\,(x_{in\_3,1}-x_{i,j}) + V_{i-1,j}(y_{i-1,j}-y_i) \qquad i = 17 \qquad \text{A.6}$$

$$H_{i,j}\frac{d}{dt} = L_{i,j}\,(x_{i+1,j}-x_{i,j}) + V_{i-1,j}(y_{i-1,j}-y_i) \qquad i = 18\ldots23 \qquad \text{A.7}$$

$$H_{i,j}\frac{d}{dt} = L_{i,j}\,(x_{i+1,j}-x_{i,j}) + V_{i-1,j}(y_{in\_3,j}-y_i) \qquad i = 24 \qquad \text{A.8}$$

$$H_{i,j}\frac{d}{dt} = L_{i,j}\,(x_{in\_4,j}-x_{i,j}) + V_{i-1,j}(y_{i-1,j}-y_i) \qquad i = 25 \qquad \text{A.9}$$

$$H_{i,j}\frac{d}{dt} = L_{i,j}\,(x_{i+1,j}-x_{i,j}) + V_{i-1,j}(y_{i-1,j}-y_i) \qquad i = 26\ldots32 \qquad \text{A.10}$$

$$H_{i,j}\frac{d}{dt} = L_{i,j}\,(x_{in\_25,j}-x_{i,j}) + V_{i-1,j}(y_{i-1,j}-y_i) \qquad i = 33 \qquad \text{A.11}$$

$$H_{i,j}\frac{d}{dt} = L_{i,j}\,(x_{i+1,j}-x_{i,j}) + V_{i-1,j}(y_{i-1,j}-y_i) \qquad i = 34\ldots40 \qquad \text{A.12}$$

$$H_{i,j}\frac{d}{dt} = L_{i,j}\,(x_{in\_6,j}-x_{i,j}) + V_{i-1,j}(y_{i-1,j}-y_i) \qquad i = 41 \qquad \text{A.13}$$

$$H_{i,j}\frac{d}{dt} = L_{i,j}\,(x_{i+1,j}-x_{i,j}) + V_{i-1,j}(y_{i-1,j}-y_i) \qquad i = 42\ldots48 \qquad \text{A.14}$$

Where the vapour composition is computed by

$$y_{i,j} = \frac{\alpha_j}{\sum_j \alpha_j x_{i,j}} \qquad \text{A.15}$$

For the components $j \in \{1,2,3\}$ and relative volatilities α.

Furthermore, some special concentrations have to be specified:

$x_{in\_2,j} = (L_8 x_{8,j} + F_0 z_j - (1-q) F_0 y_{9,j}) / L_9$	input section 2; tray no. 9	A.16
$x_{in\_1,j} = x_{liquid\_split}$	input section 1; tray no. 1	A.17
$x_{in\_4,j} = x_{liquid\_split}$	input section 4; tray no. 25	A.18
$x_{in\_6,j} = (L_{16} x_{16} + L_{40} x_{40}) / x_{41}$	liquid input section 6; tray no. 41	A.19
$y_{in\_3,j} = (V_1 y_1 + V_4 y_{25}) / V_{24}$	vapour input section 3; tray no. 24	A.20
$x_{in\_5,j} = x_{side\_splitter}$	liquid input section 5, after liquid splitter	A.21

Dynamics of liquid splitter

The liquid splitter is located between section 3 and sections ¼.

$$\begin{aligned} \frac{d}{dt} H_{liquid\ split} &= L_{24} - (L_1 + L_{25}) \\ H_{liquid\_split} \frac{d}{dt} x_{liquid\_split} &= L_{24} (x_{24} - x_{liquid\_split}) \end{aligned} \qquad \text{A.22}$$

Dynamics of side splitter

The liquid side splitter is located between section 3 and sections 4/5.

$$\begin{aligned} \frac{d}{dt} H_{side\_split} &= L_{32} - L_{33} - S \\ H_{side\_split} \frac{d}{dt} x_{side\_split} &= L_{32} (x_{32} - x_{side\_split}) \end{aligned} \qquad \text{A.23}$$

Dynamics of reboiler

This is situated between section 3 and sections ¼.

$$\begin{aligned} \frac{d}{dt} H_{reboiler} &= L_6 - V_0 - B \\ H_{reboiler} \frac{d}{dt} x_{reboiler} &= L_{in} (x_{in} - x_{reboiler}) - V_0 (y_{reboiler} - x_{reboiler}) \end{aligned} \qquad \text{A.24}$$

Dynamics of the reflux tank

This is situated between section 3 and sections 4/5.

$$\frac{d}{dt}H_{reflux\_tank} = V_0 - L_0 - D$$

$$H_{reflux\_tank}\frac{d}{dt}x_{reflux\_tank} = V_0(x_{in}-x_{reflux\_tank}) \qquad \text{A.25}$$

Liquid flow rates

$L_{i,j} = L_0$	i =1…8	A.26
$L_{i,j} = L_0 R_l$	i =9…16	A.27
$L_{i,j} = L_0 R_l + q F_0$	i =17…24	A.28
$L_{i,j} = L_0 (1-R_l)$	i =25...32	A.29
$L_{i,j} = L_0 (1-R_l) - S$	i =33...40	A.30

Vapour flow rates

$V_{i,j} = V_0 R_v + (1-q) F_0$	i = 1… 8	A.31
$V_{i,j} = V_0 R_v$	i = 9…16	A.32
$V_{i,j} = V_0 R_v + (1-q) F_0 + V_0 (1-R_v)$	i = 17…24	A.33
$V_{i,j} = V_0 (1-R_v)$	i = 25...32	A.34
$V_{i,j} = V_0 (1-R_v)$	i = 33...40	A.35

Table Captions

Figure captions

Comparison of Control Strategies for Dividing-Wall Columns

Ruben C. van Diggelen[1], Anton A. Kiss[2], Arnold W. Heemink[1]*

[1]Delft University of Technology, Institute of Applied Mathematics,

Mekelweg 4, 2628 CD Delft, The Netherlands

E-mail: A.W.Heemink@tudelft.nl, Tel: +31 (0)15 27 85813

[2]AkzoNobel Research, Development and Innovation, Process & Product Technology

Velperweg 76, 6824 BM, Arnhem, The Netherlands

E-mail: Tony.Kiss@akzonobel.com, Tel: +31 (0)26 366 1714, Fax: +31 (0)26 366 5871

KEYWORDS

Dividing-wall column, Petlyuk, advanced control, PID, LQG, GMC, LSDP, H_∞, μ-synthesis.

ABSTRACT

Conventional ternary separations progressed via thermally coupled columns such as Petlyuk configuration to a novel design that integrates two distillation columns into one shell – a setup known today as dividing-wall column (DWC). The DWC concept is a major breakthrough in distillation technology, as it brings significant reduction in the capital invested as well as savings in the operating costs. However, the integration of two columns into one shell leads also to changes in the operating mode and ultimately in the controllability of the system. Although much of the literature focuses on the control of binary distillation columns, there are just a few studies on the controllability of DWC. In this work we explore the DWC control issues and make a comparison of various control strategies based on PID loops, within a multi-loop framework (DB/LSV, DV/LSB, LB/DSV, LV/DSB) versus more advanced controllers such as LQG/LQR, GMC, and high order controllers obtained by H_∞ controller synthesis and μ-synthesis. The controllers are applied to a dividing-wall column (DWC) used in an industrial case study – the ternary separation of benzene-toluene-xylene. The performances of these control strategies and the dynamic response of the DWC is investigated in terms of products composition and flow rates, for various persistent disturbances in the feed flow rate and composition. Significantly shorter settling times can be achieved using the advanced controllers based on LQG/LQR, H_∞ controller synthesis and μ-synthesis.

1. Introduction

As a thermal separation method, distillation is one of the most important separation technologies in the chemical industry. Basically, all of the chemicals produced worldwide go through at least one distillation column on their way from crude oil to final product. Considering its many well-known benefits, distillation is and it will remain the separation method of choice in the chemical industry – with over 40 000 columns in operation around the world. Despite the flexibility and the widespread use, one important drawback is the considerable energy requirements, as distillation can generate more than 50% of plant operating cost. (Taylor et al., 2003) An innovative solution to diminish this energy consumption drawback is using advanced process integration techniques (Olujic et al., 2003).
Conventionally, a ternary mixture can be separated via a direct sequence (most volatile component is separated first), indirect sequence (heaviest component is separated first) or distributed sequence (mid-split) consisting of 2-3 distillation columns. This separation sequence evolved to the Petlyuk column configuration (Petlyuk et al., 1965) consisting of two fully thermally coupled distillation columns. Eventually, this led to the concept known today as dividing-wall column (DWC) that integrates in fact the two columns of a Petlyuk system into one column shell (Kaibel, 1987; Christiansen et al., 1997; Schultz et al., 2002; Kolbe and Wenzel, 2004). Figure 1 illustrates the most important ternary separation alternatives.

Figure 1

The name of DWC (dividing-wall column or divided wall-column) is given because the middle part of the column is split into two sections by a wall, as illustrated in Figure 1. Feed, typically containing three or more components, is introduced into one side of the column facing the wall. Deflected by the wall, the lightest component A flows upward and exits the column as top distillate while the heaviest component C drops down and is withdrawn from the bottom of the column. The intermediate boiling component B is initially entrained up and down with both streams, but the fluid that goes upward subsequently separates in the upper part and falls down on the opposite side of the wall. Similarly, the amount of B that goes toward the bottom separates in the lower part then flows up to the back side of the wall, where the entire B product is recovered by a side draw stream. Note however that using a DWC requires a proper match between the operating conditions of the two stand-alone columns in a conventional direct or indirect sequence (Becker et al., 2001).

DWC is very appealing to the chemical industry – with Montz and BASF as the leading companies (Kaibel et al., 2006) – because it can separate three or more components in a single tower, thereby eliminating the need for a second unit, hence saving the cost of building two columns and cutting operating costs by using a single condenser and reboiler. In fact, using dividing-wall columns can save up to 30% in the capital invested and up to 40% in the energy costs (Schultz et al., 2002; Isopescu et al., 2008; Kiss et al., 2009), particularly for close boiling-species (Perry's Handbook, 2008). In addition, the maintenance costs are also lower.

Compared to classic distillation design arrangements, DWC offers the following benefits:

- High purity for all three or more product streams reached in only one column.
- High thermodynamic efficiency due to reduced remixing effects.
- Lower capital investment due to the integrated design.
- Lower energy requirements compared to conventional separation sequences.
- Small footprint due to the reduced number of equipment units.

Moreover, the list of advantages can be extended when DWC is further combined with reactive distillation leading to the more integrated concept of reactive DWC (Mueller and Kenig, 2007; Kiss et al., 2009). Note however that the integration of two columns into one shell leads also to changes in the operating mode and ultimately in the controllability of the system (Wang and Wong, 2007). Therefore, all these benefits are possible only under the condition that a good control strategy is available and able to attain the separation objectives.

Although much of the literature focuses on the control of binary distillation columns, there are only a limited number of studies on the control of DWC. The brief literature review that follows makes a critical overview of the most important DWC control studies up to date.

In this work we explore the main DWC control issues and make a comparison of various control strategies based on PID loops within a multi-loop framework (DB/LSV, DV/LSB, LB/DSV, LV/DSB), more advanced controllers such as LQG/LQR, GMC, and high order controllers obtained by H_∞ controller synthesis and μ-synthesis. The performances of these control strategies and the dynamic response of the DWC is investigated in terms of products composition and flow rates, for various persistent disturbances in the feed flow rate and composition. These control strategies are applied to an industrial case study – a dividing-wall column (DWC) used for the ternary separation of benzene-toluene-xylene (physical properties listed in Table 1).

Table 1

2. Literature Review

The literature study reveals that a variety of controllers are used for distillation columns. Although there is an abundance of literature available about distillation control, most of the studies are on the control of binary separations. Some of them are interesting from a theoretic point of view, while others present a more practical approach.

Viel et al. (1997) proposed a stable control structure for binary distillation column based on a nonlinear Lyapunov controller. The controller satisfied the design goals to maintain the product qualities at their given set-points, despite the presence of typical disturbances in the feed flowrates and in the feed composition. The model used to design the controller is a relative simple constant molar overflow model. In such model pressure is taken constant, and thermal balances are neglected. The performance of the controller was compared with another nonlinear controller (Rouchon, 1990) based on the input-output linearization (IOL) technique (Isidori, 1989). Therefore, this Lyapunov based controller can achieve set-point tracking and asymptotic disturbance rejection with better robustness than in the case of using a decoupling matrix obtained by input/output linearization.

In addition to nonlinear control structures, Biswas et al. (2007) augmented IOL controllers with quadratic matrix controller (IOL-QDMC). The performance of this controller was compared to a quadratic dynamic matrix controller and input-output linearization with PI controller (IOL-PI). Consequently, the two nonlinear controllers performed better than the linear model predictive controller (QDMC). In presence of unmeasured disturbance to the process and parametric uncertainty the IOL-QDMC is much better than simple IOL-PI.

The Generic Model Control (GMC) described by Lee and Sullivan (1988) is a process model based control algorithm that incorporates the nonlinear model of the process directly within the control algorithm. In addition to this, a variant of GMC also known as Distillation Adaptive GMC (DAGMC) was applied to two typical nontrivial distillation units (Rani and Gangiah, 1991). Note that when the relative order of a nonlinear system is equal to one, the control law of GMC is the same as the control law obtained by IOL (To et al., 1996).

A different robust controller was designed by (Da-Wei Gu, 2005). The control structure consisted of a two level control: inventory control and composition control. The inventory of the non-linear model was simply done by two P controllers. Here, the inventory control is done by the level control of the tank liquid level (H_T) and the level control of the reboiler (H_R). The composition control is done by a two-degree-of freedom (2DOF) H_∞ controller obtained by a loop shaping design procedure (LSDP) and a μ-controller obtained by μ-

synthesis. The μ-controller ensures robust stability of the closed loop system and fulfillment of a mixture of time domain and frequency domain specifications. Although the design of the controller is based on a reduced linearized model, the simulation of the closed loop system with the nonlinear distillation model shows very good performance for different reference signals (Setpoint Tracking) and disturbance signals (measurement noise and time delay).

Several authors studied the design phase of the dividing-wall column (DWC) in order to improve the energy efficiency. The design stage of a DWC is very important as in this phase there are two DOF that can be used for optimization purposes. In this perspective we mention the study reported by Halvorsen and Skogestad (1997) about understanding of the steady-state behavior. The optimal solution surface of the minimal boil up is given as a function of the control variable *liquid split* (R_L) and the design variable *vapor split* (R_V) – defined in appendix. Furthermore candidate outputs are suggested that can be used to control the system such that the boil up is minimized. One of the outputs is the measure of symmetry (DTs) in the temperature profile along the column. The measure of symmetry DTs is defined by Skogestad as $DT_s = \sum(T_{1,j} - T_{4,j}) + \sum(T_{2,j} - T_{5,j})$ where $T_{i,j}$ denotes the temperature from section i at tray j. In case of optimal operation the temperature profile in the column is symmetric. Hence a 4x4 system is obtained where the inputs are reflux flowrate, vapor flowrate, side product flowrate and liquid split (L_0,V_0, S, R_L), and the measured outputs are the three product purities and DTs (x_A, x_B, x_C, DTs), respectively. A suitable set point for the variable DTs makes sure that the operating point is on the bottom of the optimal solution surface – hence the boil up related to vapor flowrate is minimized.

A more practical approach is suggested by Serra et al. (1999). A linearized model is used to obtain a feedback control by PI control. The inventory level consists of two PI loops in order to keep the liquid in the tank and the liquid in the reboiler at a nominal level. From the candidate manipulated variables: L_0, V_0, D B, S, R_L and R_V, typically the DB, LB, DV or LV is used for inventory control. The remaining variables can be used for composition control. Ideally, the controlability property of the column should be taken into account at the design stage. Serra et al. (2000) compared two designs using linear analysis tools – Morari resiliency index (MRI), condition number (CN), relative gain array (RGA), and closed loop disturbance gain (CLDG) – although non-linear analysis could also be applied (Kiss et al., 2002; 2003; 2007).

A more advanced approach for a DWC is the MPC strategy reported by Adrian et al. (2004). The MPC controller outperforms a single PI loop. Three temperatures are controlled by the

reflux ratios, the liquid split and side-draw flowrate, respectively. The disturbed variable in this case was the feed flowrate.

The null space method is a self-optimizing control method that selects the control variables as combinations of measurements (Alstad and Skogestad, 2007). For the case of a Petlyuk distillation setup this resulted into the following candidate measurements: temperature at all stages and all flowrates. Using the null space method a subset of six measurements was obtained, resulting in a practically implementation.

The energy efficiency of the DWC may be improved by allowing heat transfer through the wall (Suphanit, 2007). Although the energy savings that are obtained are small, their suggestion can be taken into account when one is designing a DWC unit.

Il Kim et al. (2007) recommended general guidelines and rules for the design of the DWC and standards for selecting control structures for the DWC. These were used later in a few studies.

A very recent control structure is proposed by Ling and Luyben (2009). Their case study resulted in an energy minimizing control structure consisting of PID controllers. They concluded that the composition of the heavy component at the top of the prefractionator is an implicit and practical way to minimize energy consumption in the presence of feed disturbances. This specific composition was controlled by the liquid split variable (R_L).

Cho et al. (2009) proposed a profile position control scheme for the control of a DWC with vapor sidedraw. Relative gain array (RGA) and singular value decomposition (SVD) analysis were used to determine optimal control configuration. Dynamic simulation showed that the profile position–product composition cascade control can keep the product purities at the desired values in the face of feed and internal disturbances.

Controller performance can be benchmarked in a systematic way based on operating records (i.e. data from plant) or using a plant model (Ordys et al., 2007). For example if a PID controller is required to control a plant, the LQG cost functions can be used to provide the lowest practically achievable performance bound. The optimal LQG based controller can be used then to compute the optimal PID controller. This optimal controller can be compared to the actual controller and hence the performance can be determined. This approach has been applied on a simulation of DWC proprietary BASF (Ordys et al., 2007).

3. Problem Statement

Following the literature review, it is clear that while a variety of controllers are used for binary distillation columns, only a few control structures were studied for dividing-wall columns (DWC). In most of the cases PID loops within a multi-loop framework controllers were used to steer the system to the desired steady state. However, control of a DWC using model predictive control has also been successfully studied (Adrian, et al 2004).
Nevertheless, there is still a gap between PID loops within a multi-loop framework control structures and a MPC strategy. Hence, the applicability and possible advantage of more advanced control strategies should be investigated. Moreover, a major problem of the previously reported case studies is the difficulty if not imposibility to make a fair comparison of the control structures, as different ternary systems were used for separation in a DWC. To solve this problem we apply all the investigated control structures to the same DWC, thus allowing a non-biased comparison of the control performace.

The general design goal is to maintain the product qualities at their given setpoints even in the presence of the disturbances. In this work, the setpoints are chosen equally for the three product compositions. Moreover, since we try to achieve a sharp separation there are no changes made to the setpoint. As a consequence, reference tracking – the performance of the overall system in case the reference changes – is not investigated. We exert two types of disturbances: 10% increase of feed flowrate and 10% increase of the molar fraction of the lightest component in the feed. Note also that the disturbances are not exerted simultaneously.

The time needed by the controller for steering the product purities in a small neighborhood of the setpoints after the exertion of disturbance is measured and used for comparison of the controller performance. Since in an industrial environment the measurements can be distorted by noise and measurement delays we carry out additional simulations using the controllers that satisfy the general design goal. Hence, the controller performance is investigated in case of a measurement delay of one minute and added measurement noise. The noise is filtered which results in a more peak shaped noise signal instead of a block signal. The gain of the filter is such that the average noise strength is 1% of the nominal measured value.

4. Dynamic Model of DWC

The dynamic model proposed in this work is used to develop a controller, hence it is recommend to use linearized liquid dynamics instead of neglecting the liquid dynamics (Skogestad, 1992). In the long run there is no difference between neglecting liquid dynamics or linearizing liquid dynamics. However, when the liquid dynamics are not neglected but simplified by a linearization, the initial response is more realistic. Hence, linearized liquid dynamics is incorporated in the model. Note that the vapor split is impractical to control hence it considered as a design variable – although with a variable vapor split the energy loss in the presence of feed disturbances is about 10 times lower than with a fixed vapor split (Alstad and Skogestad, 2007).

For the dynamic model a number of reasonable simplifying assumptions were made: 1. constant pressure, 2. no vapor flow dynamics, 3. linearized liquid dynamics and 4. neglecting the energy balances and changes in enthalpy. Note that DWC is thermo-dynamically equivalent to the Petlyuk system that is modeled using the following equations:

$$\begin{aligned} \dot{x} &= f(x, u, d, t) \\ y &= g(x) \end{aligned} \tag{1}$$

where $u = [L_0\ S\ V_0\ D\ B\ R_L\ R_V]$ is the input vector, $d = [F\ z_1\ z_2\ q]$ is the disturbance vector, x is the state vector consisting of compositions and liquid holdups and $y = [x_A\ x_B\ x_C\ H_T\ H_R]$ is the output vector.

The dynamic model is implemented in Matlab® (Mathworks, 2007) and it is based on the Petlyuk model previously reported in literature by Halvorsen and Skogestad (1997). For the detailed mathematical description of the model the reader is referred to the appendix.

Figure 2

Figure 2 illustrates the simulated dividing-wall column (DWC). The column is divided into 6 sections, each containing 8 trays, with a total of 32 trays in the main column and 16 in the prefractionator side. When disturbances are not present, feed flowrate is assumed to be F=1, feed condition q=1 (saturated liquid) and equimolar compositions of A, B and C in the feed. The liquid holdups are set as follows: for the reflux tank and the reboiler the holdup is 20, for the prefractionator the liquid holdup is 0.5, and for the main column (sections 3, 4, 5, 6) the liquid holdup is 1, 0.5, 0.5 and 1, respectively. Furthermore, according to the assumptions the vapor flow is constant inside a section:

$$V_i = V_{i-1} \tag{2}$$

In addition, the linearized approximation for the liquid flow is given by:

$$L_i \approx k_0 + k_1 H_i + k_2 V_{i-1} \tag{3}$$

where the constants k_0, k_1 and k_2 have to be chosen properly. Especially the constant k_2 have an impact on the control properties of DWC, while V is assumed to be a control variable.

Note that in the literature quite a range of set points for the product purities has been used for ternary separation. Most recent industrial examples mentioned are the separation of ternary mixtures: benzene, toluene and o-xylene (Ling and Luyben, 2009) and benzene-toulene p-xylene (Suphanit et al., 2007). The authors used for the setpoints of the product purities the values [0.99 0.99 0.99] and [0.95 0.95 0.95], respectively. In this work, we use the same ternary mixture (benzene-toluene-xylene, equivalent to A, B, C) and the reasonable setpoints [0.97 0.97 0.97] for the product specifications. Figure 3 provides the composition profiles inside the simulated DWC by means of a ternary diagram, at various feed conditions (q = 1 saturated liquid, q = 0 saturated vapour, and 0 < q < 1 mix of liquid and vapour). The bottom, side and top product are close to the left, top and right corners, respectively.

Figure 3

Linear model. A local linear model around the steady state (x*,u*)is obtained by numerical differentiation using the formula:

$$\frac{\partial f(x)}{\partial x} = \frac{f(x+h) - f(x-h)}{2h} \tag{4}$$

Hence a state space model is obtained by computing the derivative of the functions f and g with respect to alternating x or u. The model has 156 states (96 compositions for A and B, 8 compositions for A and B in the two splitters, reflux tank and reboiler; 48 tray hold-ups plus 4 additional hold-ups for the two splitters, reflux tank and reboiler) and 11 inputs (5 control, 2 design, and 4 disturbance variables), just as the nonlinear model. The quality of the linear model is clearly illustrated in Figure 4 where the nonlinear and the linear response are given on a temporary disturbance in the feed flowrate. Note that the inputs where set at nominal level and only the tank and reboiler level where controlled while they appear to be unstable.

Figure 4

5. Control Strategies

PID loops within a multi-loop framework. The most used controllers in industry are the PID controllers (Johnson and Moradi, 2005). In case of a DWC, two multi loops are need to stabilize the column and another three loops to maintain the setpoints specifying the product purities. While there are six actuators (D S B L_0 V_0 R_L) using PID loops within a multi-loop framework, many combinations are possible. However, there are only a few configurations that make sense from a practical viewpoint. The level of the reflux tank and the reboiler can be controlled by the variables L_0, D, V_0 and B respectively. Hence, there are four so called *inventory control* options to stabilize the column, the combinations: D/B, L/V, L/B and V/D to control the level in the reflux tank and the level in the reboiler (Figure 5). The part for the control of product purities is often called *regulatory control*. One actuator is left (R_L) that can be used for optimization purposes such as minimizing the energy requirements (Ling and Luyben, 2009; Halvorsen and Skogestad, 1997).

Figure 5

Moreover, closed-loop stability of the decentralized PID controls structure is an unsolved problem (Johnson and Moradi, 2005). PID loops within a multi-loop framework imply a tuning problem with many solutions and hence difficult to solve. Nevertheless, the PID loops within a multi-loop framework are more or less model independent. Hence, if the true plant is quite different than the model, it is likely that the control system will still work. Note that PI controllers in a multi-loop framework control the system via a matrix structure with only one PI controller on each column and each. The full order MIMO problem has been successfully solved and it has in addition a useful cost criterion: linear quadratic Gaussian control.

Linear Quadratic Gaussian control (LQG) is a combination of an optimal controller LQR and optimal state estimator (Kalman filter) based on a linear state-space model with measurement and process noise which minimizes the cost function:

$$J_{LQ} = \int_0^\infty x(t)^T Qx(t) + u(t)^T Ru(t)\ dt \tag{5}$$

LQG is an extension of optimal state feedback that is a solution of the *Linear Quadratic Regulation* (LQR) that assumes no process noise and that the full state is available for control. Since in case of a DWC the full state is a priori not available, and measurement noise and disturbances are assumed in the feed, the state should be estimated taking into account the disturbances. While the LQG control deals only with zero-mean stochastic noise it is not

suitable for dealing with persistent disturbances in the feed.

The resulting offset can be solved using an additional feed-forward controller – structure given in Figure 6. For example if the feed flow rate increases persistent with 10% the product flow rates also increase with 10% in order to reach a steady state. By measuring the feed flow rate the changes can be used directly to adapt the product flow rates with the same percentage. However, for persistent disturbances in feed composition and condition it is more difficult to tune the Feed Forward controller. A working solution is to extend the LQG controller with an integral action (Skogestad and Postlethwaite, 2005). The resulting controller structure is also shown in Figure 6. With an LQR controller there is no tuning problem while the optimal feedback controller is given via an Algebraic Ricatti Equation (ARE). In addition, the closed-loop system is stable with respect to zero-mean white noise. However, the obtained control structure depends heavily on the used linear model. Hence, a realistic linearized model is needed: with multivariate controller synthesis robust stability and robust performance can be obtained with respect to model uncertainty, and with non-linear control the linearization step can be avoided.

Figure 6

Non-linear control. For distillation columns the non-linear control was previously explored by Rouchon (1990). Basically the PID based controllers and LQG are linear controllers that need a linearization step in order to control a non-linear system. Most likely this leads to a loss in the control action while the plant behaves non-linear. For the control of binary distillation, non-linear control has been successfully performed. For example, it is possible to control a binary distillation column using an input–output linearizing (IOL) controller (Biswas, 2007). However the controller is based on a reduced model only considering the bottom purity in the reboiler and the top purity in the reflux drum.

Generic Model Control (GMC) is a process model-based control algorithm using the non-linear state-space model of the process, and it is a special case IOL if the system has relative order of one (Signal and Lee, 1993). This can be done directly by solving the non-linear equation for the input u:

$$\frac{\partial \hat{g}}{\partial x^T} f(x,u,d,t) = K_1 (y^* - y) + K_2 \int_0^t (y^* - y)\ dt \qquad (6)$$

The interpretation is that the derivative of the output y with respect to time follows the predefined PI-control signal at the right hand side. The full state is needed and in case the

plant is approximated by a linear model the left hand side can be replace with the linear equivalent, where y* is a vector of setpoints. The closed loop-nominal system is stable when the open-loop model is minimum phase. A linear continuous time system is minimal phase when all poles and zeros are in the left hand plane. From the pole zero map plotted in Figure 7 it can be concluded that this is not the case. As a result, non-linear control techniques like IOL and GMC are not used for the comparison study is this article.

Figure 7

Multivariable controller synthesis: LSDP. The design of a diagonal PI structure after selecting a pairing leads to a suboptimal design. In addition, the LQG/LQR controller has no guaranteed stability margin which possibly leads to problems in case of model uncertainties. The following two advanced controller synthesis methods were used in order to obtain a robust controller: loop shaping design procedure (LSDP) and the μ-synthesis procedure. Both methods were successfully applied for controller synthesis for a binary distillation column (Gu, 2005). However, in contrast to the approach of Gu, the inventory control and regulatory control problems are solved simultaneously in this work. By carrying out the H_∞ loop shaping design procedure – performed in Matlab® using the command *ncfsyn* – the plant is shaped with a pre-compensator (W_1) and a post-compensator (W_2) that is the identity matrix. W_1 is a diagonal matrix with the following transfer function on the diagonal (for i=1…5):

$$W_1(i,i) = 2 \cdot \frac{s+1}{10s} \tag{7}$$

The value 2 is chosen for the gain of the filter, in order to ensure a small steady-state error. Larger gains lead to smaller steady-state errors but worse transient response (Gu, 2005). In addition, for larger values the closed loop system is unstable in the presence of the measurements noise and time delay. Figure 8 shows the frequency response of the plant G and the shaped plant G_s, respectively.

Figure 8

The structured value μ has a maximum of 0.7686. Hence, the closed loop system is stable with respect to the modeled uncertainty. The closed loop system and the weightings, shown in Figure 9 (Gu, 2007), are described hereafter.

Figure 9

Multivariable controller μ-synthesis (D-K iteration procedure). The linear model plant G is expanded with input multiplicative uncertainty to obtain a disturbed plant G_d. The input disturbance is an uncertain gain combined with an uncertain delay:

$$W_u = \begin{pmatrix} k_1 e^{-\Theta_1 s} & & \\ & \ddots & \\ & & k_1 e^{-\Theta_1 s} \end{pmatrix} \tag{8}$$

where $k_i \in [0.8,1.2]$ and $\Theta_i \in [0,1]$ for i = 1,…,5. The matrix W_u can be splitted into two matrices:

$$\Delta = \begin{pmatrix} \Delta_1 & & \\ & \ddots & \\ & & \Delta_5 \end{pmatrix} \qquad W_\Delta = \begin{pmatrix} W_{\Delta_1} & & \\ & \ddots & \\ & & W_{\Delta_5} \end{pmatrix} \tag{9}$$

where $|\Delta_i| \leq 1$ for i=1,…,5. The functions in the matrix W_Δ are obtained via a fitting procedure in the frequency domain (Gu, 2007):

$$W_{\Delta_i} = \frac{2.2138s^3 + 15.9537s^2 + 27.6702s + 4.9050}{1s^3 + 8.3412s^2 + 21.2393s + 22.6705}, i = 1,...,5 \tag{10}$$

This function is the upper bound of 200 realizations of the relative uncertainty. Hence, an uncertainty set consisting of plants G_d is obtained, while the parameters of the uncertainty are within certain ranges. The next step is to synthesize a controller K that remains stable for all the plants G_d in the uncertainty set (*robust stability*). Robust performance is guaranteed if the structured singular value μ of the closed loop transfer function satisfies at each frequency the following condition:

$$\mu_{\hat{\Delta}}(F_L(P,K)(j\omega)) < 1, \quad \forall\omega. \tag{11}$$

The DK-iteration searches for a controller that satisfies the above condition and stabilizes the closed loop system for all plants in the uncertainty set. The performance weighting function is a diagonal matrix with wp on the diagonal:

$$W_p = \begin{pmatrix} wp & 0.03 & \cdots & \cdots & 0.03 \\ 0.03 & wp & 0.03 & & \vdots \\ \vdots & 0.03 & wp & 0.03 & \vdots \\ \vdots & & 0.03 & wp & 0.03 \\ 0.03 & \cdots & \cdots & 0.03 & wp \end{pmatrix} \qquad wp = 0.1\frac{s+3}{s+10^{-4}} \tag{12}$$

The off-diagonal elements are 0.03, such that the products and liquid levels will go to their prescribed set points. The function wp has the effect that for a low frequency range the setpoints are achieved. The functions W_u limit the control action over the frequency range $\omega \geq 150$ and the gains are chosen independently, such that in case of strong measurement noise over-steering is avoided. This results in:

$$W_u = \begin{pmatrix} wu_1 & & & & \\ & wu_2 & & & \\ & & wu_3 & & \\ & & & wu_4 & \\ & & & & wu_5 \end{pmatrix} \qquad \begin{aligned} wu_i &= g_i \frac{s+1}{s+1} \; i = 1...3 \\ wu_i &= g_i \frac{s+1}{0.01s+1} \; i = 4..5 \end{aligned} \tag{13}$$

The weights g_i are chosen to ensure good performance and robust control: $g_1=g_2=g_3=10.44$ and $g_4=g_5=0.2175$. The measurement noise on the five measurements is filtered by:

$$W_n = \begin{pmatrix} wn & & & & \\ & wn & & & \\ & & wn & & \\ & & & wn_4 & \\ & & & & wn_5 \end{pmatrix}, \quad wn = 0.01\frac{s}{s+1}, \quad wn_4 = wn_5 = 0.2\frac{s}{s+1} \tag{14}$$

The reference is linked to the output of the plant G_d via a model M. The model is represented by a diagonal matrix with zero off-diagonal elements and the following transfer functions (wm), on the diagonal:

$$wm = \frac{1}{1080s^2+288s+1} \tag{15}$$

The off-diagonal elements are zero to avoid interaction and the constants are chosen such that the settling time after an impulse is ~1500 min. Inclusion of such a model makes it easier to achieve desired dynamics. The μ-synthesis (D-K iteration procedure) – performed in Matlab® using the command *dksyn* – results in the iteration steps listed in Table 2**.**

Table 2

Robust stability analysis reveals that the maximum value of μ is 0.3629. Hence the system is stable under perturbations that satisfy: $||\Delta|| < 1/0.3629$. Likewise the maximum value of μ in case of the robust performance analysis is 0.9847. Hence the system achieves robust performance for all the specified uncertainties.

6. Results and Discussion

In the dynamic simulations performed in this study, disturbances of +10% in the feed flow rate (F) and +10% in the feed composition (x_A) were used, as these are among the most significant ones at industrial scale. Note that persistent disturbances give a better insight of the quality of the controller than zero mean disturbances, as typically after a temporary disturbance the product compositions return to their given setpoints. However, the reflux and reboiler levels are unstable and need to be stabilized. For the PI controllers of the four investigated structures the tuning parameters (proportional gain and integral term) listed in Table 3 were used, along with the control loop direction.

Table 3

The dynamic simulations were carried out in Mathworks Matlab® combined with Simulink®. The equations of the model are a system of ODE's that are solved using ODE15s solver available in Matlab. The relative tolerance (10^{-6}) and absolute tolerance (10^{-9}) make sure that the obtained solutions are reliable. Consequently, the time steps used by the solver are variable. Moreover, at any time step, the new input to the controller results in a new control signal. As shown next by the dynamic simulations, all PI control structures cope well with persistent disturbances. However, the control structure DV/LSB and LV/DSB make the DWC return to steady state only after a long time (>1000 min).

The LQG controller with feed forward control has only good results for (persistent) disturbances in the feed flowrate. For other disturbances the tuning of the feed forward terms is less straightforward. The controller has no feedback on the error term that is the difference of the setpoints and the measured values. As a result offset in the product purities appears. To solve this problem, the LQG controller is combined with an integral term.

A stop criterion is used for all test cases in order to have a fair comparison of the controllers – the simulation is stopped if the condition $\|(x_A,x_B,x_C) - (0.97,0.97,0.97)\|^2 < 1e^{-10}$ holds at time t_1 and also holds at time $t_2=t_1 + 40$ min, where $t_1<t_2$. The resulting times (smaller values means better control) are shown in Table 4.

Table 4

The effect of measurement noise on the control performance was also investigated. At the five measurements, filtered white noise was added using the following filter that should be determined according to the spectral contents of the sensor noises accompanying the measurements of the product purities and the liquid levels (Gu, 2005).

$$\text{filter} = 0.01 \cdot \frac{s}{s+1} \tag{16}$$

Hence for frequencies $\omega>1$ the damping is 0 dB and for $\omega\leq1$ there is a damping of 20 dB per decade. The gain f_{gain} =0.01 for the composition channels and 0.2 for the tank and reboiler level sensor, respectively, and the noise source is a block signal with mean 1 and sample time 0.1 minute. Consequently, the gain was selected to be 1% of the nominal measured value.
After a constant load disturbance in the feed at first instance all product purities decrease (Figure 10, left) but then, the top and bottom purities decrease significantly while the middle product purity increases. The product flow rates D and B are steered by the controller above the new nominal values in order to stabilize the product purities. The compositions load disturbance is handled faster and there is no serious overshoot (Figure 10, right). Since, the maximum difference between the setpoints and the measured product purity in case of feed flow rate disturbance is between 0.015-0.020, and approximately 0.008 in case of feed composition disturbance.

Figure 10

Unlike the previous PI control structure, DV/LSB needs a long period to stabilize the plant around the new steady state (Figure 11, left). The overshoot in the purity of xA in case of feed composition disturbance is large: approximately 0.08 (Figure 11, right).

Figure 11

The PI control structure LB/DSV controls the DWC in a similar timescale to DB/LSV (Table 4). The disturbances resulting from the changes in the nominal feed are controlled away; showing only a small overshoot in the product purities; less than 0.02 for both cases (Figure 12).

Figure 12

The control structure of the LV/DSB configuration is such that there are amplifying effects due to the outcome of the control action of both inventory and regulatory control. As a result, the feed flowrate disturbance leads to an increase of L_0 and V_0 to maintain the demanded tank and reboiler level. Consequently, the product purities increase and the levels of the tank and reboiler drop very fast due to the synergy effect of the inventory and regulatory control (Figure 13, left). This phenomenon is also present for the compositions load but less strong (Figure 13, right). Nevertheless the steady state can only be reached after a long time and the feed flow rate disturbance leads to an error of 0.05 in the purity of product B. In addition, compared to the three previous control structures, relative high flow rates are used to control the DWC: $L_0 > 1.1$ and $V_0 > 1.3$.

Figure 13

Figure 14

Figure 14 shows that RGA number vs frequency plot. This clearly distinguish between the LV/DSB and DB/LSV control structures, where the DB/LSV option is preferable to LV/DSB. However, the RGA number for the other structures (LB/DSV and DV/LSB) have similar values, located in between the RGA number of the LV/DSB and DB/LSV structures.

Nevertheless, there is a performance discrepancy that can be explained by investigating the absolute RGA matrix at s=0.0392 (Eq. 20) and conclude that the pairing x_A-V and x_B-V is more effective than x_B-L and x_C-L. Similar behavior is expected for other frequences. From the multi-loop structure with the best RGA number (DB/LSV) we can obtain LB/DSV or DV/LSB via two permutations of the input variables respectively. As a result the variable V for controlling H_R has a bad impact on the product compositions, worst than the case where L is used for controlling H_T in the LB/DSV configuration.

$$|\,\mathrm{RGA}\,| = \begin{pmatrix} 1.0360 & 0.0019 & 0.1509 & 0 & 0 \\ 0.9283 & 0.6016 & 0.4661 & 0 & 0 \\ 0.8753 & 0.4789 & 1.3645 & 0 & 0 \\ 0 & 0 & 0 & 1 & 0 \\ 0 & 0 & 0 & 0 & 1 \end{pmatrix} \qquad (17)$$

While the LQG controller results in optimal state feedback in case of zero-mean noise, problems occur in case of persistent disturbance. Hence, the LQG controller needs to be expanded in order to handle the load disturbances. Combined with the feed forward controller the feed flow rate disturbance can easily be controlled and results in a small settling time (Figure 15, left). In case of compositions disturbance there is no clear relationship between the amount of input and output – as it was for flowrate – and hence the feed forward leads to bad control resulting in a different steady state error (Figure 15, right).

Figure 15

The LQG combined with an integral action stabilizes the column around the demanded setpoints for all the disturbances (Figure 16). In both cases the maximum error in the product compositions is less then 0.005. Furthermore, there is a striking contrast between settling time after a feed flow rate disturbance and a feed composition disturbance: in the latter case the settling time is much longer.

Figure 16

The controller obtained by the LSDP (of order 164) is implemented and the results are shown in Figure 17. The application of this advanced controller leads to significantly shorter settling times than the best PI control structures. Remarkably, the maximal offset error in the product compositions are less then 0.002.

Figure 17

Figure 18 shows that the μ-controller (of order 218) is able to steer the system to the desired steady state after persistent disturbance. Similar to the LSDP-controller the settling time is significantly shorter compared to the PI control structures. And the maximal error in the product compositions is less then 0.002. Moreover, the settling time of the system controlled by the μ-controller is the smallest of all compared control structures.

Figure 18

In addition to the previous scenarios, noise and a time delay of 1 minute was added to each measurement channel. The added measurement noise is filtered using the filter described by the previous equation (16). This simulation was carried out only for the PI control structure DB/LSV, LQG with Integral action, LSDP-controller and the μ-controller as these controllers lead to the shortest settling times. The impact of noise and delay on the LB/DSV PI structure is expected to be comparable with DB/LSV. The dynamic simulation of the PI control structure DB/LSV with measurement noise is shown in Figure 19.

Figure 19

The regulatory part of the control structure (DB) is controlling the tank level and the reboiler level. The measurements noise has more impact on the flow rates D and B than the other three flow rates (Figure 19, right). In addition, the persistent disturbance results in a serious offset for $t < 500$ minutes. However, the control structure is robust to the measurement noise and time delays.

In order to have a fair comparison with the PI control structure, the scales on the Y-axis are the same. The results for the LQG with Integral action control structure (Figure 20) shows similar chaotic behavior in the product composition compared with the PI control structure. Nevertheless, the maximal deviation in the product composition is less than 0.008 and the persistent disturbance is no longer visible after approximately $t > 200$ minutes. While the weighting of the integral error for the product compositions is much larger compared to the liquid levels, the noise has more impact on the control signals L_0, V_0 and S. In addition, the input weightings are also different: the weightings on L0 and V0 are larger than the weighting on S, and the weightings on S is larger than the weightings on B and D. Hence, there is a trade off in a fast control action and measurement noise reduction.

Figure 20

The high order LSDP-controller is more sensitive to noise as shown by the chaotic behavior of the product purities plotted in Figure 21. The closed loop stable remains stable but when synthesizing the controller the noise source is not taken into account. In the absence of measurement noise the control action is such that the settling time is short.

Figure 21

The effect of measurement noise and delay on the system controlled by the μ-controller is shown in Figure 22**.** While there is chaotic behavior in the product compositions the control actions are very calm despite the present noise. Also, the maximum deviation in the product composition is small – less than 0.008.

Figure 22

Note that all the control structures investigated were tested for a large number of disturbances, but here we limit only to the ones that are relevant at industrial scale. Although the reported disturbances are not exerted at the same time, no serious problems – such as instability or lack of capability to reach the setpoints – were observed in case of simultaneous disturbances. The same holds for a decrease of 10% in the feed flow rate or feed composition. The exerted noise is filtered and the gain is approximately 1% of the nominal value on the channel. In an industrial case the filter should correspond to the measurement sensor. Moreover, there is a need to consider the dynamics of the actuators (e.g. time constants, stiction) in evaluating the controller performance (Srinivasan and Rengaswamy, 2005; Shoukat Choudhury et al., 2006). However, for the DWC studied in this work, the timescale of the changes in product purities and liquid levels is in minutes – hence the neglection of the actuator time constant and stiction is expected to be realistic.

Remarkably, PI control structures are already for a long time the celebrated controllers in the chemical industry (Johnson and Moradi, 2005). Several reasons are given for their success:

1. Simplicity of the control structure,
2. Robustness with respect to model uncertainties and disturbances,
3. Relatively easy manual stabilization of the process with PID loops within a multi-loop framework, when an actuator or sensor fails.

The LQG control structure offers optimal state estimation and an optimal control with respect to the cost function (5), providing that the matrices Q and R are chosen in an appropriate way. Unlike LQG, many control variables have to be chosen for the PID loops within a multi-loop

framework. In addition, the LQG control structure guarantees stability of the closed loop system consisting of a linearized DWC, whereas the stability problem of the PID loops within a multi-loop framework is still open (Johnson and Moradi, 2005). The full model is nonlinear and the optimal state estimation and optimal control holds only for the linearized model. However, as shown by Figure 4 this should not lead to problems. Moreover, the dynamic simulations showed no control or stability problems of the closed loop system. Furthermore, there is a trade off between a short settling time in the case of no measurement delay and noise, and a very smooth control action in case of measurement noise. A short settling time results in a more chaotic control if noise is present.

The LSDP-controller has difficulties to cope with the measurement noise. The μ-controller has the shortest settling times and a relatively good behaviour when measurement noise and delay is present. Unlike the μ-controller, controller reduction of the LSDP-controller leads to serious problems in the presence of the measurement noise and delay. As a result, the computer needs much more time to carry out a simulation of the DWC controlled by a LSDP-controller compared the other control structures.

In addition to the controllers compared in this work, Model Predictive Control (MPC) is a serious candidate for controlling non-linear processes. Efficient implementations of non-linear MPC in industrial cases were already reported for several non-linear processes (Kiss et al., 1999; Nagy et al., 2007, Simon et al., 2008, 2009; Roman et al., 2009) and in particular DWC (Adrian et al, 2003). However, more advanced controllers such as MPC are out of the scope of the current study.

7. Conclusions

The comparison of control strategies performed in this work – based on a dividing-wall column separating the ternary mixture benzene-toluene-xylene – provides significant insight into the controllability of DWC, and gives important guidelines for selecting the appropriate control structure. The dynamic model of the DWC used in this study is not a reduced one, but a full-size non-linear model that is representative for industrial separations. Although the application of non-linear based controllers is very appealing – since linearization is not necessary – the general model controller (GMC) is not applicable in practice for the DWC as the open-loop model is not minimum phase.

Due to practical considerations based on the physical flows, there are basically four control strategies possible based on PID loops within a multi-loop framework: DB/LSV, DV/LBS, LB/DSV, LV/DSB. The results of the dynamic simulations show that DB/LSV and LB/DSV are the best control structures among the decentralized multivariable PI structured controllers, being able to handle persistent disturbances in reasonable short times. However, the DV/LBS and LV/DSB structures needed very long settling times, in case of persistent disturbances.

The DWC model is not only non-linear but also a true multi-input multi-output (MIMO) system, hence the applicability of a MIMO control structure starting with a LQG controller was also investigated. With the LQG controller there is an optimal tuning with respect to the corresponding cost function. In order to cope with persistent disturbances two options were explored: feed forward control and addition of an integral action. The LQG combined with a feed forward has good results for a persistent disturbance in the feed flowrate. However, for changes in the feed composition and condition it is difficult to find a good tuning. Moreover, other persistent disturbances than the ones used for tunning cannot be controlled with LQG. Nevertheless, combining LQG with an integral action and reference input solves the problem. Depending on the expected measurement noise the cost function can be determined. Moreover, robustness against measurement noise results in a more conservative tuning.

The loop-shaping design procedure (LSDP) used in this work leads to a feasible μ-controller that has some additional benefits, while specific model uncertainties can be incorporated in the control structure. However, reduction of the LSDP controller (order 164) is not possible since the reduced controller is unable to control the column. In contrast, the μ-controller can be reduced from order 218 to only 25 and still having a good control performance. In the DWC case described here, the obtained μ-controller is able to minimize the settling time when handling persistent disturbances. While PI control structures are also able to control the DWC,

significantly shorter settling times can be achieved using MIMO controllers. Moreover, persistent disturbance are also controlled faster using a MIMO controller.

Acknowledgment

We thank Dr. ir. Karel Keesman (Wageningen University and Research Centre, NL) for the helpful discussions, as well as Prof. Da-Wei Gu (Leicester University, UK) and Prof. Sigurd Skogestad (Norwegian University of Science and Technology) for the technical support. The financial support given by AkzoNobel to Ruben van Diggelen during his internship and final M.Sc. project is also gratefully acknowledged.

Supporting Information

This information is available free of charge via the Internet at http://pubs.acs.org.

Notation

B	bottom product flow rate
D	distillate product flow rate
d	disturbance vector
e	error signal
F	feed flow rate
f, g	functions
f_{gain}	filter gain
F_L	closed loop transfer function
G_d	plant from the uncertainty set
G_s	shaped plant
H_i	liquid holdup
H_R	liquid holdup in reboiler
H_T	liquid holdup in reflux tank
I	identity matrix
K	controller
K_1, K_2	control constants
k_i	constant hydraulic factor $i \in \{0, 1, 2\}$
K_r	reference tracking part of controller
K_y	output feedback part of controller
L_0	reflux flow rate
n	noise signal
N	number of trays
P	plant
q	feed condition
Q	weight matrix on state
r	reference signal
R	weight matrix on input
R_L	ratio liquid split
R_V	ratio vapor split
S	side product flow rate
T	temperature
t	time
u	control vector
V_0	vapor flow rate
W_1	pre-compensator matrix
W_2	post-compensator matrix
W_n	noise shaping filter
W_p	performance action weighting
W_u	control action weighting
x	state vector
x_A	top composition, component A
x_B	side composition, component B
x_C	bottom composition, component C
$x_{i,j}$	liquid composition
y	output vector
y^*	setpoint vector
$y_{i,j}$	vapor composition
z_1	feed composition, component A
z_2	feed composition, component B
α_j	relative volatility
Δ	uncertainty matrix
Θ	time delay constant
μ_Δ	structured singular value

Subscripts

i	tray number $i \in \{1 \ldots N\}$
j	component $j \in \{1, 2, 3\}$

References

1. Adrian R., Schoenmakers H., Boll M., MPC of integrated unit operations: Control of a DWC, Chemical Engineering & Processing, 43 (2004), 347-355.
2. Alstad V., Skogestad S., Null space method for selecting optimal measurement combinations as controlled variables, Industrial & Engineering Chemistry Research, 46 (2007), 846-853.
3. Becker H., Godorr S., Kreis H., Partitioned distilliation columns - why, when & how, Journal of Chemical Engineering, January (2001), 68-74.
4. Biswas P. P., Ray S., Samanta A. N., Multi-objective constraint optimizing IOL control of distillation column with nonlinear observer, Journal of Process Control, 17 (2007), 73-81.
5. Cho Y., Kim B., Kim D., Han M., Lee M., Operation of divided wall column with vapor sidedraw using profile position control, Journal of Process Control, 19 (2009), 932-941.
6. Gu D.W., Robust control design with Matlab®, Chapter 11, Springer, 2005.
7. Halvorsen I. J., Skogestad S., Optimizing control of Petlyuk distillation: understanding the steady-state behaviour, Computers & Chemical Engineering, 21 (1997), 249-254.
8. Il Kim K., Lee M., Park S., Dynamic simulation for the structural design of the divided wall column for different feed composition and various separation features, International Conference on Control, Automation and Systems, Vol. 1-6 (2007), 1988-1992.
9. Isidori A., Nonlinear control systems: an introduction, Springer Verlag, 1989.
10. Isopescu R., Woinaroschy A., Draghiciu L., Energy reduction in a divided wall distillation column, Revista de Chimie, 59 (2008), 812-815.
11. Johnson M. A., Moradi H., PID control: new identification and design methods, Springer Verlag, London, 2005.
12. Kaibel B., Jansen H., Zich E., Olujic Z., Unfixed dividing wall technology for packed and tray distillation columns, Distillation and Absorption, 152 (2006), 252-266.
13. Kaibel G., Distillation columns with vertical partitions, Chemical Engineering Technology, 10 (1987), 92–98.
14. Kiss A. A., Agachi S. P., Model Predictive Control of temperature of a PVC emulsion process, Hungarian Journal of Industrial Chemistry, 27 (1999), 117-124.
15. Kiss A. A., Bildea C. S., Dimian A. C., Iedema P. D., State multiplicity in CSTR-Separator-Recycle polymerization systems, Chemical Engineering Science, 57 (2002), 535-546.

16. Kiss A. A., Bildea C. S., Dimian A. C., Iedema P. D., State multiplicity in PFR-Separator-Recycle polymerization systems, Chemical Engineering Science, 58 (2003), 2973-2984.
17. Kiss A. A., Bildea C. S., Dimian A. C., Design and control of recycle systems by non-linear analysis, Computers & Chemical Engineering, 31 (2007), 601-611.
18. Kiss A. A., Pragt H., van Strien C., Reactive Dividing-Wall Columns - How to get more with less resources?, Chemical Engineering Communications, 196 (2009), 1366-1374.
19. Kister H., Can we believe the simulation results?, Chemical Engineering Progress, October 2002, 52-58.
20. Kolbe B., Wenzel S., Novel distillation concepts using one-shell columns, Chemical Engineering & Processing, 43 (2004), 339-346.
21. Lee P.L., Sullivan G.R., Generic Model Control (GMC), Computers & Chemical Engineering, 12 (1988), 573-580.
22. Ling H., Luyben W. L., New control structure for divided-wall columns, Industrial & Engineering Chemistry Research, 48 (2009), 6034-6049.
23. MathWorks Inc., MATLAB® – Robust Control Toolbox Manual, 2007.
24. Mueller I., Kenig E. Y., Reactive distillation in a Dividing Wall Column – rate-based modeling and simulation, Industrial & Engineering Chemistry Research, 46 (2007), 3709-3719.
25. Nagy Z. K., Mahn B., Franke R., Allgöwer F., Evaluation study of an efficient output feedback nonlinear model predictive control for temperature tracking in an industrial batch reactor, Control Engineering Practice, 15 (2007), 839-850.
26. Olujic Z., Kaibel B., Jansen H., Rietfort T., Zich E., Frey G., Distillation column internals/configurations for process intensification, Chemical & Biochemical Engineering Quarterly, 17 (2003), 301-309.
27. Ordys A., Uduehi D., Johnson M., Process control performance assessment – from theory to implementation, Springer, London, 2007.
28. Perry R. H., Green D. W., Perry's chemical engineers' handbook, 8th Edition, McGraw-Hill, 2008.
29. Petlyuk F. B., Platonov V. M., Slavinskii D. M., Thermodynamically optimal method for separating multicomponent mixtures, International Chemical Engineering, 5 (1965), 555-561.
30. Rani K. Y., Gangiag K., Adaptive Generic Model Control: dual composition control of distillation, AIChe Journal, 37 (1991), 1634-1644.

31. Roman R., Nagy Z. K., Cristea M. V., Agachi S. P., Dynamic modelling and nonlinear model predictive control of a Fluid Catalytic Cracking Unit, Computers & Chemical Engineering, 33 (2009), 605-617.
32. Rouchon P., Dynamic simulation and nonlinear control of distillation columns. Ph.D. thesis, Ecole des Mines de Paris, France, 1990.
33. Schultz M. A., Stewart D. G., Harris J. M., Rosenblum S. P., Shakur M. S., O'Brien D. E., Reduce costs with dividing-wall columns, Chemical Engineering Progress, May (2002), 64-71.
34. Serra M., Espuña A., Puigjaner L., Control and optimization of the divided wall column, Chemical Engineering and Processing, 38 (1999), 549-562.
35. Serra M., Espuña A., Puigjaner L., Study of the divided wall column controllability: influence of design and operation, Computers & Chemical Engineering, 24 (2000), 901-907.
36. Shoukat Choudhury M. A. A., Shah S. L., Thornhill N. F., Shook D. S., Automatic detection and quantification of stiction in control valves, Control Engineering Practice, 14 (2006), 1395-1412.
37. Signal P. D., Lee P. L., Robust stability and performance analysis of Generic Model Control, Chemical Engineering Communications, 124 (1993), 55-76.
38. Simon L. L., Kencse H., Hungerbuhler K., Optimal rectification column, reboiler vessel, connection pipe selection and optimal control of batch distillation considering hydraulic limitations, Chemical Engineering and Processing, 48 (2008), 938-949.
39. Simon L. L., Nagy Z. K. , Hungerbuhler K., Model based control of a liquid swelling constrained batch reactor subject to recipe uncertainties, Chemical Engineering Journal, 153, 2009, 151–158.
40. Skogestad S., Dynamics and control of distillation columns – a critical survey, IFAC-symposium DYCORD+'92, Maryland, April 27-29, 1992.
41. Skogestad S., Postlethwaite I., Multivariable Feedback Control, 2nd edition, Wiley, 2005.
42. Srinivasan R., Rengaswamy R., Control loop performance assessment. 1. A qualitative approach for stiction diagnosis, Industrial & Engineering Chemistry Research, 44 (2005), 6708–6718.
43. Suphanit B., Bischert A., Narataruksa P., Exergy loss analysis of heat transfer across the wall of the dividing-wall distillation column, Energy, 32 (2007), 2121-2134.

44. Taylor R., Krishna R., Kooijman H., Real-world modeling of distillation, Chemical Engineering Progress, 99 (2003), 28-39.
45. To L.C., Nonlinear control techniques in alumina refineries, Ph.D. thesis, Curtin University of Technology, 1996.
46. Viel F., Busvelle A., Gauthiers J.P., A stable control structure for binary distillation columns, International Journal of Control, 67 (1997), 475-505.
47. Wang S. J., Wong D. S. H., Controllability and energy efficiency of a high-purity divided wall column, Chemical Engineering Science, 62 (2007), 1010-1025.

Appendix

Dynamic model of DWC

The nonlinear model of the DWC is described by the following mathematical equations:

$$\dot{x} = f(x, u, d, t)$$
$$y = g(x) \qquad \text{A.1}$$

where $u = [L_0\ S\ V_0\ D\ B\ R_L\ R_V]$ and $d = [F\ z_1\ z_2\ q]$. Furthermore, the state vector x consists of 104 compositions for the first two components and 52 liquid holdups. The output vector is given by $y=[x_A\ x_B\ x_C\ H_T\ H_R]$.

State equations.

Numbering is from top to bottom starting in the prefractionator and then continuing in the main column. Overall, the DWC has 6 sections (S1-S6) that are clearly illustrated in Figure 2.

$$H_i \frac{dx_{i,j}}{dt} = L_{i,j}\,(x_{liquid\_split,j} - x_{i,j}) + V_{i-1,j}(y_{i-1,j} - y_i) \qquad i = 1 \qquad \text{A.2}$$

$$H_i \frac{dx_{i,j}}{dt} = L_{i,j}\,(x_{i+1,j} - x_{i,j}) + V_{i-1,j}(y_{i-1,j} - y_i) \qquad i = 2\ldots8 \qquad \text{A.3}$$

$$H_i \frac{dx_{i,j}}{dt} = L_{i,j}\,(x_{in\_2,j} - x_{i,j}) + V_{i-1,j}(y_{i-1,j} - y_i) \qquad i = 9 \qquad \text{A.4}$$

$$H_i \frac{dx_{i,j}}{dt} = L_{i,j}\,(x_{i+1,j} - x_{i,j}) + V_{i-1,j}(y_{i-1,j} - y_i) \qquad i = 10\ldots16 \qquad \text{A.5}$$

$$H_i \frac{dx_{i,j}}{dt} = L_{i,j}\,(x_{in\_3,1} - x_{i,j}) + V_{i-1,j}(y_{i-1,j} - y_i) \qquad i = 17 \qquad \text{A.6}$$

$$H_i \frac{dx_{i,j}}{dt} = L_{i,j}\,(x_{i+1,j} - x_{i,j}) + V_{i-1,j}(y_{i-1,j} - y_i) \qquad i = 18\ldots23 \qquad \text{A.7}$$

$$H_i \frac{dx_{i,j}}{dt} = L_{i,j}\,(x_{i+1,j} - x_{i,j}) + V_{i-1,j}(y_{in\_3,j} - y_i) \qquad i = 24 \qquad \text{A.8}$$

$$H_i \frac{dx_{i,j}}{dt} = L_{i,j}\,(x_{in\_4,j} - x_{i,j}) + V_{i-1,j}(y_{i-1,j} - y_i) \qquad i = 25 \qquad \text{A.9}$$

$$H_i \frac{dx_{i,j}}{dt} = L_{i,j}\,(x_{i+1,j} - x_{i,j}) + V_{i-1,j}(y_{i-1,j} - y_i) \qquad i = 26\ldots32 \qquad \text{A.10}$$

$$H_i \frac{dx_{i,j}}{dt} = L_{i,j}\,(x_{in\_25,j} - x_{i,j}) + V_{i-1,j}(y_{i-1,j} - y_i) \qquad i = 33 \qquad \text{A.11}$$

$$H_i \frac{dx_{i,j}}{dt} = L_{i,j}\,(x_{i+1,j} - x_{i,j}) + V_{i-1,j}(y_{i-1,j} - y_i) \qquad i = 34\ldots40 \qquad \text{A.12}$$

$$H_i \frac{dx_{i,j}}{dt} = L_{i,j}\,(x_{in\_6,j} - x_{i,j}) + V_{i-1,j}(y_{i-1,j} - y_i) \qquad i = 41 \qquad \text{A.13}$$

$$H_i \frac{dx_{i,j}}{dt} = L_{i,j}\,(x_{i+1,j} - x_{i,j}) + V_{i-1,j}(y_{i-1,j} - y_i) \qquad i = 42\ldots48 \qquad \text{A.14}$$

where the liquid holdup is given by:

$$\frac{dH_i}{dt} = L_{i+1} - L_i \qquad \text{A.15}$$

and the vapor composition is computed by:

$$y_{i,j} = \frac{\alpha_j}{\sum_j \alpha_j x_{i,j}} \qquad \text{A.16}$$

For the components $j \in \{1,2,3\}$ and relative volatilities α.

Furthermore, some special concentrations have to be specified:

$x_{in\_2,j} = (L_8 x_{8,j} + F_0 z_j - (1-q) F_0 y_{9,j}) / L_9$	input section 2; tray no. 9	A.17
$x_{in\_1,j} = x_{liquid\_split}$	input section 1; tray no. 1	A.18
$x_{in\_4,j} = x_{liquid\_split}$	input section 4; tray no. 25	A.19
$x_{in\_6,j} = (L_{16} x_{16} + L_{40} x_{40}) / x_{41}$	liquid input section 6; tray no. 41	A.20
$y_{in\_3,j} = (V_1 y_1 + V_4 y_{25}) / V_{24}$	vapor input section 3; tray no. 24	A.21
$x_{in\_5,j} = x_{side\_splitter}$	liquid input section 5, after liquid splitter	A.22

Dynamics of liquid splitter

The liquid splitter is located between section 3 and sections 1/4.

$$\begin{aligned} \frac{d}{dt} H_{liquid\ split} &= L_{24} - (L_1 + L_{25}) \\ H_{liquid\_split} \frac{d}{dt} x_{liquid\_split} &= L_{24} (x_{24} - x_{liquid\_split}) \end{aligned} \qquad \text{A.23}$$

Dynamics of side splitter

The liquid side splitter is located between section 3 and sections 4/5.

$$\begin{aligned} \frac{d}{dt} H_{side\_split} &= L_{32} - L_{33} - S \\ H_{side\_split} \frac{d}{dt} x_{side\_split} &= L_{32} (x_{32} - x_{side\_split}) \end{aligned} \qquad \text{A.24}$$

Dynamics of reboiler

This is situated between section 3 and sections 1/4.

$$\begin{aligned} \frac{d}{dt}H_{reboiler} &= L_6\text{-}V_0 - B \\ H_{reboiler}\frac{d}{dt}x_{reboiler} &= L_{in}(x_{in}\text{-}x_{reboiler})\text{-}V_0(y_{reboiler} - x_{reboiler}) \end{aligned} \qquad \text{A.25}$$

Dynamics of the reflux tank

This is situated between section 3 and sections 4/5.

$$\begin{aligned} \frac{d}{dt}H_{reflux\_tank} &= V_0 - L_0 - D \\ H_{reflux\_tank}\frac{d}{dt}x_{reflux\_tank} &= V_0(x_{in}\text{-}x_{reflux\_tank}) \end{aligned} \qquad \text{A.26}$$

Liquid flow rates

$L_{i,j} = L_0\ R_L$	i =1…8	A.27
$L_{i,j} = L_0\ R_L + qF_0$	i =9…16	A.28
$L_{i,j} = L_0$	i =17…24	A.29
$L_{i,j} = L_0\ (1\text{-}R_L)$	i =25...32	A.30
$L_{i,j} = L_0\ (1\text{-}R_L) - S$	i =33...40	A.31
$L_{i,j} = L_0 + qF_0 - S$	i =41...48	A.32

Vapor flow rates

$V_{i,j} = V_0\ R_v\text{+}(1\text{-}q)\ F_0$	i = 1… 8	A.33
$V_{i,j} = V_0\ R_v$	i = 9…16	A.34
$V_{i,j} = V_0\ R_v\text{+}(1\text{-}q)\ F_0 + V_0\ (1\text{-}R_v)$	i = 17…24	A.35
$V_{i,j} = V_0\ (1\text{-}R_v)$	i = 25...32	A.36
$V_{i,j} = V_0\ (1\text{-}R_v)$	i = 33...40	A.37
$V_{i,j} = V_0$	i = 41...48	A.38

Note that the DWC model considered in this work makes use of theoretical stages, hence there is no difference made in terms of column internals (trays or packing). Nevertheless, from a practical viewpoint, the HETP is assumed to be the same on both sides of the column if packing is used as internals. The potential HETP differences between the two sides of the column can be avoided by proper design as well as control measures (Kister, 2002; Olujic et al., 2003; Kaibel et al., 2006).

Tables

Table 1. Physical properties of the investigated ternary system: benzene, toluene, and xylene.

Physical property	Benzene	Toluene	Xylene
Molecular formula	C_6H_6	C_7H_8	C_8H_{10}
Molecular weight	78.11	92.14	106.17
Density (kg/m^3)	878.6	866.9	860.0
Viscosity (cP at 20°C)	0.652	0.590	0.620
Critical pressure (bar)	48.95	41.08	35.11
Critical temperature (°C)	288.9	318.6	343.05
Melting temperature (°C)	5.53	– 94.97	13.26
Boiling temperature (°C)	80.09	110.63	138.36

Table 2. Results of the multivariable μ-synthesis (D-K iterative procedure).

Iteration	Controller order	Maximum value of μ	Achieved γ
1	194	14.4	16.1
2	204	1.4	1.5
3	218	0.985	1.038

Table 3. Tuning parameters of PI controllers.

DB/LSV	P (%/%)	I (min)	D (min)	Control direction
xA → L	3	80	0	+
xB → S	3	80	0	–
xC → V	3	80	0	+
Tank Level → D	0.5	100	0	–
Reboiler Level → B	0.5	100	0	–

DV/LSB	P (%/%)	I (min)	D (min)	Control direction
xA → L	1	100	0	+
xB → S	1	100	0	–
xC → B	1	100	0	–
Tank Level → D	0.1	400	0	–
Reboiler Level → V	0.1	400	0	–

LB/DSV	P (%/%)	I (min)	D (min)	Control direction
xA → D	3	75	0	–
xB → V	3	75	0	+
xC → S	3	75	0	+
Tank Level → L	0.5	400	0	–
Reboiler Level → B	0.5	400	0	–

LV/DSB	P (%/%)	I (min)	D (min)	Control direction
xA → D	1	100	0	–
xB → S	1	100	0	–
xC → B	1	100	0	–
Tank Level → L	0.5	400	0	–
Reboiler Level → V	0.5	400	0	–

Table 4. Settling time to reach steady state for different persistent disturbances.

Control structure	Settling time (min)	Settling time (min)
	+10% Feed flowrate	*+10% x_A in feed*
DV/LSB	>> 1000	>> 1000
LV/DSB	>> 1000	>> 1000
LB/DSV	790	561
DB/LSV	714	525
LQR/LGQ (Integral action)	510	839
LQR/LGQ (Feed forward)	432.5	N/A
LSDP	645	569
μ-controller	642	569

Figure captions

Figure 1. Separation of a ternary mixture via direct distillation sequence (top), Petlyuk configuration (center) and dividing-wall column (bottom).

Figure 2. Schematics of the simulated dividing-wall column

Figure 3. Composition profile inside the dividing-wall column, as ternary diagram for two cases: saturated liquid feed (q=1, left) and liquid-vapor feed (q=0.5, right).

Figure 4. Comparison between the non-linear and linearized system: response after a non-persistent disturbance of +10% in the feed flow rate for 20 minutes (t=40..60)

Figure 5. Control structures based on PID loops within a multi-loop framework: DB/LSV, DV/LSB, LB/DSV, LV/DSB.

Figure 6. LQG controller with feed-forward controller (top), LQG controller extended with integral action (bottom).

Figure 7. Pole-zero map of the linearized system

Figure 8. The frequency response of the plant G (-) and of the shaped plant(--).

Figure 9. The closed-loop interconnection structure of the DWC system with weighted outputs; the dashed box represents a plant G_d from the uncertainty set.

Figure 10. Dynamic response of the DB/LSV control structure, at a persistent disturbance of +10% in the feed flow rate (left) and +10% x_A in the feed composition (right)

Figure 11. Dynamic response of the DV/LSB control structure, at a persistent disturbance of +10% in the feed flow rate (left) and +10% xA in *the* feed composition (right)

Figure 13. Dynamic response of the LV/DSB control structure, at a persistent disturbance of +10% in the feed flow rate (left) and +10% x_A in the feed composition (right)

Figure 14. RGA number vs frequency, for the PID loops within a multi-loop framework.

Figure 15. Dynamic response of LQG controller with feed forward, at a persistent disturbance of +10% in the feed flow rate (left) and +10% x_A in the feed composition (right).

Figure 16. Dynamic response of the LQG combined with Integral action control structure, at a persistent disturbance of +10% in the feed flow rate (left) and +10% x_A in the feed composition (right).

Figure 17. Dynamic response of the LSDP-controller, at a persistent disturbance of +10% in the feed flow rate (left) and +10% x_A in the feed composition (right).

Figure 18. Dynamic response of the μ-controller, at a persistent disturbance of +10% in the feed flow rate (left) and +10% x_A in the feed composition (right).

Figure 19. Dynamic response of the DWC with the DB/LSV control structure, at a persistent disturbance of +10% at t=50min in the feed flow rate while there is white measurement noise and a time delay.

Figure 20. Dynamic response of the DWC with the LQG with Integral action control structure, at a persistent disturbance of +10% at t=50min in the feed flow rate while there is white measurement noise and a time delay.

Figure 21. Dynamic response of the DWC with the LSDP-controller, at a persistent disturbance of +10% at t=50min in the feed flow rate while there is white measurement noise and a time delay.

Figure 22. Dynamic response of the DWC with the μ-controller, at a persistent disturbance of +10% at t=50min in the feed flow rate while there is white measurement noise and a time delay.

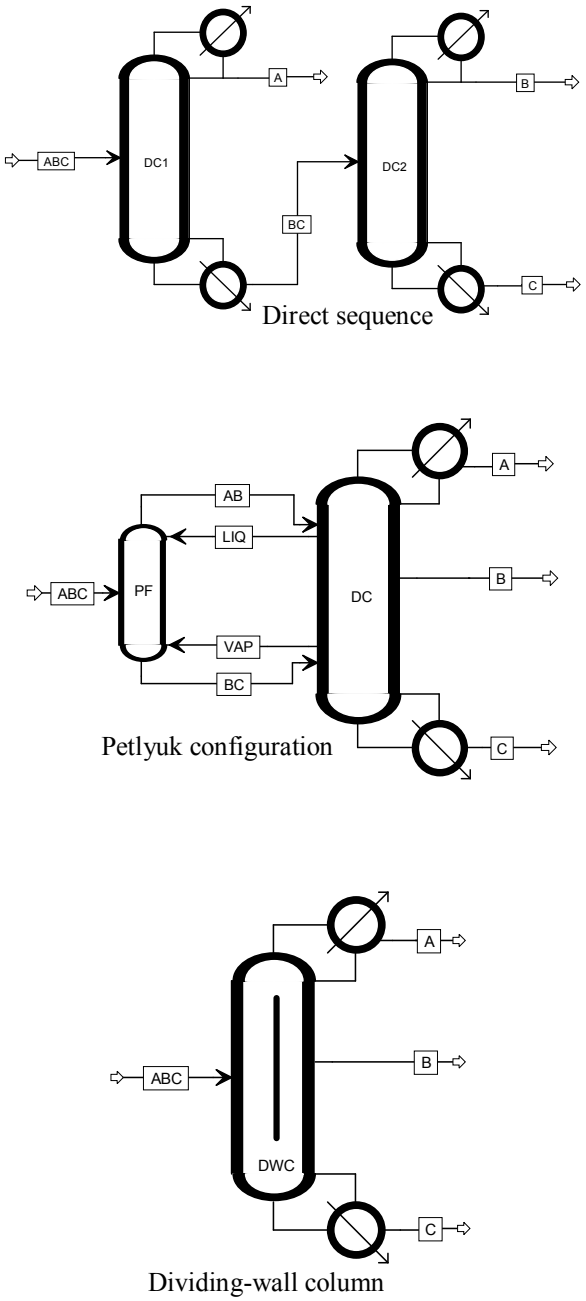

Figure 1. Separation of a ternary mixture via direct distillation sequence (top), Petlyuk configuration (center) and dividing-wall column (bottom).

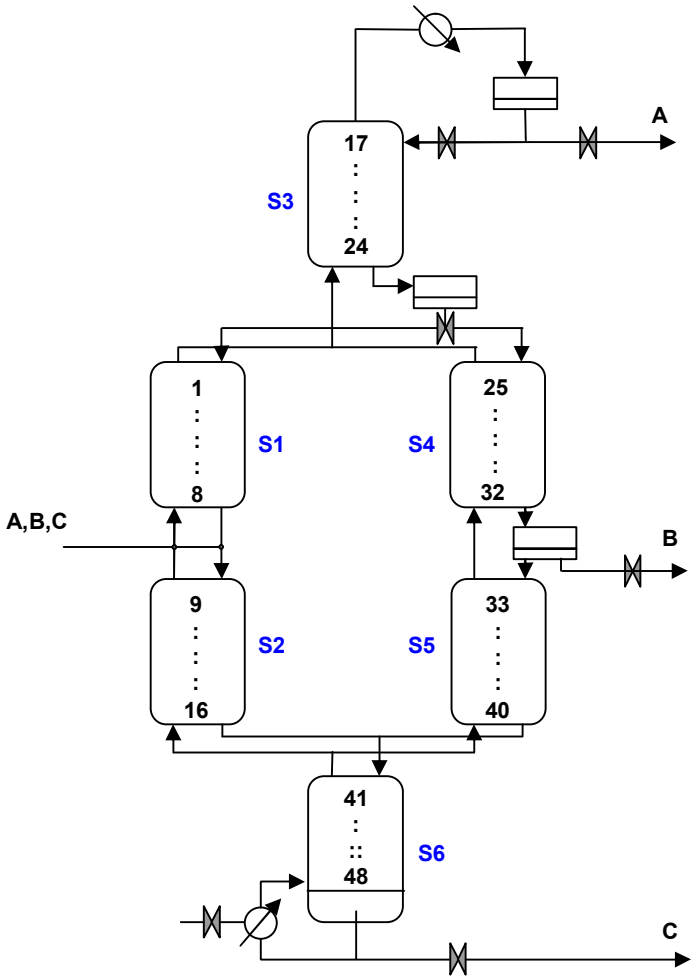

Figure 2. Schematics of the simulated dividing-wall column.

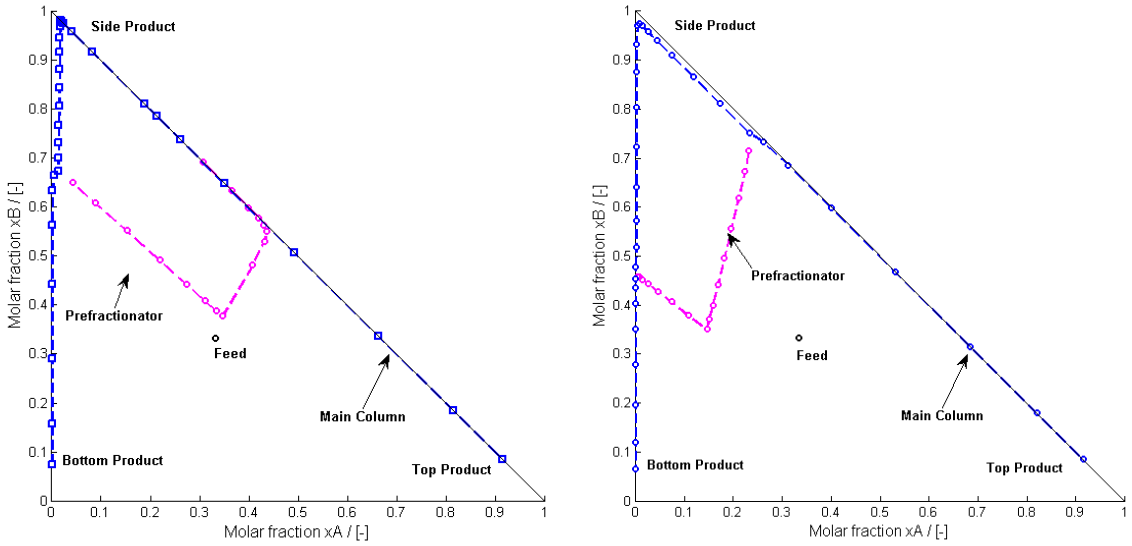

Figure 3. Composition profile inside the dividing-wall column, as ternary diagram for two cases: saturated liquid feed (q=1, left) and liquid-vapor feed (q=0.5, right).

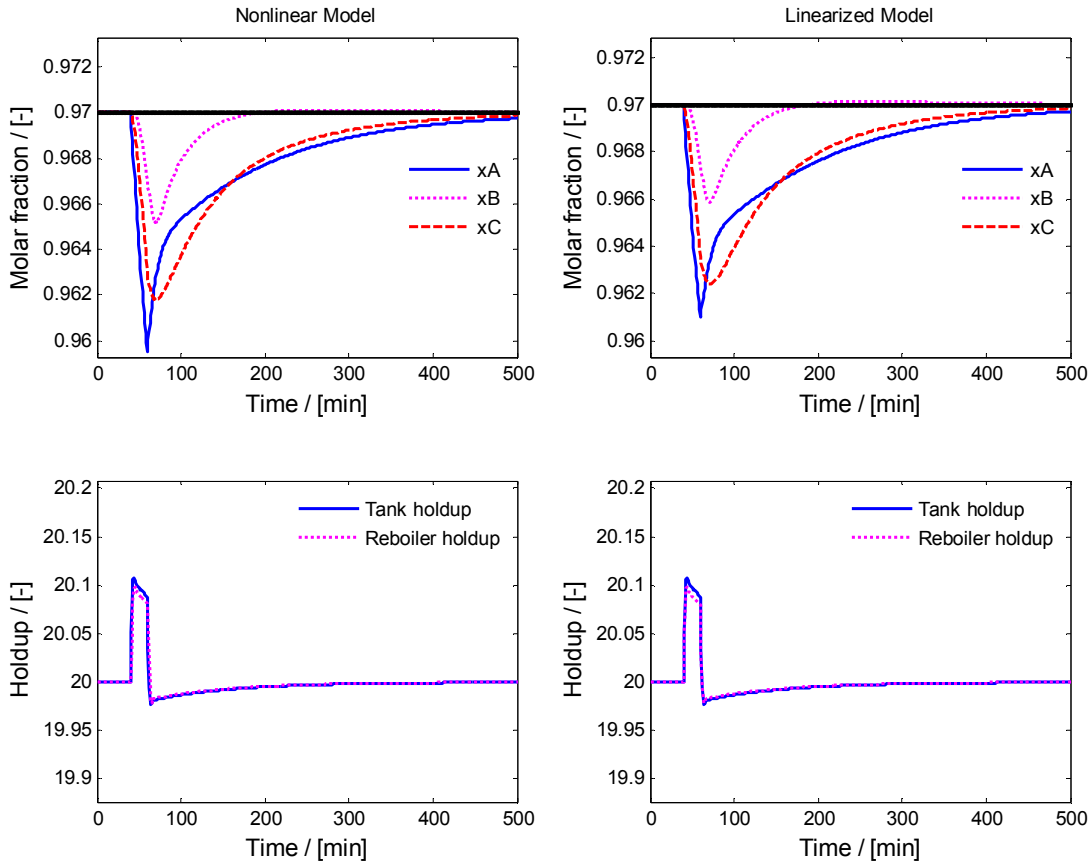

Figure 4. Comparison between the non-linear and linearized system: response after a non-persistent disturbance of +10% in the feed flow rate for 20 minutes (t=40..60)

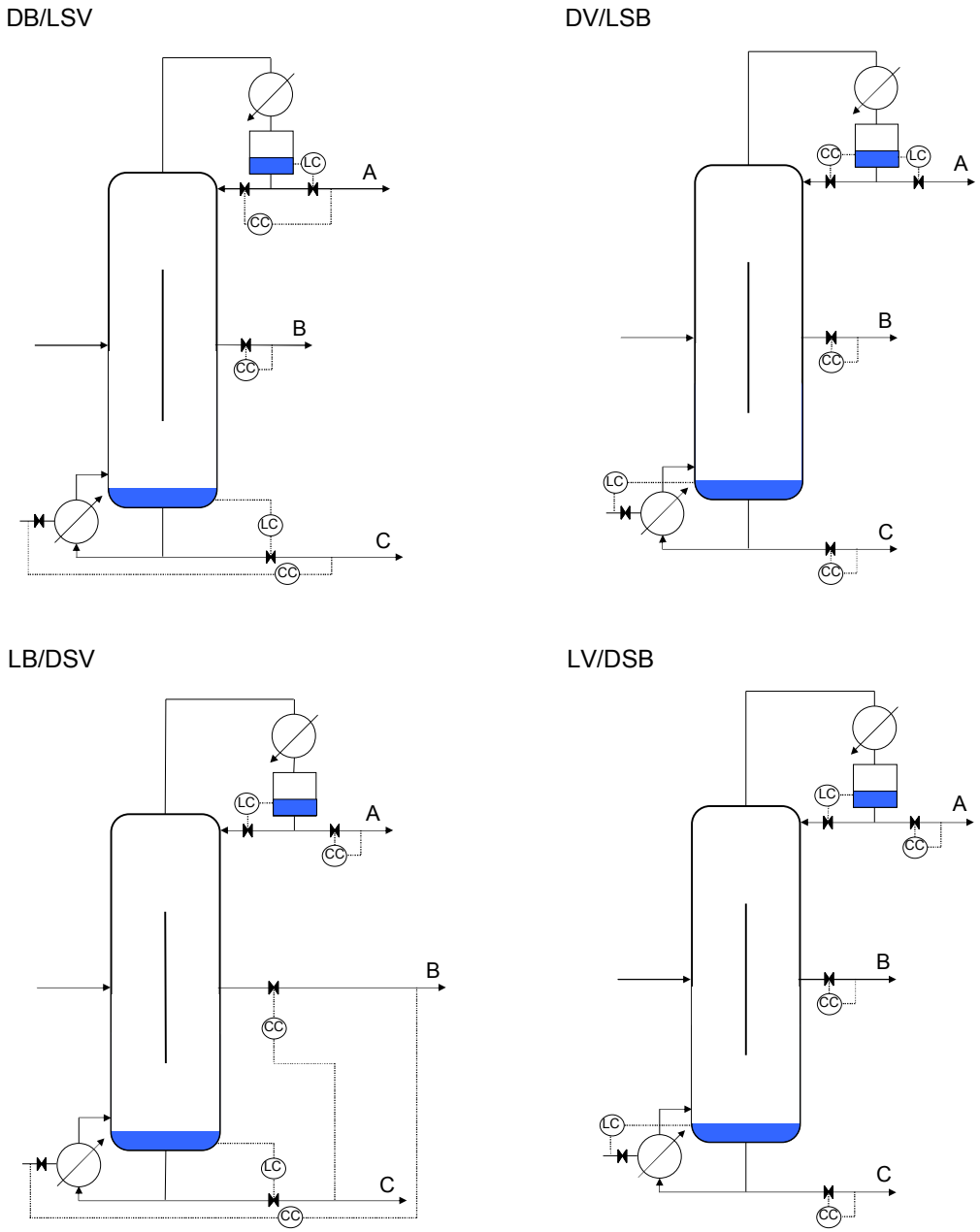

Figure 5. Control structures based on PID loops within a multi-loop framework: DB/LSV, DV/LSB, LB/DSV, LV/DSB.

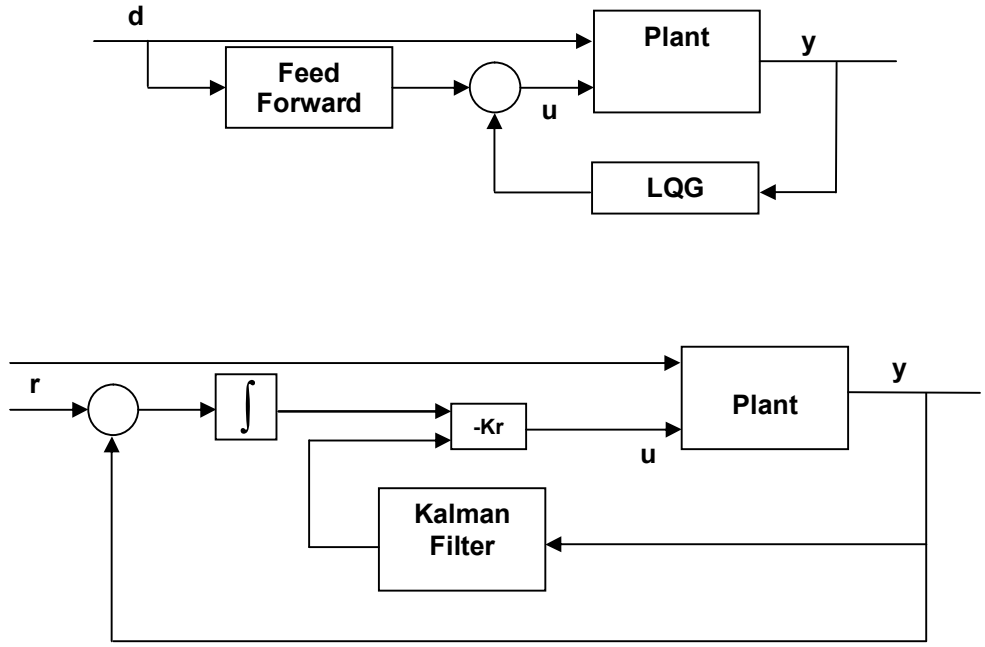

Figure 6. LQG controller with feed-forward controller (top), LQG controller extended with integral action (bottom).

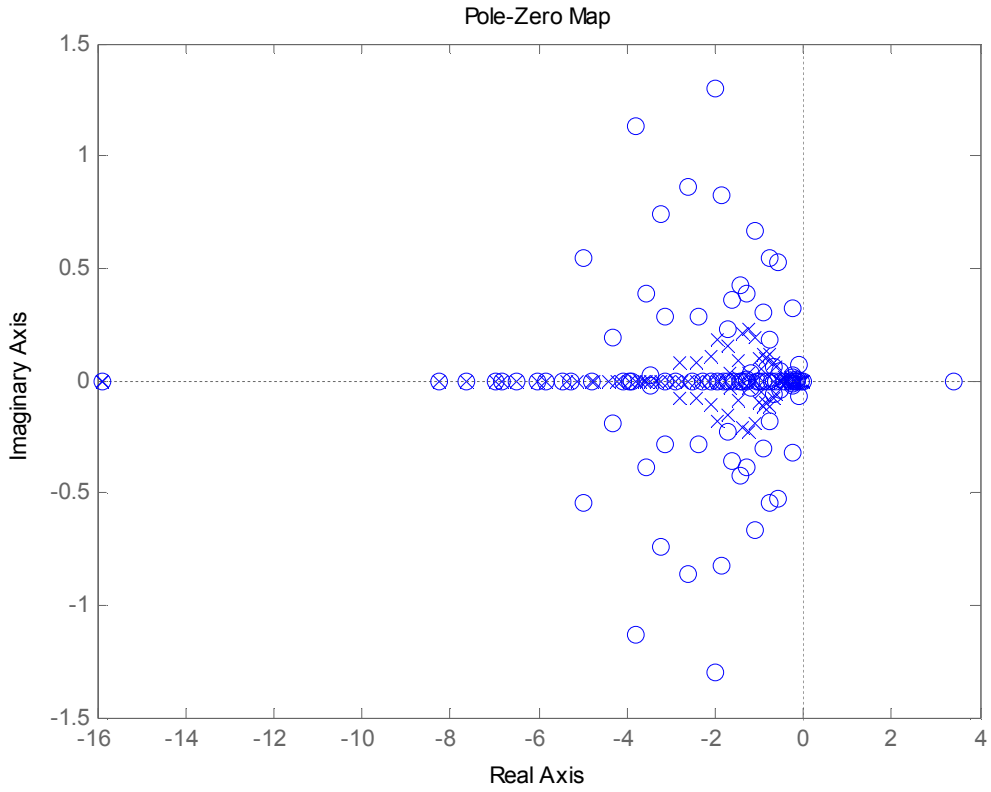

Figure 7. Pole-zero map of the linearized system.

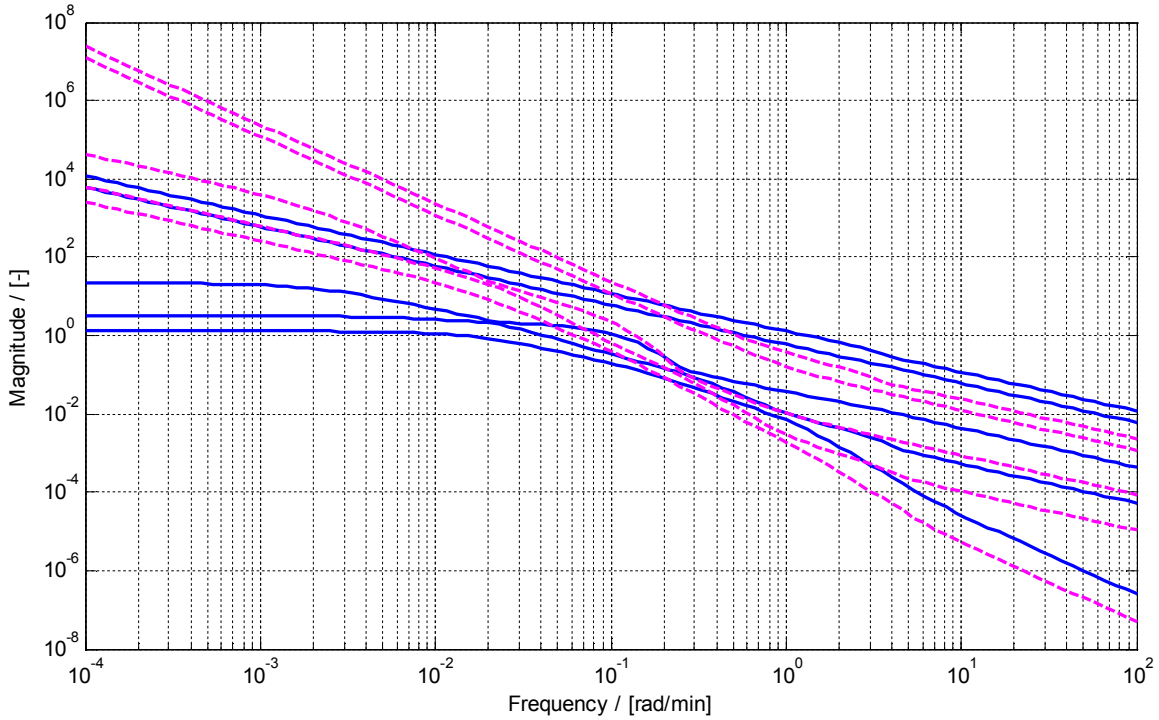

Figure 8. The frequency response of the plant G (-) and of the shaped plant(--).

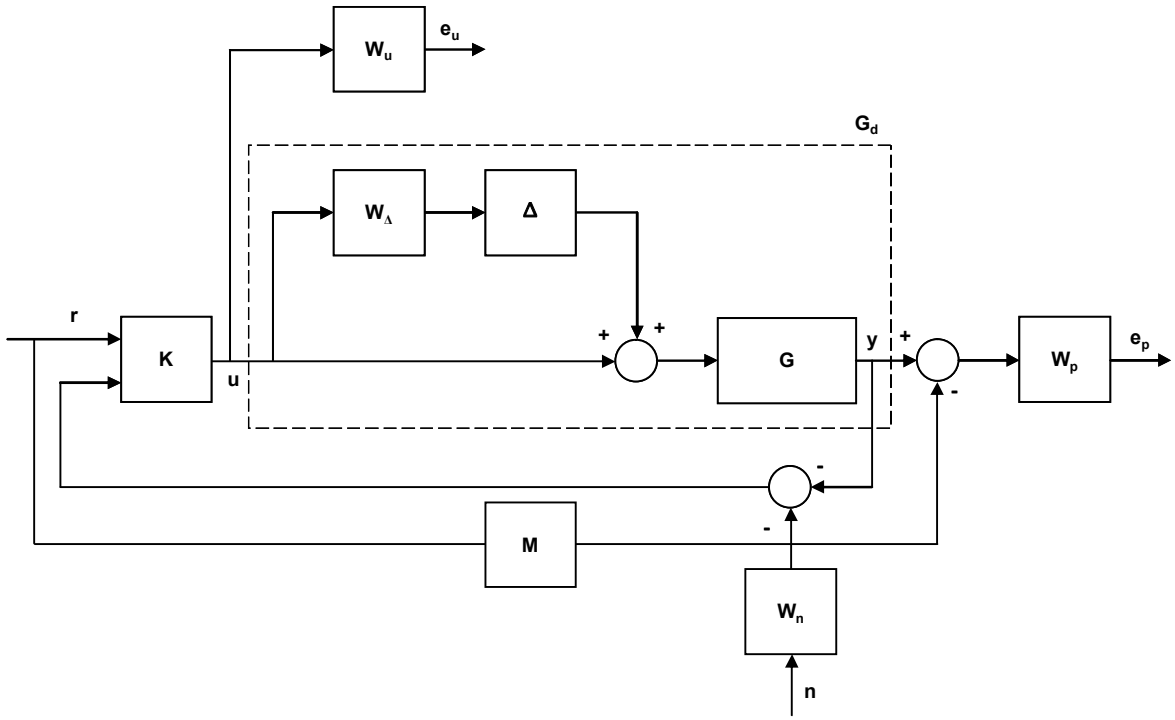

Figure 9. The closed-loop interconnection structure of the DWC system with weighted outputs; the dashed box represents a plant G_d from the uncertainty set.

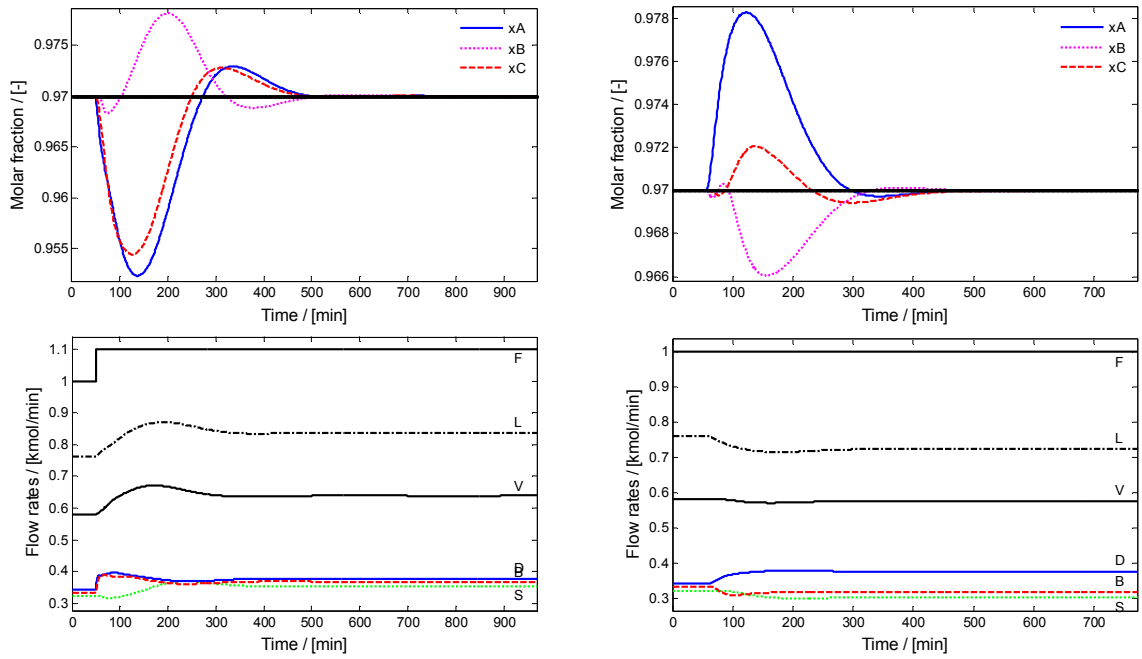

Figure 10. Dynamic response of the DB/LSV control structure, at a persistent disturbance of +10% in the feed flow rate (left) and +10% x_A in the feed composition (right)

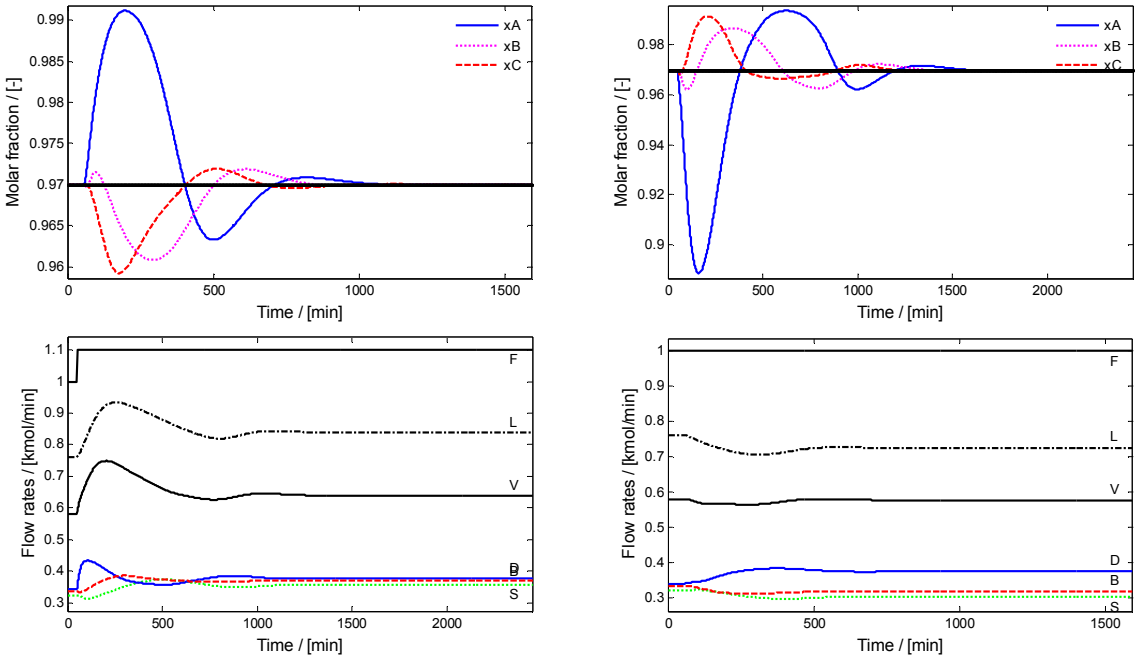

Figure 11. Dynamic response of the DV/LSB control structure, at a persistent disturbance of +10% in the feed flow rate (left) and +10% x_A in the feed composition (right)

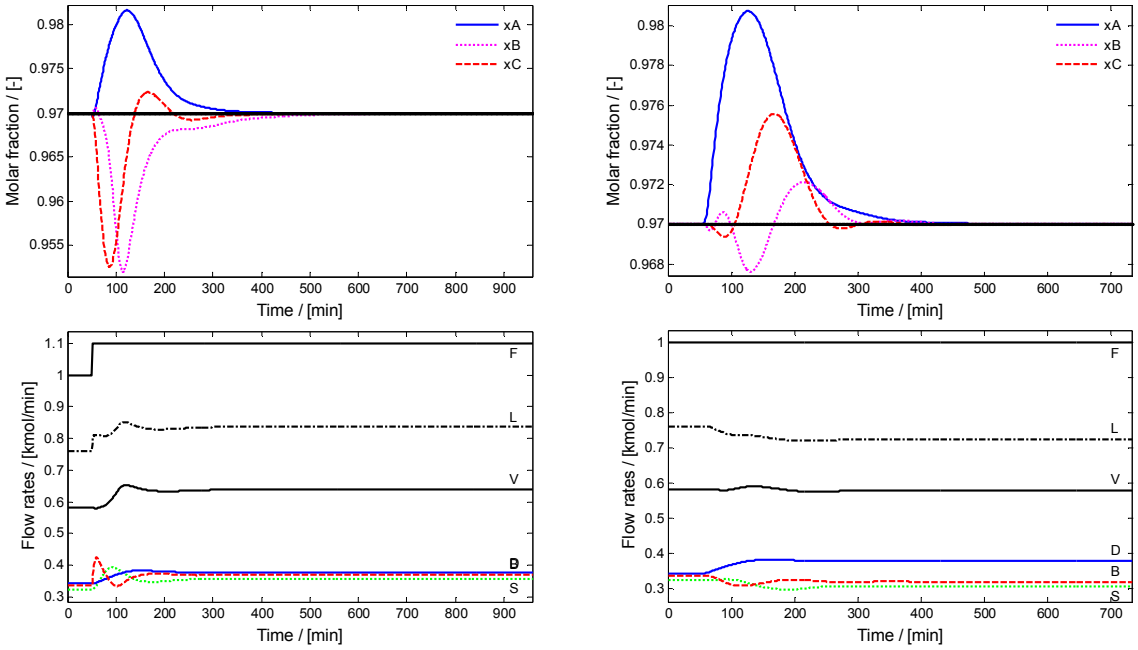

Figure 12. Dynamic response of the LB/DSV control structure, at a persistent disturbance of +10% in the feed flow rate (left) and +10% xA in the feed composition (right)

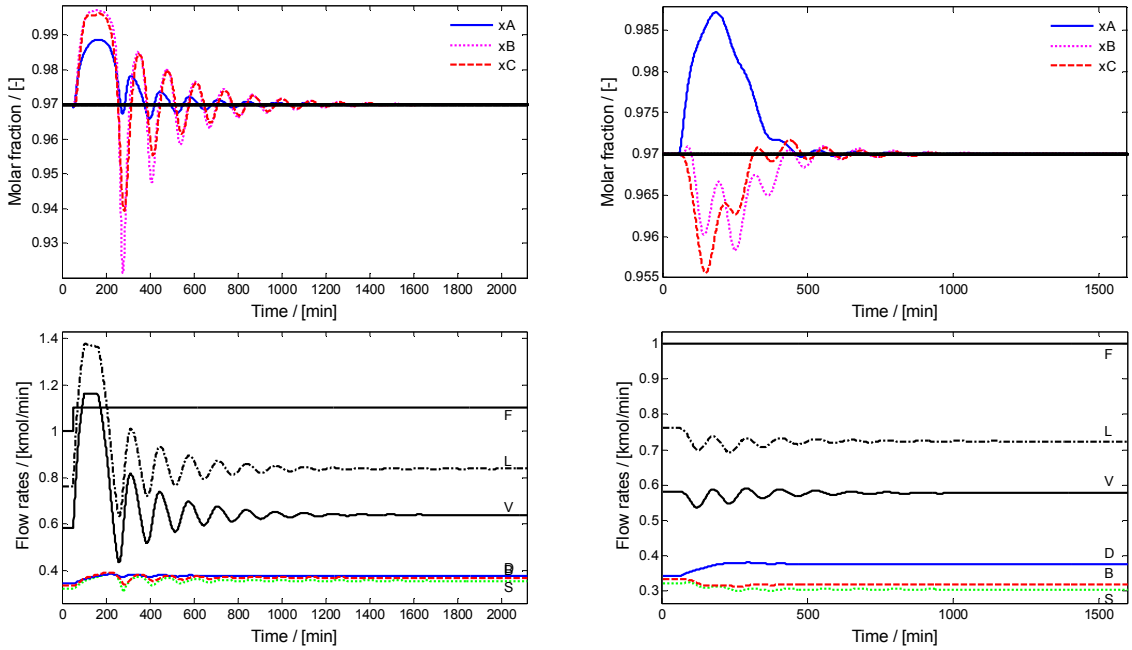

Figure 13. Dynamic response of the LV/DSB control structure, at a persistent disturbance of +10% in the feed flow rate (left) and +10% x_A in the feed composition (right)

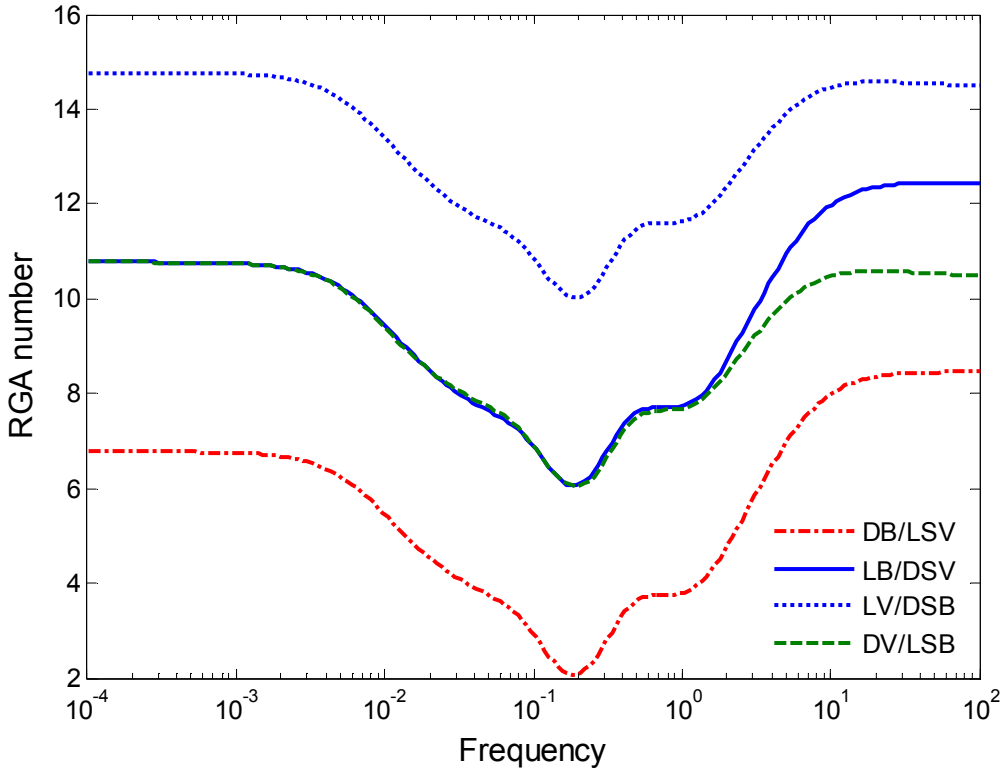

Figure 14. RGA number vs frequency, for the PID loops within a multi-loop framework.

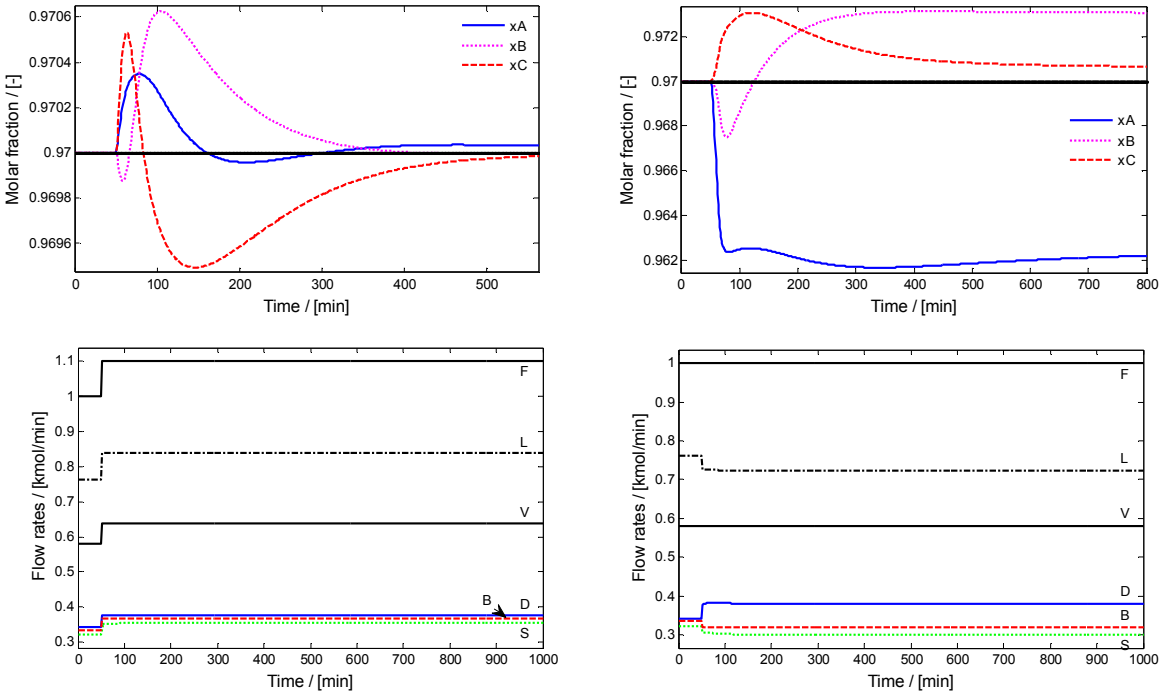

Figure 15. Dynamic response of LQG controller with feed forward, at a persistent disturbance of +10% in the feed flow rate (left) and +10% x_A in the feed composition (right).

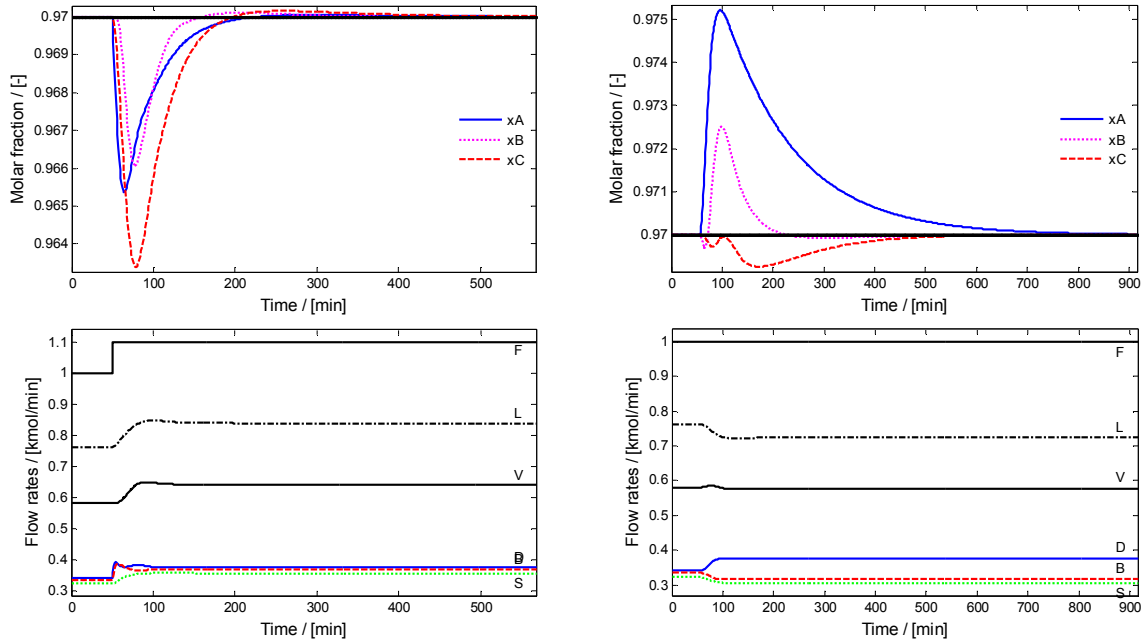

Figure 16. Dynamic response of the LQG combined with Integral action control structure, at a persistent disturbance of +10% in the feed flow rate (left) and +10% x_A in the feed composition (right).

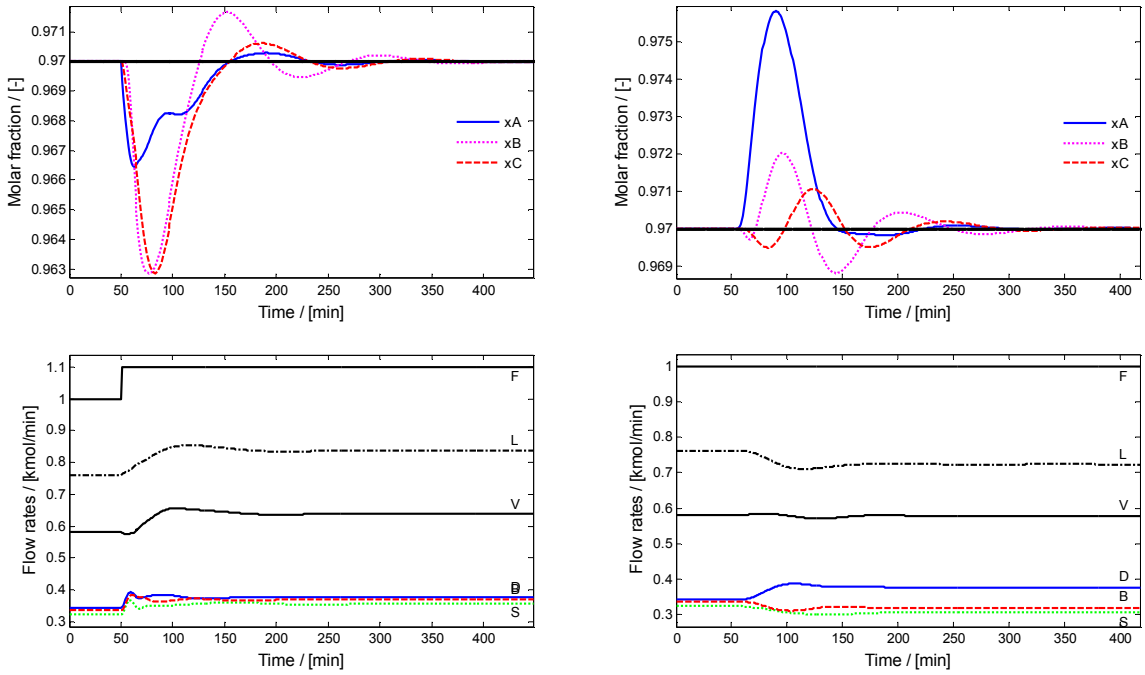

Figure 17. Dynamic response of the LSDP-controller, at a persistent disturbance of +10% in the feed flow rate (left) and +10% x_A in the feed composition (right).

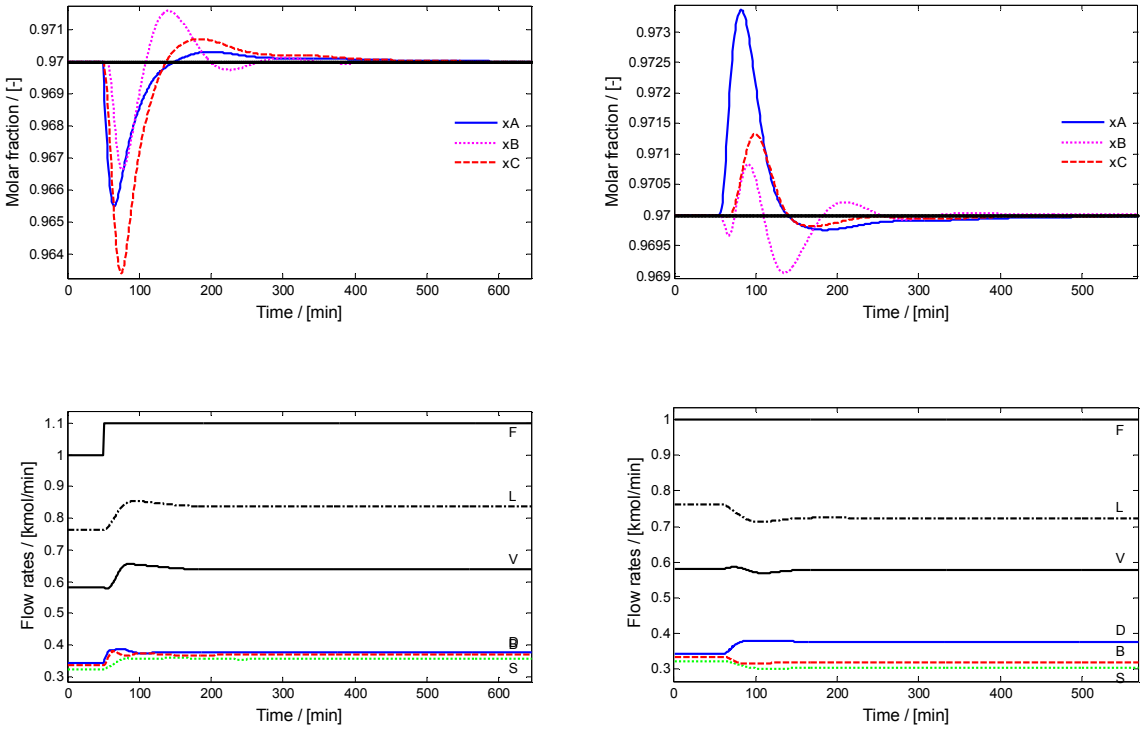

Figure 18. Dynamic response of the μ-controller, at a persistent disturbance of +10% in the feed flow rate (left) and +10% x_A in the feed composition (right).

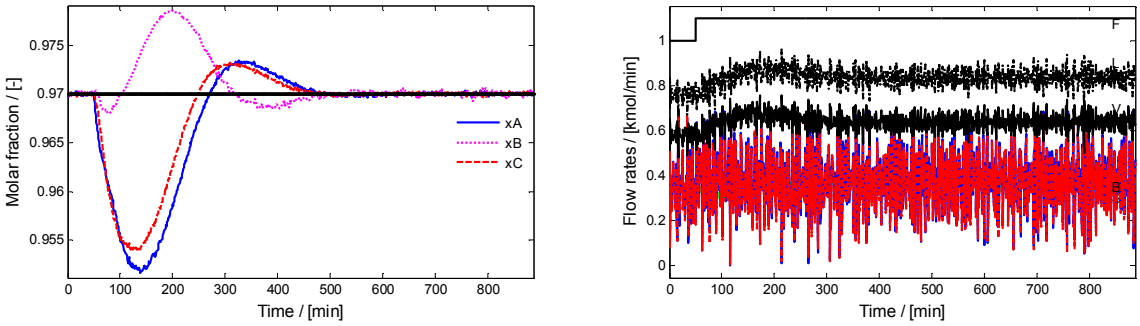

Figure 19. Dynamic response of the DWC with the DB/LSV control structure, at a persistent disturbance of +10% at t=50min in the feed flow rate while there is white measurement noise and a time delay.

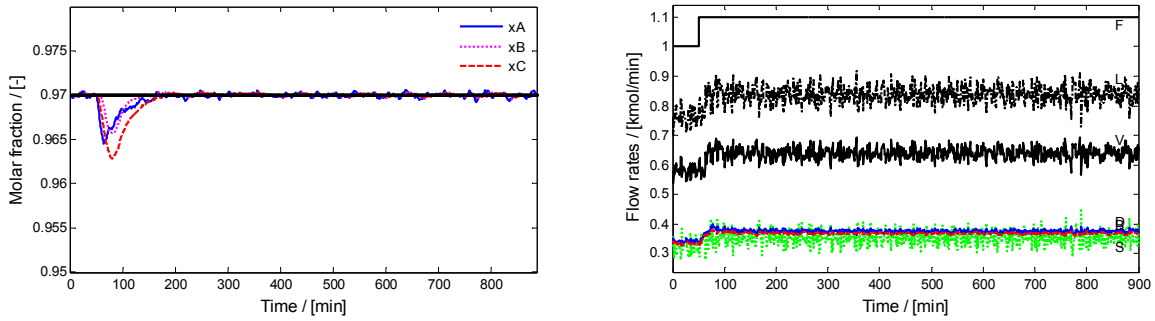

Figure 20. Dynamic response of the DWC with the LQG with Integral action control structure, at a persistent disturbance of +10% at t=50min in the feed flow rate while there is white measurement noise and a time delay.

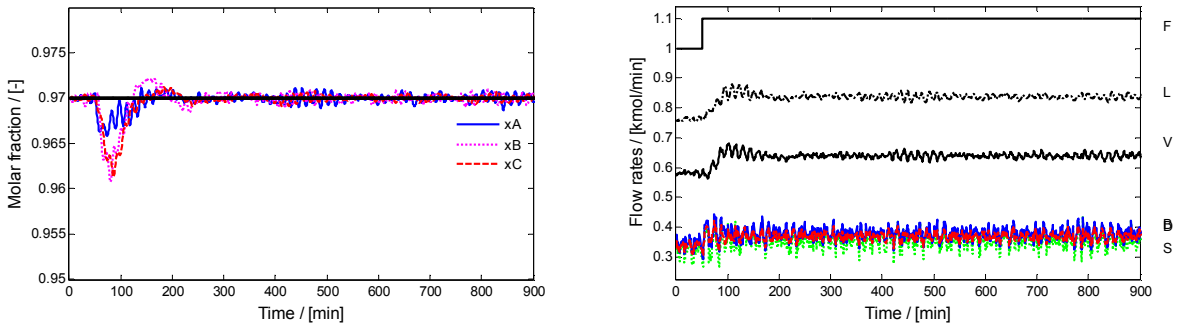

Figure 21. Dynamic response of the DWC with the LSDP-controller, at a persistent disturbance of +10% at t=50min in the feed flow rate while there is white measurement noise and a time delay.

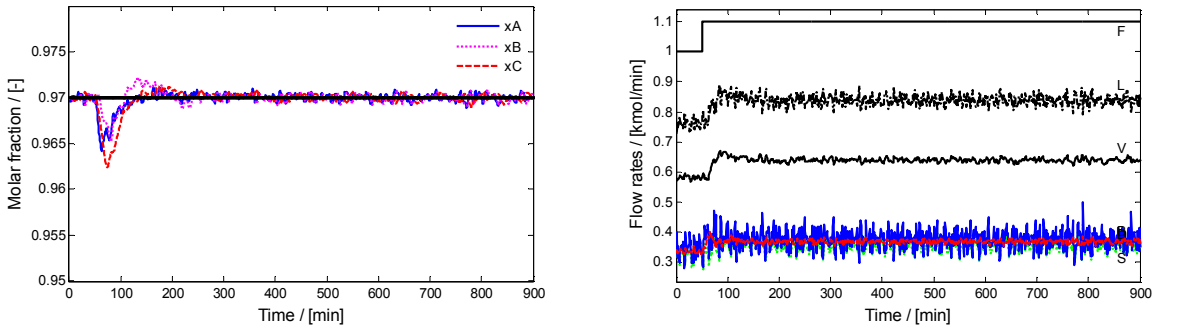

Figure 22. Dynamic response of the DWC with the μ-controller, at a persistent disturbance of +10% at t=50min in the feed flow rate while there is white measurement noise and a time delay.